Fortschritt-Berichte VDI

VDI

Reihe 3

Verfahrenstechnik

Dipl.-Ing. Sebastian Recker,
Düsseldorf

Nr. 951

Systematic and Optimization-Based Synthesis and Design of Chemical Processes

Berichte aus der
Aachener Verfahrenstechnik - Prozesstechnik

RWTH Aachen University

Systematic and Optimization-Based Synthesis and Design of Chemical Processes

Systematischer und optimierungsbasierter Entwurf chemischer Prozesse

Von der Fakultät für Maschinenwesen der
Rheinisch-Westfälischen Technischen Hochschule Aachen
zur Erlangung des akademischen Grades eines
Doktors der Ingenieurwissenschaften
genehmigte Dissertation

vorgelegt von

Sebastian Recker

Berichter: Universitätsprofessor Dr.-Ing Wolfgang Marquardt
Universitätsprofessor Dr.-Ing Hannsjörg Freund

Tag der mündlichen Prüfung: 10.03.2017

Fortschritt-Berichte VDI

Reihe 3

Verfahrenstechnik

Dipl.-Ing. Sebastian Recker,
Düsseldorf

Nr. 951

Systematic and Optimization-Based Synthesis and Design of Chemical Processes

Berichte aus der
Aachener Verfahrenstechnik - Prozesstechnik

RWTH Aachen University

Recker, Sebastian
Systematic and Optimization-Based Synthesis and Design of Chemical Processes
Fortschr.-Ber. VDI Reihe 3 Nr. 951. Düsseldorf: VDI Verlag 2017.
124 Seiten, 31 Bilder, 26 Tabellen.
ISBN 978-3-18-395103-1, ISSN 0178-9503,
€ 48,00/VDI-Mitgliederpreis € 43,20.

Für die Dokumentation: Conceptual Process Design – Process Optimization – Shortcut Model for Kinetically-Controlled Reactor Networks – Rigorous Optimization – MINLP

In industrial practice, conceptual process design is typically conducted by repetitive simulation studies, which require detailed design specifications in an early design phase. Guided by heuristics, these iterative solution procedures result in high manual effort and, in addition, no guarantee concerning the quality of the solution can be given. Optimization-based design methods provide a tremendous potential to accelerate and improve conceptual process design. For this purpose, a synthesis framework for the optimization-based design of chemical processes is presented in this thesis. Powerful shortcut and rigorous evaluation methods for reaction and distillation are presented. These methods are computationally efficient in order to allow an optimization-based design of large-scale chemical processes. Various industrial case studies illustrate the application of the novel approaches and highlight their benefits.

Bibliographische Information der Deutschen Bibliothek
Die Deutsche Bibliothek verzeichnet diese Publikation in der Deutschen Nationalbibliographie; detaillierte bibliographische Daten sind im Internet unter http://dnb.ddb.de abrufbar.

Bibliographic information published by the Deutsche Bibliothek
(German National Library)
The Deutsche Bibliothek lists this publication in the Deutsche Nationalbibliographie (German National Bibliography); detailed bibliographic data is available via Internet at http://dnb.ddb.de.

D82 (Diss. RWTH Aachen University, 2017)

Als Manuskript gedruckt. Printed in Germany.
ISSN 0178-9503
ISBN 978-3-18-395103-1

Vorwort

Die vorliegende Arbeit entstand während meiner Zeit als wissenschaftlicher Mitarbeiter der Aachener Verfahrenstechnik - Prozesstechnik und Systemverfahrenstechnik der RWTH Aachen. Mein besonderer Dank gilt meinem Doktorvater, Herrn Professor Dr.-Ing. Wolfgang Marquardt, für die Förderung und Unterstützung während dieser Zeit. Ohne seine Begeisterungsfähigkeit und Offenheit wäre diese Arbeit nicht möglich gewesen. Weiterhin danke ich Herrn Professor Dr.-Ing. Hannsjörg Freund für die Übernahme des Koreferats. Zudem danke ich Herrn Professor Dr. rer. nat. Werner Schomburg für die Übernahme des Prüfungsvorsitzes. Herrn Prof. Alexander Mitsos, Ph.D. danke ich für seine Teilnahme als Prüfungsbeisitzer und besonders für seine Unterstützung während meiner Zeit als Mitarbeiter der Aachener Verfahrenstechnik - Systemverfahrenstechnik.

Bei allen Mitarbeitern des Lehrstuhls bedanke ich mich für die freundschaftliche und kollegiale Atmosphäre, in der ich sowohl das Forschen als auch andere gemeinsame Aktivitäten sehr genossen habe. Insbesondere innerhalb der Synthesegruppe war der fachliche Austausch mit Andreas Harwardt, Christian Redepenning und Kirsten und Mirko Skiborowski stets produktiv und hatte einen großen Anteil am Gelingen dieser Arbeit. Vielen Dank für die wunderbare Zeit nicht nur auf der Arbeit, sondern auch abseits des Insitutes. Manuel Dahmen, Christian Redepenning und Kirsten und Mirko Skiborowski danke ich darüber hinaus für das Korrekturlesen dieser Arbeit.

Weiterhin hat die interdisziplinäre Zusammenarbeit im EU-Projekt SYNFLOW mir immer wieder geholfen, über den berühmten Tellerrand hinaus zu schauen und die eigene Forschung zu hinterfragen. Besonderer Dank gilt hierbei den Kollegen Herrn Dr. Charles Gordon, Herrn Dr. Marco Haumann, Frau Dr. Lisa Völk und Frau Olga Walz für ihre Unterstützung.

Ich möchte mich auch bei allen Studenten bedanken die mich während dieser Zeit durch HiWi-Tätigkeiten und studentischen Abschlussarbeiten in meiner Arbeit am Lehrstuhl unterstützt haben. Insbesondere Jannik Burre, Flemming Holtorf und Vinzent Strobel möchte ich an dieser Stelle für ihren Einsatz danken.

Mein größter Dank gilt meinen Eltern, meiner Frau Eva und unserer Tochter Annabelle für ihr Unterstützung und Liebe.

Düsseldorf, im März 2017 *Sebastian Recker*

Contents

Nomenclature

Abbreviations

1-MODE 1-methoxy-2,7-octadiene

3-MODE 3-methoxy-1,7-octadiene

AIC Akaike's information criterion

AR attainable region

CSTR continuous stirred-tank reactor

DSR differential sidestream reactor

ETBE ethyl tert-buthyl ether

EtOH ethanol

FAM feed angle method

G Gibbs free energy

H enthalpy

IB isobutene

IMes 1,3-dimesityl-imidazol-2-ylidene

IMI incremental model identification

LCA life cycle analysis

LP linear program

MeOH methanol

MESH mass, equilibrium, summation and enthalpy

MINLP mixed-integer nonlinear programming

nBa n-butane

NCC nonlinear complementarity constraints

NLP nonlinear programming

NMP N-methylpyrrolidone

OED optimal experiment design

Pd palladium

PFR plug flow reactor

PNFA process network flux analysis

PNFA reaction network flux analysis

RBM rectification body method

ROM reduced-order model

TAC total annualized cost

TON turnover number

TPP triphenylphosphine

TS threefold sulfonated derivative

VLE vapor liquid equilibrium

VRC vapor recompression column

Indices

act active

adJolly adjusted jolly mechnanism

B boil-up

c component

cap capital

Cat catalyst

ci column intervals

cl	clearance
comp	compressor
cs	column shell
D	distillate
dipa	dipalladium-bisally mechnanism
E	entrainer
emp	empirical
f	feed
fp	feed pinch
hx	heat exchanger
i	reaction device
in	inlet
Jolly	jolly mechnanism
k	reaction
KW	cooling water
L	liquid
n	tray
op	operating
out	outlet
pre	precursor
pv	pressure vessel
R	reactor
Raw	raw material
Reac	reaction
Sep	separation

sp	saddle pinch
V	vapor

Symbols

α	angle	$[-]$
α	heat transfer coefficient	$[W/(m^2K)]$
ΔH_R	enthalpy of reaction	$[J/mol]$
η_{comp}	isentropic compression efficiency	$[-]$
κ	isentropic exponent	$[-]$
μ	relaxation parameter	$[-]$
ν	stoichiometric coefficient	$[-]$
Φ	economic potential	[$]
$\boldsymbol{n}$	normal vector	$[-]$
$\boldsymbol{W}$	weighting matrix	$[-]$
A	exchange area	$[m^2]$
B	boil-up molar flow	$[mol/s]$
b	binary decision variable	$[mol/s]$
C	cost	[$]
c	continuous decision variable	$[-]$
c_p	specific heat capacity	$[J/K]$
D	diameter	$[m)]$
D	distillate molar flow	$[mol/s]$
E	entrainer flow rate	$[mol/s]$
E_a	activation energy	$[kJ/mol]$
F	F-factor	$[Pa^0.5]$
F	feed flow rate	$[mol/s]$

f_c	capital charge factor	$[-]$
H	height	$[m]$
H	hold up	$[m^3]$
h	specific enthalpy	$[J/mol]$
k	heat transfer coefficient	$[kW/(m^2K)]$
k	reaction rate constant	$[mol/(m^3s)]$
k_0	pre-exponential factor	$[mol/(m^3s)]$
L	liquid molar flow	$[mol/s]$
M_v	molar volume	$[m^3/kmol]$
MF	module factor	$[-]$
MPF	material pressure factor	$[-]$
N	molar flow	$[mol/s]$
n	column tray	$[-]$
n	reactor element	$[-]$
n_c	number of components	$[-]$
n_i	number of reaction devices	$[-]$
n_t	number of reactor tubes	$[-]$
N_{col}	number of column trays in final design	$[-]$
N_T	number of column trays	$[-]$
p	pressure	$[bar]$
P_{comp}	compressor power duty	$[kW]$
Q	heat stream	$[kW]$
Q_B	reboiler heat duty	$[kW]$
Q_D	condenser heat duty	$[kW]$
R	rate of formation	$[mol/(l\ s)]$

R	reflux molar flow	$[mol/s]$
R_g	ideal gas constant	$[J/(molK)]$
T	temperature	$[K]$
V	vapor molar flow	$[mol/s]$
V	volume	$[m^3]$
v	velocity	$[m/s]$
x	liquid mole fraction	$[-]$
y	vapor mole fraction	$[-]$
z	mole fraction	$[-]$

Abstract

In industrial practice, conceptual process design is typically conducted by repetitive simulation studies, which require detailed design specifications in an early design phase. Guided by heuristics, these iterative solution procedures result in high manual effort and, in addition, no guarantee concerning the quality of the solution can be given. Optimization-based design methods provide a tremendous potential to accelerate and improve conceptual process design.

Various authors have therefore suggested the use of surrogate models, which do not require detailed specifications. Others have developed methods for the optimization-based process design by means of superstructure optimization. Marquardt, Kossack and Kraemer (2008) proposed a framework for an optimization-based design of hybrid separation processes, which combines shortcut and rigorous evaluation steps. This framework has been successfully demonstrated for conceptual design of various processes (see, e.g., Krämer, Harwardt, Bronneberg and Marquardt, 2011).

In this thesis, the process design framework of Marquardt et al. (2008) is extended towards the optimization-based design of reaction-separation processes. For this purpose, powerful shortcut and rigorous evaluation methods for reactor networks and reaction-separation processes are proposed. It is important to emphasize that all of these methods are developed to be computationally efficient in order to allow an optimization-based design and analysis of large-scale processes. As a consequence, cost-optimal process solutions can be obtained with considerably less effort compared to the use of tedious repetitive simulation studies. It also has to be stressed that the performance of all methods is validated by large-scale industrial case studies. Thus, it is shown that the process design framework can contribute decisively towards the sustainable solution of today's challenging design problems in chemical engineering.

Kurzfassung

Die Verknappung fossiler Rohstoffe, steigender Wettbewerbsdruck und die Forderung nach nachhaltiger Produktion treiben die Suche nach effizienteren Produktionsprozessen an. Diese Prozesse werden in einem kreativen Entwurfsprozess entwickelt, wobei heutzutage neue Prozessvarianten häufig anhand von Erfahrungswissen und Heuristiken generiert und anschließend mit Hilfe von Synthesewerkzeugen evaluiert werden. Alternativ bieten optimierungsbasierte Entwurfsmethoden das Potential die Entwicklung neuer, innovativer Prozesse zu unterstützen.

Bei der Optimierung von Reaktions- und Trennprozessen mit rigorosen Modellen entstehen sehr große Gleichungssysteme, die auf Grund ihrer starken Nichtlinearität nur schwer zu lösen sind. Um die Komplexität der Modelle zu reduzieren, können in einem ersten Schritt Näherungsverfahren verwendet werden. Hierdurch kann zunächst die strukturelle Vielfalt der Prozessvarianten reduziert werden. Diese Herangehensweise bietet den Vorteil einer sehr kompakten Formulierung der Optimierungsprobleme. Bei der Optimierung von Reaktions- und Trennverfahren mit Näherungsverfahren werden üblicherweise Gleichgewichtsreaktoren modelliert und das dafür nötige Reaktionsgleichgewicht mit Hilfe thermodynamischer Gleichungen bestimmt. Der optimale Betriebspunkt kann jedoch von diesem Reaktionsgleichgewicht abweichen. Daher wird in dieser Arbeit ein kinetik-basiertes Näherungsverfahren für Reaktornetzwerke vorgestellt, welches das, durch eine Verschaltung beliebiger Reaktortypen, erreichbare Gebiet abbilden kann. Darauf aufbauend wird eine systematische Initialisierung der rigorosen Modelle vorgestellt, mit deren Hilfe die Robustheit und Effizienz der rigorosen Optimierung verbessert werden kann.

Um den Entwurf von katalytischen Prozessen zu unterstützen wird anschließend eine Heuristik für die Generierung von katalytischen Prozessvarianten entwickelt. Diese Heuristik integriert nicht nur die Entscheidungen, die an die Auswahl des Katalysators gekoppelt sind, in den Entwurfsprozess. Sie adressiert auch die für den Entwurfsprozess notwendigen Laborexperimente und dient somit als Forschungswerkzeug zur Planung und Auswertung von Laborversuchen.

Zuletzt werden die Schlussfolgerungen über die Bedeutung und Anwendbarkeit von Näherungsverfahren und rigorosen Optimierungsmethoden für den Entwurf von Reaktions- und Trennprozessen zusammengefasst und offene Fragestellungen abgeleitet.

1 Introduction

1.1 Conceptual design of chemical processes

Depleting natural resources, increasing international competition, and the desire for sustainability foster the chemical industry to pursue more efficient processes. The conceptual design paves the way for the efficiency of a process and is therefore not only one of the most complex, but also one of the most important tasks in the development of a new chemical process. It comprises the selection of suitable unit operations, their combination and interconnection in a general flowsheet structure as well as the rough sizing and costing of equipment. The choices made in this early design stage already set the course for a successful process, as they typically account for about 80% of the final cost of the entire process (Biegler, Grossmann and Westerberg, 1997). While modern commercial process simulators allow the evaluation of complex flowsheets with a multitude of unit operations and recycle streams, new process variants are often generated based on expert-knowledge and heuristics involving problem decomposition. Examples are the hierarchical approach to conceptual design (Douglas, 1988) or the onion model (Smith and Linnhoff, 1988) which pragmatically decompose the design task into subproblems for the reactor network, the separation and recycle system, as well as the heat exchanger network design. These dependent subproblems are consequently assessed in subsequent steps, to reduce complexity in the extremely large design space. Consequently, most of the approaches to conceptual process design deal only with one of these specific subproblems.

A recent database search (Cremaschi, 2015) yielded over 1200 publications in the main areas of reactor network, distillation-based separation systems, and reaction-separation process design with at least a linear increase in the total number of publications over the last two decades (cf. Figure 1.1). However, less than 20% of the contributions deal with the design of reaction-separation processes, since the simultaneous optimization of the design subproblems is still a computationally difficult problem (Kallrath, 2000). In the following, a broad overview on the existing design methods is provided. Hereby, only the key features are outlined, while a more comprehensive presentation of the technical details can be found in the cited literature.

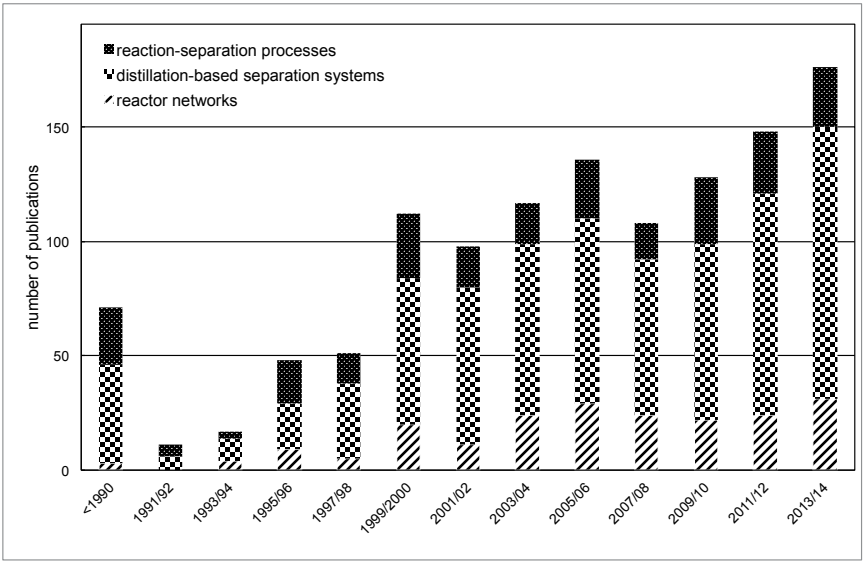

Figure 1.1: Number of process design publications.

1.1.1 Design methods for reactor networks

Existing design methods for reactor networks can be grouped into four main areas: heuristics, attainable region concepts, dynamic optimization, and superstructure optimization. Reactor selection heuristics can be classified into criteria based on experience and model evaluation (Schembecker, Dröge, Westhaus and Simmrock, 1995, Till, Sand, Engell, Schembecker and von Trotha, 2003). In many cases, the heuristics are easy to apply, easy to use, and may result in an appropriate choice of a reactor network for common reaction classes. However, these criteria may hinder the development of innovative reactor concepts and the potential of their application to complex systems is limited.

In order to assess attainable performance targets of arbitrary reactor networks Horn (1964) introduced the concept of attainable regions (AR), a geometrical approach which can be directly used for synthesizing optimal reactor configurations for a given feed and known reaction kinetics. In some appropriately chosen state space the AR refers to the set of all product compositions which can be reached by any possible reactor network employing only reaction and mixing. The boundary of the AR is of special interest, as it represents the maximum achievable product compositions. In fact, any reachable reactor product can be realized by parallel, serial or serial-parallel configurations of plug flow reactors (PFRs) (Feinberg and Hildebrandt, 1997), continuous stirred-tank reactors

(CSTRs) (Feinberg, 2000a), or differential sidestream reactors (DSRs) (Feinberg, 2000b). Since the set of all attainable product compositions is derived graphically, the classical AR approach can only be applied to problems which can be reduced to at most three dimensions (Rooney, Hausberger, Biegler and Glasser, 2000). In order to overcome this limitation, computational techniques were developed to apply the AR concept to higher dimensional problems (Abraham and Feinberg, 2004). Kauchali, Rooney, Biegler, Glasser and Hildebrandt (2002) formulate a linear program (LP) to analyze candidate ARs by discretization of the concentration space into an arbitrarily large number of points. This model represents a large network of completely connected CSTRs which can be used to approximately determine the optimal operating point of arbitrary reactor networks consisting of CSTRs, PFRs and DSRs. However, due to the discretization of the concentration space, the number of equations and variables grows exponentially with the number of components. Thus, problems with more than three components can easily lead to models with thousands of equations and possibly millions of variables (Kauchali et al., 2002). Clearly, modern LP solvers can handle large-scale problems, but reaction processes with a typical, industrially relevant number of raw materials, intermediates, and (by-)products will result in extremely large problems, which scale with the number of chemical components involved.

A different approach of assessing attainable performance targets of reactor networks can be traced back to Denbigh (1944) and has been extended by several authors (see, e.g., Bilous and Amundson, 1956, Aris, 1961, Horn, 1961). It uses the concept of dynamic optimization of an elementary process function (Freund and Sundmacher, 2008). A fluid element is tracked on its way along a (spatially or temporally) resoluted reaction coordinate. During its evolution, the state of the fluid element defined by concentrations, temperature, and pressure can be manipulated by reaction as well as heat and mass fluxes. Thus, an optimal state trajectory of the element in thermodynamic state space can be decided. An analysis of this trajectory provides insight into the choice of promising reactor networks. The technical approximation of the optimal route by an appropriate reactor design can subsequently be addressed by sequentially increasing the level of detail of the reactor models (Peschel, Freund and Sundmacher, 2010). Consequently, this sequential approach can help to develop innovative reactor concepts and does provide detailed information about reactor sizing in the last step.

Optimal sizing information can also be determined by means of superstructure optimization, for which flowsheet structure, operating conditions and equipment sizes are simultaneously optimized. A superstructure for reactor network synthesis is generally composed of a set of pre-defined reactor types, e.g., isothermal (Kokossis and Floudas, 1990) or non-isothermal (Kokossis and Floudas, 1994, Pahor, Kravanja and Iri Bedenik, 2001) CSTRs

and PFRs, or CSTRs and cross flow reactors (Schweiger and Floudas, 1999). In contrast to the AR, the possible connections between the reactors must be specified a priori, though the best connection as well as the existence of the specified reactors are identified as a result of superstructure optimization, where the possible connections between reactors are represented by integer variables in the model. Additionally, the performance characteristics of many reactor networks are similar. For example, a cascade of CSTRs may approximate a PFR very well. Therefore, finding the best combination from a technical and economic point of view can become very difficult. This problem can be addressed by means of simple superstructures, which only include the most promising combinations. However, such simplifications may result in a loss of the optimal reactor network in the superstructure. Hence, modeling for superstructure optimization requires always a trade-off between the number of combinations included in the superstructure, the uniqueness of the solution, and the complexity of solving the resulting mathematical programming problem.

1.1.2 Design methods for distillation-based separation systems

Heuristics also play an important role for the design of separation systems (Siirola and Rudd, 1971, Barnicki and Fair, 1990). Hereby, potential unit operations are selected on the basis of thermodynamic insight, if physical properties of the pure components and the mixture to be separated are available (Jaksland, Gani and Lien, 1995). Available software packages (Kirkwood, Locke and Douglas, 1988, Seuranen, Hurme and Pajula, 2005) which support the design of separation systems try to combine thermodynamic analysis and heuristic rules.

Since distillation is typically the initial choice, especially in the context of bulk chemical or fuel production processes, significant progress has been made towards the design of distillation-based separation systems. For zeotropic mixtures all basic and thermally-coupled configurations can already be derived automatically (Shah and Agrawal, 2010). However, only few publications address the generation of process variants for azeotropic distillation processes, since the inherent distillation boundaries limit the attainable degree of separation. To analyze the feasibility of a distillation sequence, Ryll, Blagov and Hasse (2012) introduced (piecewise) linear approximations of the distillation boundaries and used them for the minimization of the recycle stream in a pre-defined process flowsheet. The authors extended the approach to heterogeneous azeotropic distillation processes (Ryll, Blagov and Hasse, 2014) by integrating another linear approximation approach for the miscibility gap to describe the separation in a decanter (Ryll, Blagov and Hasse, 2013). However, due to the inherent ∞/∞ assumptions (Blagov and Hasse, 2002), this method does not provide any information on column sizes or the required energy demand, while it is also limited to systems with at most four components. Classical shortcut methods

like the Fenske-Underwood-Gilliland method (see, e.g., Doherty and Malone, 2001) can be applied to azeotropic mixtures by treating azeotropes as pseudo components (Liu, Jobson, Smith and Wahnschafft, 2004). However, in order to accurately describe the non-ideality of azeotropic mixtures more rigorous distillation column models need to be utilized. Skiborowski, Harwardt and Marquardt (2014a) present an overview of such methods and their extensions for extractive and heteroazeotropic distillation processes.

Hybrid separation processes should be considered if a separation by distillation alone is not possible or inefficient. A hybrid separation process is defined as the combination of at least two different unit operations, contributing to the same separation task (Franke, Gorak and Strube, 2004). While such processes offer significant potential for improvement, their consideration also extends the design space drastically and thus makes design more challenging. Skiborowski, Harwardt and Marquardt (2013) present a review of available computational methods for the conceptual design of distillation-based hybrid processes for the separation of liquid mixtures.

1.1.3 Design methods for reaction-separation processes

In industrial practice, the structure of a reaction-separation process is often pragmatically fixed using heuristics, known solutions of similar problems, and experience. Common heuristics for reaction-separation processes as, e.g., published by Douglas (1988), Smith and Linnhoff (1988) or Upadhye, Qi and Huber (2011), usually start with the design of a suitable reactor network. Only after finalizing this, the separation and recycle system and, if appropriate, the heat exchanger network are designed in subsequent steps. The feasibility and the cost of the proposed process candidates are then determined by repetitive simulation studies, where the operating points and unit specifications of feasible alternatives are often determined by spreadsheet calculations and rules of thumbs (Luyben, 2010; 2011). Although the decomposition of the design procedure might be necessary to reduce the design space, it might come at the price of missing a superior solution. One important connection, which is interrupted by such a decomposition, is the recycle between the reaction and the separation system. In complex chemical processes optimizing the reaction system with respect to a reaction performance criterium does not necessarily yield the best process-wide solution. High conversion towards the desired product, e.g., can in many reaction systems lead to unfavored side products. These side products can complicate the thermodynamic mixture behavior and may lead to high cost for separation. Therefore, it might be beneficial to decrease the conversion and to recover and recycle the non-converted raw material. Consequently, integrated design of reaction and separation can potentially identify operating points that differ from the individual optimization of the subsystems.

Graphical approaches such as GH-plots (Fox, Hildebrandt, Glasser and Patel, 2013)

can help to facilitate the integrated design of reaction and separation. Enthalpy (H) and Gibbs free energy (G) depicting the flows of heat and work respectively, are determined for all unit processes and are graphically represented as vectors in the GH-space. By manipulating the vectors in the graph, the overall material, energy, and work balances can be determined, before any flowsheet exists. Furthermore, these vectors can be used to construct a flowsheet which represents a thermodynamically efficient process. Based on such an initial flowsheet design, phenomena-based synthesis methods (Ismail, Pistikopoulos and Papalexandri, 1999, Ismail, Proios and Pistikopoulos, 2001, Lutze, Román-Martinez, Woodley and Gani, 2012, Babi, Holtbruegge, Lutze, Gorak, Woodley and Gani, 2015) can be used to derive further process variants. These methods identify the phenomena involved in each task and manipulate and recombine them to generate sustainable and intensified process designs, which include hybrid and/or intensified unit operations.

Another promising approach for generating process variants, which is currently limited to processes without recycles, uses the concept of operating windows (Steimel, Harrmann, Schembecker and Engell, 2013a;b). An operating window is herein defined by a set of intervals describing the feasible ranges of properties in the material streams linking the process units. By considering the operating window of one process unit the corresponding downstream section can be developed, even if the actual design and operating point is not yet fixed. During process synthesis, the operating windows are gradually narrowed until all process units have been fixed and the flowsheet can be evaluated.

To facilitate the design of innovative and economically attractive process concepts, promising variants should be identified in an early design stage to narrow down the usually large number of possible variants and to reduce the effort for rigorous process design. In particular, shortcut methods can be used to determine performance bounds, which can be used to robustify subsequent rigorous optimization. For reaction-separation processes such bounds can be predicted by a steady-state design of a process only involving sharp separations and ideal CSTRs (Feinberg and Ellison, 2001, Feinberg, 2002). Alternatively, bounds can be predicted by optimizing a species-dependent residence time distribution function (Balakrishna and Biegler, 1993, Freund and Sundmacher, 2008), which is similar to the concept of elementary process functions for reactor networks, or by optimization of superstructures consisting of mass exchanger and separation task units (Linke and Kokossis, 2003). Although these process performance bounds can help to understand when no configurative innovation will produce further improvements, they do not allow identifying drawbacks regarding the optimal process structure. Therefore, those methods are more suited as an analysis rather than a design tool.

Shortcut methods for distillation can provide a lower limit on the operational cost of a previously specified separation. In combination with reactor shortcuts they can be used for

a fast screening of the performance of different variants of reaction-separation processes. Ryll et al. (2014) coupled equilibrium and conversion reactor models with the ∞/∞-method for distillation to determine the operating points with minimal recycle flows for all flowsheet candidates. Kossack, Refinius, Brüggemann and Marquardt (2007) coupled Gibbs reactor models with the thermodynamically sound rectification body method (RBM) (Bausa, von Watzdorf and Marquardt, 1998) to estimate an approximate lower bound for operating cost. Hentschel, Peschel, Freund and Sundmacher (2014) combined elementary process functions for the reactor models with the Fenske-Underwood-Gilliland method to optimize total cost of reaction-distillation processes. The utilization of these computationally efficient shortcut methods allows a ranking of possible flowsheet alternatives or even an optimization of flowsheet superstructures, which embed several process variants (Gassner and Maréchal, 2009a;b). However, in the likely case of recycles the change of operating points in any unit will affect the performance of the entire process. Therefore, the simultaneous treatment of kinetically-controlled reactor networks and separators for non-ideal mixtures is desirable. To the authors' knowledge, such methods have not been reported yet. Another drawback of these shortcut methods is that they do not provide information on equipment sizing, which determines the investment cost of the process. Therefore, the optimal trade-off between investment and operating cost cannot be determined.

An optimal equipment design can be computed by optimization of rigorous unit models, for example, by coupling derivative-free optimization algorithms and rigorous process simulators (Gross and Roosen, 1998, Vázquez-Ojeda, Segovia-Hernández, Hernández, Hernández-Aguirre and Kiss, 2013). This approach is limited by the reliability of the process simulator, as the optimization algorithm cannot distinguish between simulator errors due to violated process constraints or convergence failures. Additionally, these derivative-free methods are often unable to find optimal solutions even in the absence of constraints and integer variables when the number of degrees of freedom exceeds about ten, which is already the case for small flowsheets (Rios and Sahinidis, 2013). To leverage the potential of specialized simulation software, surrogate models (also known as reduced-order models (ROMs)) can be trained by rigorous simulation for later use in simulation-based optimization (Caballero and Grossmann, 2008, Fahmi and Cremaschi, 2012). As these models do not make use of physical simplifications, highly accurate surrogate models often have a complex functional form, which is disadvantageous in algebraic optimization, e.g., of reaction-separation processes, where smaller, compact algebraic forms are desirable (Cozad, Sahinidis and Miller, 2014).

In principle all design variables can be directly optimized using mixed-integer nonlinear programming (MINLP) (Kokossis and Floudas, 1991, Smith and Pantelides, 1995, Papalexandri and Pistikopoulos, 1996, Grossmann, Caballero and Yeomans, 1999). There-

fore, the resulting mathematical programming problem has to comprise of a model representing process units that account for all feasible process configurations. Because the resulting problems are difficult to set up and solve (Westerberg, 2004), a systematic procedure is necessary to facilitate the use of deterministic superstructure optimization of entire reaction-separation processes in industrial practice.

Systematic and optimization-based design approaches which facilitate the simultaneous optimization of the design subproblems can increase the efficiency within the conceptual design phase and allow for the development of improved and innovative processes. In order to improve the conceptual design of separation processes, Marquardt, Kossack and Kraemer (2008) and Dowling and Biegler (2015) have proposed process design frameworks for equation-oriented optimization of hybrid separation processes. The systematic and optimization-based framework for the design of hybrid separation processes proposed by Marquardt et al. (2008) has been used and demonstrated for conceptual design of various processes (see, e.g., Krämer, Harwardt, Bronneberg and Marquardt, 2011). This framework combines thermodynamically sound shortcut methods and rigorous mixed-integer nonlinear programming. The design task is separated into three distinctive steps: In the first step, different flowsheet structures are generated. In the second step, these alternative flowsheets are evaluated with shortcut methods to screen for the most promising process alternatives, which are finally modeled rigorously and optimized in the third step to calculate operating point and sizing information and finally to determine the cost-optimal process design. Since a number of alternative flowsheets have already been eliminated, only a few optimization runs are necessary in this final step. The optimization is further improved through an excellent initialization with the results from the shortcut step.

A thorough application of the process design framework requires the availability of reliable and computationally efficient methods for each of the different steps. Within the last 15 years, the process design group at Aachener Verfahrenstechnik - Process Systems Engineering has developed shortcut methods, rigorous optimization methodologies and the previously mentioned process design framework to facilitate a systematic, optimization-based design of (hybrid) separation processes with a focus on distillation. The theses of Bausa (2001), Brüggemann (2005), Urdaneta (2005), and Wallert (2007) focused on the development of shortcut methods for homogeneous and heterogeneous azeotropic, reactive and extractive distillation, as well as hybrid processes where distillation is supplemented by crystallization. Kossack (2010) and Krämer (2012) extended the scope to combine shortcut methods with rigorous optimization of single columns, column networks and hybrid separation processes. Harwardt (2013) extended the developed optimization-based design methods to account for the new challenges of separations for processing of biorenewables and included the subproblem of heat integration into the design framework. Most recently,

Skiborowski (2015) further improved the existing methods and proposed novel computational approaches to support the design process and to ease the application of optimization-based design methods especially for the separation of heterogeneous mixtures and hybrid separation processes.

1.2 Aim and structure of this thesis

While the process design framework is in principle applicable to all kinds of processes, its application was until now restricted to separation processes only. The optimization-based design of reaction-separation processes did not get appropriate attention, due to the size and complexity of these problems. Several nonlinear reaction and separation unit models embedded in a flowsheet, recycle loops that have to be optimized, and nonlinearities of the underlying non-ideal thermodynamic and reaction kinetic models complicate numerical evaluation and require an extension of the framework. This thesis addresses these limitations and proposes a systematic procedure for the optimization-based design of reaction-separation processes. Chapter 2 presents extensions to the framework of Marquardt et al. (2008) to account for the systematic design of reaction-separation processes. The necessary extensions of both, the shortcut evaluation methodology for the pre-selection of flowsheets and the rigorous optimization procedure integrate existing and new approaches. While shortcut tools for separation processes are already routinely utilized, commonly used reactor shortcuts are limited because the achievable product compositions are restricted to chemical equilibrium (Ismail et al., 2001). However, optimal reaction-separation processes might not operate at the limiting points of chemical equilibrium and therefore a kinetically controlled reactor shortcut is presented. The application of the framework is illustrated in this chapter with two academic case studies based on literature data and specifications. One bottleneck of this framework is the generation of alternative flowsheet variants which is still based on heuristics and expert knowledge. This is especially a limitation for catalytic processes, since the selection of an appropriate catalyst is not addressed by common heuristics. To overcome this limitation, a systematic design procedure for the generation of variants for catalytic processes is presented in Chapter 3. Within this systematic design procedure, laboratory experiments are integrated to identify the necessary reaction kinetic models and to facilitate the finding of innovative catalytic processes. Subsequently, Chapter 4 investigates the conceptual design of a novel catalytic process for butadiene telomerization. Hereby, the systematic procedure for the generation of variants presented in Chapter 3 as well as the optimization-based methods presented in Chapter 2 are utilized to design a novel process for this industrially relevant reaction. This industrial case studies emphasizes how the tools and methods presented in this thesis facilitates the con-

ceptual design of chemical processes from kinetic investigations to flowsheet optimization. Finally, Chapter 5 gives a summary of this thesis and provides an overview of the identified strengths and weaknesses in the design methodology for reaction-separation processes.

1.3 Previous publication of results

This thesis originates from the research performed by the author at Aachener Verfahrenstechnik - Process Systems Engineering. Most results are in preparation for publication or have already been published. The following list gives an overview on the results that have been already published:

- The content of Chapter 2 has to some extent been published in *Computers & Chemical Engineering* (Recker, Skiborowski, Redepenning and Marquardt, 2015) and *Computer Aided Chemical Engineering* (Recker and Marquardt, 2012, Recker, Skiborowski, Redepenning and Marquardt, 2014).
- The contents of Chapters 3 and 4 have to some extent been published in *Journal of Catalysis* (Völkl, Recker, Niedermaier, Kiermaier, Strobel, Maschmeyer, Cole-Hamilton, Marquardt, Haumann and Wasserscheid, 2015).

Additional contributions were made to other collaborative research projects that are not covered by this thesis, in particular:

- An overview on a systematic sequential and iterative model-based design strategy, which argues for a paradigm shift to properly address the requirements of model-based design of future bio-based value chains (Marquardt, Harwardt, Recker, Viell and Voll, 2012).
- A first idea on the integration of model identification and process optimization (Recker, Kerimoglu, Harwardt, Tkacheva and Marquardt, 2013). Rather than decoupling model identification and process optimization, information from process optimization are used to design optimal experiments for improving the quality of the kinetic model given the intended use of the model. The Fisher Information Matrix is heuristically modified such that sensitivities, which describe the influence of parametric uncertainties on the economic objective used in process optimization, are utilized as weights for optimal experimental design.
- A pinch-based shortcut method for the performance screening of isothermal extraction columns which allows the automated screening of more than 3,500 solvents within one hour computational time (Redepenning, Recker and Marquardt, 2016).

2 A unifying framework for conceptual process design

The current interest in the development of more efficient processes has drawn attention towards the optimization-based design of reaction-separation processes. The limitations of available design methods can be overcome by an adequate combination of different methods in a systematic design framework. It extends the design framework for separation processes of Marquardt et al. (2008) by including the degrees of freedom related to reactor networks and to the interconnection of reaction and separation units in a flowsheet. It aims at the simultaneous optimization of the flowsheet structure, the unit specifications and the operating points of integrated reaction-separation processes. Certainly, the simultaneous inclusion of all possible design options into an automated framework is highly desirable but quickly leads to combinatorial explosion. In combination with non-linear models used to describe the reaction, mass and heat transfer phenomena that occur in the processing units, the resulting synthesis problem is beyond the scope of existing optimization technology, even for relative small problems. Therefore, a hierarchical procedure to guide the decision-making process of conceptual process design is proposed in this chapter and illustrated in Figure 2.1. In a first step of the procedure, possible process variants are generated. They are then evaluated by means of shortcut calculations in a second step. Consequently, the results are used for an efficient initialization of the rigorous optimization models. To account for the non-ideal behavior of the mixtures involved and the multiple recycles, the reaction and separation units are optimized simultaneously, since variations in the performance of any unit will affect the performance of the whole process. The process design framework as a procedure of incremental refinement and successive initialization allows for a hierarchical synthesis of the cost optimal process, while taking into account multiple flowsheet alternatives.

Although the workflow suggested by the design framework appears to be linear in nature, it is important to note that each of the steps involves synergetic input across the other steps of the framework. The intention is that by using the framework the development team will start their research on a selection of initial process options which are evaluated by shortcut methods. The result of the shortcut evaluation will be a ranking of the initial flowsheet

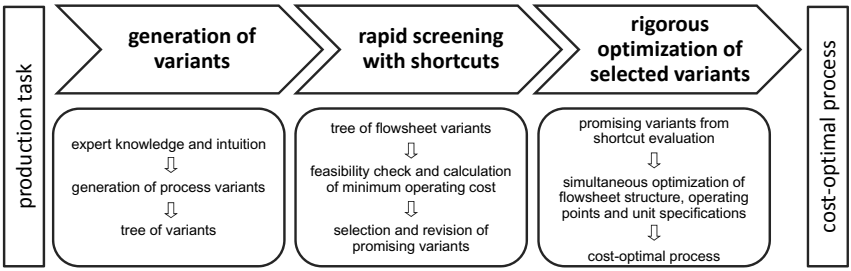

Figure 2.1: Framework for the systematic design of reaction-separation processes.

candidates based on their minimum operating cost. Based on this ranking some of the flowsheet candidates can be discarded. An analysis of the shortcut results indicates where further process improvements might be useful and additional variants can be generated and evaluated based on the shortcuts. After all generated variants are screened and ordered according to the results of the shortcut screening, the cost-optimal production process can be identified by rigorous optimization of the promising variants. The necessary tools, which are employed in the various steps of the design framework, are described in the following.

2.1 Variant generation

In the first step of the proposed framework, possible flowsheet alternatives for the desired production task are generated. For reactor networks (cf. Section 1.1.1) or for zeotropic multicomponent distillation with simple columns (cf. Section 1.1.2) the generation of flowsheets can be automated. However, for reaction-separation processes, we still need to create flowsheet alternatives manually based on heuristics and expert knowledge because, to date, no examples of generally applicable automatic flowsheet generation procedures are known from the literature. As mentioned in Section 1.1.3, phenomena-based synthesis methods (Lutze et al., 2012, Babi et al., 2015) or methods based on the concept of operating windows (Steimel et al., 2013a;b) can help to overcome this limitation, but are not automatically applicable to general reaction-separation processes yet.

2.2 Optimization with shortcut models

Considering the large number of possible process candidates, it is clear that not all possible flowsheet alternatives can be covered by simulation studies or rigorous optimization in case of complex processes. The framework therefore relies on shortcut tools to calculate the

minimum operating cost of each process and to determine a few economically attractive flowsheet designs. While shortcut tools for separation processes are already routinely utilized, commonly used reactor shortcuts such as Gibbs reactors are of limited use because the achievable product compositions are restricted to chemical equilibrium (Ismail et al., 2001). However, optimal reaction-separation processes might not operate at the limiting points of chemical equilibrium. Especially in case of parallel or consecutive reactions reaching chemical equilibrium might be unfavorable. In fact, processes involving catalytic reactions often operate far away from chemical equilibrium, since catalyst cost are an important economic factor. Also reaction hold-up and residence time might be restricted due to economic or safety reasons. Therefore, integrated reaction-separation processes cannot be properly assessed during the early stages of design, because powerful shortcut methods for kinetically controlled reactor networks are still lacking. Consequently, a novel shortcut method for reactor networks is necessary, which allows the optimization of integrated reaction-separation processes.

2.2.1 Reactor shortcut

As introduced by Feinberg and Ellison (2001), arbitrary reactor networks can be represented by a network of completely connected ideally mixed reaction devices. However, the exponential growth of the number of variables and equations of the LP problem introduced by Kauchali et al. (2002) permits the application to systems of relevant size. The explosion of the problem size can however be avoided, if the problem is formulated without the discretization of the concentration space as sketched in Figure 2.2. Here a state-space representation is used to formulate the reactor network consisting of an arbitrary connection of reaction devices of arbitrary volume. The mathematical model is an NLP which is further described in the following.

The inlet stream to the reactor network N_0 is split into the bypass stream $N_{0,out}$ and the streams $N_{0,i}$ entering n_i reaction devices. The mole balance reads as

$$0 = N_0 - N_{0,out} - \sum_{i=1}^{n_i} N_{0,i}. \tag{2.1}$$

The outlet stream N_{out} consists of the bypass stream and the streams $N_{i,out}$ leaving the devices. The mole balance reads as

$$0 = N_{out} - N_{0,out} - \sum_{i=1}^{n_i} N_{i,out}. \tag{2.2}$$

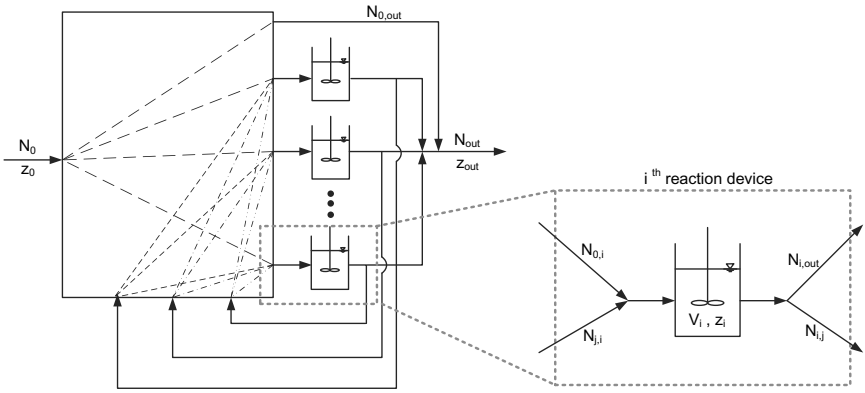

Figure 2.2: State-space representation of the superstructure formulation of the reactor network model.

Furthermore, the mole fraction of the outlet flow for component c ($z_{out,c}$) is related to the mole fraction of the inlet flow $z_{0,c}$ and the mole fraction inside the devices $z_{i,c}$ by

$$0 = N_{out} z_{out,c} - N_{0,out} z_{0,c} - \sum_{i=1}^{n_i} N_{i,out} z_{i,c}, \qquad c = 1, \ldots, n_c. \tag{2.3}$$

The outlet streams leaving the ideally mixed reaction devices are calculated from

$$0 = \left(N_{i,out} + \sum_{j=1}^{n_i} N_{i,j} \right) - \left(N_{0,i} + \sum_{j=1}^{n_i} N_{j,i} \right) - V_i \sum_{c=1}^{n_c} \sum_{k=1}^{n_R} R_{k,c}, \qquad i = 1, \ldots, n_i, \tag{2.4}$$

where $N_{i,j}$ represents the stream leaving device i and entering device j. V_i is the device volume, and $R_{k,c}$ indicates the rate of formation k for component c. Thus, the equations for the mole fractions read as

$$0 = \left(N_{i,out} + \sum_{j=1}^{n_i} N_{i,j} \right) z_{i,c} - \left(N_{0,i} z_{0,c} + \sum_{j=1}^{n_i} N_{j,i} z_{j,c} \right) - V_i \sum_{k=1}^{n_R} R_{k,c}, \qquad c = 1, \ldots, n_c, \quad i = 1, \ldots, n_i. \tag{2.5}$$

The number of equations describing this reactor model is $(n_i + 1)n_c + 2 + n_i$. It therefore

scales linearly with the number of components n_c and the number of reaction devices n_i. As only few reaction devices are needed to approximate most reactor systems (Feinberg and Ellison, 2001), the NLP embedding this reactor model is capable to approximate the optimal operating point for industrially reactor networks. This way, a synthesis method can be devised at the expense of replacing the LP problem of Kauchali et al. (2002) by an NLP problem. Moreover, an analysis of the optimal device connectivity also allows to deduce the optimal reactor system. If, e.g., all devices are of similar volume and arranged in a sequence, a tubular reactor may be used.

The degrees of freedom of this reactor shortcut model comprise the streams entering the devices $N_{0,i}$, the interconnecting streams between the devices $N_{i,j}$, as well as the device volumes V_i and, if appropriate, the device temperatures T_i. Following the CSTR equivalence principle (Feinberg and Ellison, 2001) $s+1$ devices should be sufficient for the calculations, with s being the rank of the underlying network of chemical reactions. In this work, ten devices found to be sufficient for all calculations.

2.2.2 Separation shortcut

The reactor shortcut model forms the core of a shortcut evaluation of integrated reaction-separation processes. Together with established shortcut models for separation units it forms the basis for a shortcut-based optimization of an integrated reaction-separation process. In this work, the feed angle method (FAM), which has been proposed by Krämer et al. (2011), is utilized as shortcut model for distillation columns. This pinch-based method does not rely on numerous tray-to-tray calculations and can be applied to ideal mixtures as well as homogeneous and heterogeneous azeotropic distillation columns. In this thesis, all separations are feed pinch controlled. For homogeneous mixtures with more than three components therefore a hyperplane defined by the feed pinch (fp) and the relevant saddle pinches (sp) is constructed by means of the normal vector $\boldsymbol{n}_{sp,fp}$. Assuming that the feed pinch is located in the stripping section, the saddle pinches are specified by the equations for a balance envelope around the rectifying section:

$$0 = V_{sp} - L_{sp} - D, \tag{2.6}$$

$$0 = V_{sp} y_{sp,c} - L_{sp} x_{sp,c} - D x_{D,c}, \quad c = 1, \ldots, n_c - 1, \tag{2.7}$$

$$0 = V_{sp} h_{V,sp} - L_{sp} h_{L,sp} - D h_D + Q_D, \tag{2.8}$$

$$1 = \sum_{c=1}^{n_c} x_{sp,c}, \quad 1 = \sum_{c=1}^{n_c} y_{sp,c}, \tag{2.9}$$

$$y_{sp,c} = K_{sp,c}(\boldsymbol{x}_{sp}, T_{sp}, p)x_{sp,c}, \quad c = 1, \ldots, n_c - 1, \tag{2.10}$$
$$h_{V,sp} = h_V(\boldsymbol{x}_{sp}, T_{sp}, p), \tag{2.11}$$
$$h_{L,sp} = h_L(\boldsymbol{x}_{sp}, T_{sp}, p), \tag{2.12}$$

where L_n, $\boldsymbol{x}_n$, $h_{L,n}$ and V_n, $\boldsymbol{y}_n$, $h_{V,n}$ represent the total flow rate, composition and enthalpy for the liquid phase and the vapor phase on tray n. D, $\boldsymbol{x}_D$ and h_D are the flow rate, composition and enthalpy of the distillate stream and Q_D the energy demand of the condenser. Accordingly, the feed pinch is specified by the equations for a balance envelope around the stripping section:

$$0 = L_{fp} - V_{fp} - B, \tag{2.13}$$
$$0 = L_{fp}x_{fp,c} - V_{fp}y_{fp,c} - Bx_{B,c}, \quad c = 1, \ldots, n_c - 1, \tag{2.14}$$
$$0 = L_{fp}h_{L,fp} - V_{fp}h_{V,fp} - Bh_B + Q_B, \tag{2.15}$$
$$1 = \sum_{c=1}^{n_c} x_{fp,c}, \quad 1 = \sum_{c=1}^{n_c} y_{fp,c}, \tag{2.16}$$
$$y_{fp,c} = K_{fp,c}(\boldsymbol{x}_{fp}, T_{fp}, p)x_{fp,c}, \quad c = 1, \ldots, n_c - 1, \tag{2.17}$$
$$h_{V,fp} = h_V(\boldsymbol{y}_{fp}, T_{fp}, p), \tag{2.18}$$
$$h_{L,fp} = h_L(\boldsymbol{x}_{fp}, T_{fp}, p), \tag{2.19}$$

where B, $\boldsymbol{x}_B$ and h_b are the flow rate, composition and enthalpy of the boil-up stream and Q_B the energy demand of the reboiler. The angle α between the line connecting the feed pinch with the tray above the feed pinch and the hyperplane is consequently given by

$$\cos(\alpha) = \frac{\boldsymbol{n}_{sp,fp}^T(\boldsymbol{x}_{n_f-1} - \boldsymbol{x}_{fp})}{||\boldsymbol{n}_{sp,fp}||_2 \; ||\boldsymbol{x}_{n_f-1} - \boldsymbol{x}_{fp}||_2}, \tag{2.20}$$

whereby the stage above the feed tray is specified by

$$0 = V_{n_F} - L_{n_F-1} - D, \tag{2.21}$$
$$0 = V_{n_F}y_{n_F,c} - L_{n_F-1}x_{n_F-1,c} - Dx_{D,c}, \quad c = 1, \ldots, n_c - 1, \tag{2.22}$$
$$0 = V_{N_F}h_{V,n_F} - L_{n_F-1}h_{L,n_F-1} - Dh_D + Q_D, \tag{2.23}$$
$$1 = \sum_{c=1}^{n_c} x_{n_F-1,c}, \quad 1 = \sum_{c=1}^{n_c} y_{n_F-1,c}, \tag{2.24}$$
$$y_{n_F-1,c} = K_{n_F-1,c}(\boldsymbol{x}_{n_F-1}, T_{n_F-1}, p)x_{n_F-1,c}, \quad c = 1, \ldots, n_c - 1, \tag{2.25}$$
$$h_{V,n_F-1} = h_V(\boldsymbol{y}_{n_F-1}, T_{n_F-1}, p), \tag{2.26}$$
$$h_{L,n_F-1} = h_L(\boldsymbol{x}_{n_F-1}, T_{n_F-1}, p). \tag{2.27}$$

When the tray is located in the hyperplane, the normal vector is perpendicular to the line connecting the feed pinch and the tray such that $\cos(\alpha)$ becomes zero. Consequently, this model allows to approximate the situation of minimum energy demand of a distillation column by demanding that

$$cos(\alpha) \leq \epsilon \tag{2.28}$$

for a sufficient small ϵ.

In this work, an improved formulation of the FAM (Skiborowski, 2015) is used. Instead of setting an angle between two composition vectors numerically to zero, the novel FAM formulation utilizes a linear dependency of several composition vectors to describe the situation of minimum energy demand. Hence, this novel formulation avoids the highly nonlinear equation for calculation of the vector norm required for the original angle criteria.

The FAM determines minimum energy demand and requires full specification of outlet compositions and flow rates. This allows the aggregation of this model with the NLP reactor shortcut to one NLP problem for optimization of a complete reaction-separation process.

2.2.3 Solution procedure

In order to optimize a complete reaction-separation process comprising several units, the models for the reaction and separation units are connected by streams with variable flow rates and compositions. The degrees of freedom are only increased by the number of split factors of occurring purge streams and the flow rates of the process feeds. As mentioned before, the FAM can be integrated into the flowsheet for the optimization of an entire reaction-separation process. However, due to the strong nonlinearities of the underlying equation system, the FAM requires the specification of the pinch topology and an initialization of the relevant pinch points. In contrast to shortcut evaluations of separation processes, where often simple mass balances are sufficient to initialize the unit models, the treatment of integrated reaction-separation processes requires a more advanced initialization to provide the required information on the pinch points for the FAM. Therefore, we initialize the shortcut optimization model with simple splitters and fixed energy demands. After each initialization step, a rigorous search for pinch points using the RBM (Bausa et al., 1998) is performed. The energy demands for the splitters are updated until the change is small enough such that the pinch topologies of the separation systems do not change. These preparatory calculations are in this work executed manually, but can in principle be automated. Afterwards, the optimization of the entire reaction-separation process can be performed with the aforementioned shortcut models, including the FAM.

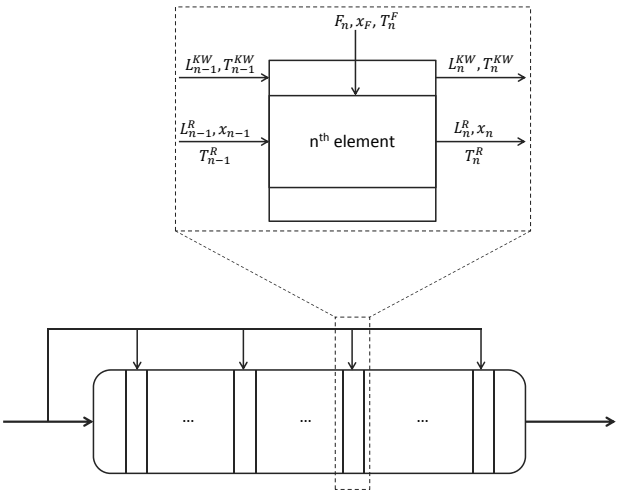

Figure 2.3: Discretized multi-tube DSR element

2.3 Optimization with rigorous models

The evaluation of a reaction-separation process with shortcut models provides a good approximation of the performance potential of a process variant enabling a comparison of different process flowsheets with respect to operating cost. However, no conclusions can be drawn regarding optimal equipment sizing and capital cost. This information can only be gained by a rigorous optimization of the entire process with an economic objective function and more detailed unit models. In the following, the rigorous models for multi-tube differential sidestream reactors, continuous stirred-tank reactors as well as distillation columns used in this thesis are presented.

2.3.1 Multi-tube differential sidestream reactor

The rigorous optimization model for a multi-tube differential sidestream reactor (DSR) comprises of mole and energy balances for finite volume elements of a reactor tube (cf. Figure 2.3). In this work, a Radau-II collocation model with three stages is used for disrcetization. The collocation method subdivides each finite reactor element into three collocation points (Carey and Finlayson, 1975). The collocation method constructs a polynomial for which the differential equations for mass (or more precise mole) and energy are satisfied at the initial and at each collocation point. The weighting matrix

$$\boldsymbol{W} = \begin{pmatrix} \frac{88-7\sqrt{6}}{360} & \frac{296-169\sqrt{6}}{1800} & \frac{-2+3\sqrt{6}}{225} \\ \frac{296+169\sqrt{6}}{1800} & \frac{88+7\sqrt{6}}{360} & \frac{-2-3\sqrt{6}}{225} \\ \frac{16-\sqrt{6}}{36} & \frac{16+\sqrt{6}}{36} & \frac{1}{9} \end{pmatrix} \tag{2.29}$$

results from the specific distribution of the collocation points (Deuflhard and Bornemann, 1994). Total mole balances for the first element of a reactor are given by

$$\begin{pmatrix} L^R_{1,1} \\ L^R_{2,1} \\ L^R_{3,1} \end{pmatrix} = \begin{pmatrix} \frac{F_1}{n_t} \\ \frac{F_1}{n_t} \\ \frac{F_1}{n_t} \end{pmatrix} + V_1 \cdot \boldsymbol{W} \cdot \sum_{c=1}^{n_c} \begin{pmatrix} R_{1,1,c} \\ R_{2,1,c} \\ R_{3,1,c} \end{pmatrix} \tag{2.30}$$

and for the other elements by

$$\begin{pmatrix} L^R_{1,n} \\ L^R_{2,n} \\ L^R_{3,n} \end{pmatrix} = \begin{pmatrix} L^R_{3,n-1} + \frac{F_n}{n_t} \\ L^R_{3,n-1} + \frac{F_n}{n_t} \\ L^R_{3,n-1} + \frac{F_n}{n_t} \end{pmatrix} + V_n \cdot \boldsymbol{W} \cdot \sum_{c=1}^{n_c} \begin{pmatrix} R_{1,n,c} \\ R_{2,n,c} \\ R_{3,n,c} \end{pmatrix}, \qquad n = 2, \ldots, N_{max}. \tag{2.31}$$

These balances include the distribution of the feed $F = \sum_{n=1}^{N_{max}} F_n$ with mole fraction x_c^F into the n_t reactor tubes. Component mole balances for the first element are given by

$$\begin{pmatrix} L^R_{1,1} x_{1,1,c} \\ L^R_{2,1} x_{2,1,c} \\ L^R_{3,1} x_{3,1,c} \end{pmatrix} = \begin{pmatrix} \frac{F_1}{n_t} x_c^F \\ \frac{F_1}{n_t} x_c^F \\ \frac{F_1}{n_t} x_c^F \end{pmatrix} + V_1 \cdot \boldsymbol{W} \cdot \begin{pmatrix} R_{1,1,c} \\ R_{2,1,c} \\ R_{3,1,c} \end{pmatrix}, \qquad c = 1, \ldots, n_c \tag{2.32}$$

and for the other elements by

$$\begin{pmatrix} L^R_{1,n} x_{1,n,c} \\ L^R_{2,n} x_{2,n,c} \\ L^R_{3,n} x_{3,n,c} \end{pmatrix} = \begin{pmatrix} L^R_{3,n-1} x_{3,n-1,c} + \frac{F_n}{n_t} x_c^F \\ L^R_{3,n-1} x_{3,n-1,c} + \frac{F_n}{n_t} x_c^F \\ L^R_{3,n-1} x_{3,n-1,c} + \frac{F_n}{n_t} x_c^F \end{pmatrix} + V_n \cdot \boldsymbol{W} \cdot \begin{pmatrix} R_{1,n,c} \\ R_{2,n,c} \\ R_{3,n,c} \end{pmatrix},$$
$$c = 1, \ldots, n_c, \quad n = 2, \ldots, N_{max}. \tag{2.33}$$

Hereby, V_n is the element's volume and $R_{n,c} = R(x_{n,c})$ is the rate of formation for component c. L_n^R is the flowrate of the liquid phase leaving element n with concentration $x_{n,c}$. The outlet temperature of the volume element T_n^R results from the energy balance for the reactants which is for the first reactor element given by

$$\begin{pmatrix} L^R_{1,1} h_{1,1} \\ L^R_{2,1} h_{2,1} \\ L^R_{3,1} h_{3,1} \end{pmatrix} = \begin{pmatrix} \frac{F_1}{n_t} h^F \\ \frac{F_1}{n_t} h^F \\ \frac{F_1}{n_t} h^F \end{pmatrix} + \alpha A_1^J \cdot \boldsymbol{W} \cdot \begin{pmatrix} T^{KW}_{1,1} - T^R_{1,1} \\ T^{KW}_{2,1} - T^R_{2,1} \\ T^{KW}_{3,1} - T^R_{3,1} \end{pmatrix} + V_1 \cdot \boldsymbol{W} \cdot \sum_{c=1}^{n_c} \Delta H_{R,c} \begin{pmatrix} R_{1,1,c} \\ R_{2,1,c} \\ R_{3,1,c} \end{pmatrix} \tag{2.34}$$

and for the other elements by

$$\begin{pmatrix} L^R_{1,n}h_{1,n} \\ L^R_{2,n}h_{2,n} \\ L^R_{3,n}h_{3,n} \end{pmatrix} = \begin{pmatrix} L^R_{3,n-1}h_{3,n-1} + \frac{F_n}{n_t}h^F \\ L^R_{3,n-1}h_{3,n-1} + \frac{F_n}{n_t}h^F \\ L^R_{3,n-1}h_{3,n-1} + \frac{F_n}{n_t}h^F \end{pmatrix} + \alpha A^J_n \cdot \boldsymbol{W} \cdot \begin{pmatrix} T^{KW}_{1,n} - T^R_{1,n} \\ T^{KW}_{2,n} - T^R_{2,n} \\ T^{KW}_{3,n} - T^R_{3,n} \end{pmatrix}$$
$$+ V_n \cdot \boldsymbol{W} \cdot \sum_{c=1}^{n_c} \Delta H_{R,c} \begin{pmatrix} R_{1,n,c} \\ R_{2,n,c} \\ R_{3,n,c} \end{pmatrix}, n = 2, \ldots, N_{max}. \tag{2.35}$$

The equations for the cooling water temperature read as

$$0 = \frac{F^{KW}}{n_t} c_p^{KW} \begin{pmatrix} T^{KW}_{1,1} - T^{KW}_F \\ T^{KW}_{2,1} - T^{KW}_F \\ T^{KW}_{3,1} - T^{KW}_F \end{pmatrix} - \alpha A^J_1 \cdot \boldsymbol{W} \cdot \begin{pmatrix} T^{KW}_{1,1} - T^R_{1,1} \\ T^{KW}_{2,1} - T^R_{2,1} \\ T^{KW}_{3,1} - T^R_{3,1} \end{pmatrix}, \tag{2.36}$$

$$0 = \frac{F^{KW}}{n_t} c_p^{KW} \begin{pmatrix} T^{KW}_{1,n} - T^{KW}_{3,n-1} \\ T^{KW}_{2,n} - T^{KW}_{3,n-1} \\ T^{KW}_{3,n} - T^{KW}_{3,n-1} \end{pmatrix} - \alpha A^J_n \cdot \boldsymbol{W} \cdot \begin{pmatrix} T^{KW}_{1,n} - T^R_{1,n} \\ T^{KW}_{2,n} - T^R_{2,n} \\ T^{KW}_{3,n} - T^R_{3,n} \end{pmatrix}, \qquad n = 2, \ldots, N_{max}. \tag{2.37}$$

α represents the heat transfer coefficient, A^J_n the reactor jacket area and $\Delta H_{R,c}$ the heat of reaction. Neglecting the heat of mixing, the enthalpy h_n is calculated by

$$h_n = h(x_{n,c}, T_n) = \sum_{c=1}^{n_c} x_{n,c} \int_{T_o}^{T_n} c_{p,c}\, dt \tag{2.38}$$

with

$$\int_{T_o}^{T_n} c_{p,c}\, dt = K_{1,c}(T_n - T_0) + K_{2,c}\frac{T_n^2 - T_0^2}{2} + K_{3,c}\frac{T_n^3 - T_0^3}{3}$$
$$+ K_{4,c}\frac{T_n^4 - T_0^4}{4} + K_{5,c}\frac{T_n^5 - T_0^5}{5} \tag{2.39}$$

and the coefficients $K_{1,c} - K_{5,c}$. The constraint

$$v_R = \frac{F M_v}{n_t \frac{\Pi D^2}{4}} \geq 0.5 \frac{m}{s} \tag{2.40}$$

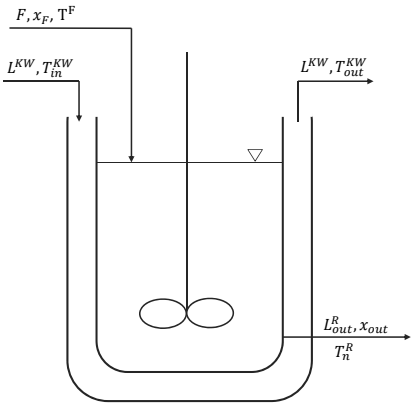

Figure 2.4: CSTR reactor

ensures a minimal velocity v_R of the reaction mixture to prevent back-mixing in the reactor (Hagen, 2004). M_v denotes the molar volume of the feed and D the diameter of each tube. If the sidestreams F_n, for $n = 2, \ldots, N_{max}$, are set to zero this model reduces to a PFR.

Throughout this thesis the cost correlations presented by Guthrie (1969) have been utilized. The utilization of these non-linear cost model allows a direct implementation into the rigorous optimization problem. The cost correlations are non-linear functions of performance relevant properties and include the aspect of economy of scale. The cost correlations provide the base cost in US-$ with 1969 purchasing power, which is updated by the Marshall and Swift index. The Marshall and Swift index $MS-index_{today}$ is set to 1536.5. Material and pressure correction factors MPF are used to account for operating conditions, construction materials beyond carbon steel and other design options for the equipment. The module factor MF accounts for installation of the equipment including piping and process control. According to Guthrie (1969), the capital cost for the reactor can be determined by

$$C_{cap} = \frac{MS-index_{today}}{MS-index_{1969}} \$5000 \left(\frac{A^J n_R[ft^2]}{400 ft^2} \right)^{0.64} (MPF + MF - 1) \tag{2.41}$$

The material pressure factor MPF is 3.14 for a fixed-bed reactor, the module factor MF is 3.6.

2.3.2 Continuous stirred-tank reactor

A CSTR can be modeled as sketched in Figure 2.4. Component mole balances are given by

$$0 = L^R_{out} x_{out,c} - F x^F_c + V_R R_c, \qquad c = 1, \ldots, n_c \tag{2.42}$$

and the total mole balance by

$$0 = L^R_{out} - F + V_R \sum_{c=1}^{n_c} R_c. \tag{2.43}$$

The outlet temperature of the reactor results from the energy balance

$$0 = L^R_{out} h^R_{out} - F h^F + \alpha A^J (T^{KW}_{out} - T^R_{out}) + V \sum_c R_c \Delta H_{R,c} \tag{2.44}$$

with reactor volume V. Similarly, the outlet cooling water temperature T^{KW}_{out} is computed from

$$0 = L^{KW} c^{KW}_p (T^{KW}_{out} - T^{KW}_{in}) - \alpha A^J (T^{KW}_{out} - T^R_{out}). \tag{2.45}$$

The capital cost for a CSTR is determined by the diameter D_{CSTR} and the height H_{CSTR}. They consist of the cost for a pressure vessel C_{pv}

$$C_{pv} = \frac{MS-index_{today}}{MS-index_{1969}} \$1000 \left(\frac{D_{CSTR}[ft]}{3ft}\right)^{1.05} \left(\frac{H_{CSTR}[ft]}{4ft}\right)^{0.81} (MPF + MF - 1) \tag{2.46}$$

with material and pressure correction factor $MPF = 2.25$ and the module factor $MF = 4.23$ and the cost for a shell-and-tube heat exchanger

$$C_{hx} = \frac{MS-index_{today}}{MS-index_{1969}} \$5000 \left(\frac{\pi D_{CSTR}[ft] H_{CSTR}[ft]}{400 ft^2}\right)^{0.77} (MPF + MF - 1) \tag{2.47}$$

with pressure correction factor $MPF = 3.75$ and module factor $MF = 3.29$.

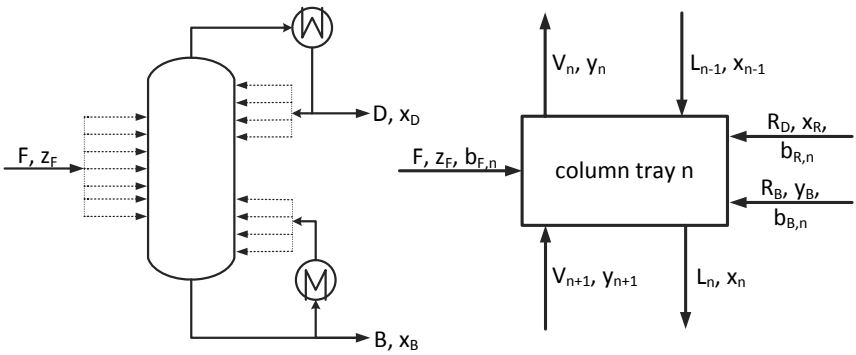

Figure 2.5: Superstructure for a simple distillation column (left) and balance envelope for a general column tray (right).

2.3.3 Simple distillation column

The superstructure for a simple distillation column is based on the model presented by Krämer, Kossack and Marquardt (2009) and is illustrated in Figure 2.5. Hereby, the number of equilibrium trays in the rectifying and stripping sections are optimized by the variable location of the feed tray and the reflux and boil-up location.

Equilibrium tray model

Each equilibrium tray is described by the **m**ass, **e**quilibrium, **s**ummation and ent**h**alpy (MESH) equations. Mass (or more precise component mole) and energy balances for each column tray n are given by

$$\begin{aligned} L_n x_{n,c} + V_n y_{n,c} = L_{n-1} x_{n-1,c} + V_{n+1} y_{n+1,c} + F z_{F,i} b_{F,n} \\ + R_D x_{R,c} b_{R,n} + R_B y_{B,c} b_{B,n}, \quad c = 1, ..., n_c, \end{aligned} \tag{2.48}$$

and

$$\begin{aligned} L_n h_{L,n} + V_n h_{V,n} = L_{n-1} h_{L,n-1} + V_{n+1} h_{V,n+1} + F h_F b_{F,n} \\ + R_D h_{L,R} b_{R,n} + R_B h_{V,B} b_{B,n}, \end{aligned} \tag{2.49}$$

where L_n, $\boldsymbol{x}_n$, $h_{L,n}$ and V_n, $\boldsymbol{y}_n$, $h_{V,n}$ represent the total flow rate, composition and enthalpy for the liquid phase and the vapor phase on the tray. F, R_D, R_B, $\boldsymbol{z}_F$, $\boldsymbol{x}_R$, $\boldsymbol{y}_B$ and h_F, $h_{L,R}$, $h_{V,B}$ are the flow rates, compositions and enthalpies of the feed, reflux and boil-up streams.

Whether they are directed to tray n is determined by the binary decision variables $b_{F,n}$, $b_{R,n}$ and $b_{B,n}$. The summation constraints for the liquid and vapor phase compositions are given by

$$\sum_{c=1}^{n_c} x_{n,c} = 1, \tag{2.50}$$

$$\sum_{c=1}^{n_c} y_{n,c} = 1. \tag{2.51}$$

The vapor composition $\boldsymbol{y}$, the equilibrium temperature $\boldsymbol{T}$ and molar enthalpies $\boldsymbol{h}_L$ and $\boldsymbol{h}_V$ are represented in the optimization model by means of simple equations of implicit functions

$$\begin{bmatrix} \boldsymbol{y} \\ \boldsymbol{T} \end{bmatrix} = f_{VLE}(\boldsymbol{x}, p), \tag{2.52}$$

$$\begin{bmatrix} \boldsymbol{h}_L \\ \boldsymbol{h}_V \end{bmatrix} = h_{VLE}(\boldsymbol{x}, p). \tag{2.53}$$

The right hand sides of Equations 2.52 and 2.53 constitute numerical values of the properties on the left, which are determined by an external function "hiding" the equations of the vapor-liquid equilibrium (VLE) calculations.

External function

Although modern gradient-based optimization algorithms in principle enable the solution of problems with thousands of equations, the VLE calculations are integrated into the equation-based optimization by means of an external routine to increase the robustness of the optimization problem as proposed by Skiborowski, Harwardt and Marquardt (2014b). The main idea behind the external routine is the simplification of the optimization model by placing the calculation of the physical properties inside a so-called external function. This eliminates a number of highly nonlinear equations from the overall optimization problem while adapted solvers can be used for the underlying thermodynamic routines. In each iteration of the optimization, a set of values of variables is transferred from the modeling environment GAMS (Brooke, Kendrick, Meeraus and Raman, 2005) to the external function. Inside the external function the VLE calculations are performed using the transferred variable values. To integrate the results of these calculations into the optimization problem, they need to be formulated in the form of equality constraints, which are treated as external equations inside of GAMS. In addition to these constraints also the gradients with respect to the variables are required and therefore calculated in the external function.

Since the external functions are implemented in a dynamic link library (DLL) there is some overhead for communication, but the robustness of the optimization problem is increased significantly (Skiborowski et al., 2014b).

MINLP column model

The MINLP column model comprises the MESH equations (Equations 2.48 - 2.53) for each column tray in the superstructure ($n = 2, ..., N_{T-1}$). The mass and energy balances for the (total) condenser ($n = 1$) and the (partial) reboiler ($n = N_T$) are given by

$$0 = V_{n+1}y_{n+1,c} - (D + R_D)x_{n,c}, \quad n = 1,\ c = 1, .., n_c, \tag{2.54}$$

$$0 = V_{n+1}h_{V,n+1} - (D + R_D)h_{L,n} + Q_D, \quad n = 1, \tag{2.55}$$

$$0 = L_{n+1}x_{n+1,c} - Bx_{n,c} - R_B y_{n,c}, \quad n = N_T,\ c = 1, .., n_c, \tag{2.56}$$

$$0 = L_{n+1}h_{L,n+1} - Bh_{L,n} - R_B h_{V,n} + Q_B, \quad n = N_T. \tag{2.57}$$

The compositions and enthalpies of the reflux and boil-up stream are given by

$$0 = x_{R,c} - x_{1,c}, \quad c = 1, ..., n_c, \tag{2.58}$$

$$0 = h_{L,R} - h_{L,1}, \tag{2.59}$$

$$0 = y_{N_T,c} - y_{B,c}, \quad c = 1, ..., n_c, \tag{2.60}$$

$$0 = h_{V,N_T} - h_{V,B} \tag{2.61}$$

and the liquid flow rate for tray 1 and the vapor flow rate for tray N_T are given by

$$0 = L_1 \tag{2.62}$$

and

$$0 = V_{N_T}. \tag{2.63}$$

Closure relations and additional constraints apply for the binary variables modeling feed, reflux and boil-up locations:

$$\sum_{n=1}^{N_T} b_{F,n} = 1, \tag{2.64}$$

$$\sum_{n=1}^{N_T} b_{B,n} = 1, \tag{2.65}$$

$$\sum_{n=1}^{N_T} b_{R,n} = 1, \tag{2.66}$$

$$\sum_{k=1}^{n} b_{B,k} + b_{F,n+1} \leq 1, \quad n = 1, ..., N_T - 1, \tag{2.67}$$

$$\sum_{k=n}^{N_T} b_{R,k} + b_{F,n-1} \leq 1, \quad n = 2, ..., N_T, \tag{2.68}$$

$$\sum_{k=1}^{n} b_{F,k} + b_{R,n+1} \leq 1, \quad n = 1, ..., N_T - 1, \tag{2.69}$$

$$\sum_{k=n}^{N_T} b_{F,k} + b_{B,n-1} \leq 1, \quad n = 2, ..., N_T. \tag{2.70}$$

The Equations 2.67 - 2.70 hereby ensure that the feed is located below the reflux from the condenser and above the boil-up stream. The number of column trays in the final design is calculated based on the binaries for the location of reflux and boil-up streams

$$N_{col} = N_T - \sum_{n=1}^{N_T} \left(\sum_{k=1}^{n} b_{B,k} + \sum_{k=n}^{N_T} b_{R,k} \right) + 2. \tag{2.71}$$

The column diameter D_{col} for a specific tray n is determined by the vapor load of the column (Bauer, 1997)

$$D_{col,n} = \sqrt{\frac{4V_n}{F\Pi} \sqrt{\frac{RT_n \sum_c y_{n,c} M_c}{p}}}, \tag{2.72}$$

with molar masses M_c and the F-factor F, which is assumed to be 2 $Pa^{0.5}$. While the column diameter should be determined as $\max_n D_{col,n}$, a single tray is selected and fixed in the optimization for simplicity, instead of introducing the highly nonlinear equation for every tray. The height of the column

$$H_{col} = N_{col} H_{tray} + H_{cl} \tag{2.73}$$

is calculated based on the number of equilibrium trays N_{col}, a height value for a single tray H_{tray} and a clearance for liquid distributors, demister, etc. H_{cl}. For all calculations a height $H_{tray} = 0.5\ m$ and an additional clearance $H_{cl} = 4\ m$ are assumed. The heat exchange areas A_{hx} are determined by

$$A_{hx} = \frac{Q_B}{\Delta T_{reb} k_{reb}} \tag{2.74}$$

for a reboiler, and

$$A_{hx} = \frac{Q_D}{\Delta T_{con} k_{con}} \tag{2.75}$$

for a condenser. ΔT_{reb} and ΔT_{con} are the (logarithmic) mean temperature differences, and k_{reb} and k_{con} are the heat transfer coefficients for the reboiler and condenser. For all calculations $k_{reb} = 1\frac{kW}{m^2K}$ and $k_{con} = 2\frac{kW}{m^2K}$ are assumed, which are typical values for shell and tube exchangers (Roetzel and Spang, 2013).

Capital cost estimation

The capital cost for a simple distillation column consists of the investment cost for the column shell C_{cs}, the cost for column intervals C_{ci} and the cost for heat exchangers C_{hx}:

$$C_{cap} = C_{cs} + C_{ci} + C_{hx}. \tag{2.76}$$

The investment cost for the column shell C_{cs} is determined by the diameter D_{col} and the height H_{col} for the cylindrical pressure vessel:

$$C_{cs} = \frac{MS{-}index_{today}}{MS{-}index_{1969}} \$1000 \left(\frac{D_{col}[ft]}{3ft}\right)^{1.05} \left(\frac{H_{col}[ft]}{4ft}\right)^{0.81} (MPF + MF - 1). \tag{2.77}$$

The material and pressure correction factor MPF is 2.25, the module factor MF is 4.23. The investment cost for column internals C_{ci} is also determined by the diameter D_{col} and the height H_{col} of the column shell:

$$C_{ci} = \frac{MS{-}index_{today}}{MS{-}index_{1969}} \$1000 \left(\frac{D_{col}[ft]}{3ft}\right)^{1.05} \left(\frac{H_{col}[ft]}{4ft}\right)^{0.81} (MPF + MF - 1). \tag{2.78}$$

Sieve trays with 18 inch tray spacing made of stainless steel result in a material and pressure correction factor MPF of 3.1. The module factor MF is 1.0. The investment cost for heat exchangers C_{hx} is determined by the heat exchanger area A_{hx}:

$$C_{hx} = \frac{MS{-}index_{today}}{MS{-}index_{1969}} \$5000 \left(\frac{A_{hx}[ft^2]}{400ft^2}\right)^{0.77} (MPF + MF - 1). \tag{2.79}$$

A kettle reboiler design is chosen for the reboiler, resulting in a material and pressure correction factor MPF of 3.8. A floating head condenser results in a material and pressure correction factor MPF of 3.75. The module factor MF for heat exchangers is 3.29.

Model reformulation

Krämer et al. (2009) have proposed a robust and efficient optimization strategy for complex large-scale distillation processes for multi-component azeotropic mixtures. This strategy is based on a suitable initialization procedure and a continuous reformulation of the MINLP problem by adding additional nonlinear complementarity constraints (NCC). Instead of solving the MINLP problem directly, the problem is solved as a series of successively relaxed MINLP problems by means of a NLP solver. To finally obtain a discrete solution, so-called NCC-functions are introduced as additional nonlinear constraints (Stein, Oldenburg and Marquardt, 2004). As presented by Krämer et al. (2009), Fischer-Burmeister functions are used as NCC functions and introduced as inequality constraints. Therefore, the binary variable $b_{F,n}$ is substituted by a continuous variable $0 \leq c_{F,n} \leq 1$. Similar to the binary variables, the sum of all these continuous variables is restricted by the summation constraint

$$\sum_{n=1}^{N_T} c_{F,n} = 1. \tag{2.80}$$

To determine an integer solution, the Fischer-Burmeister functions are introduced as inequality constraints for all N_T possible feed trays:

$$c_{F,n} + \sum_{m \neq n} c_{F,m} - \sqrt{c_{F,n}^2 + \left(\sum_{m \neq n} c_{F,m} \right)^2} \leq \mu, \quad n = 1, ..., N_T. \tag{2.81}$$

During optimization, the relaxation parameter μ is reduced to $\mu = 0$ in several steps of the solution procedure. Thus, the final solution represents a solution to the original MINLP problem.

2.3.4 Reactive distillation column

For a reactive distillation column, the mass balances for each column tray (Equation 2.48) are substituted, as described by Harwardt, Kraemer, Rüngeler and Marquardt (2011), by

$$\begin{aligned} L_n x_{n,c} + V_n y_{n,c} = {} & L_{n-1} x_{n-1,c} + V_{n+1} y_{n+1,c} + F z_{F,c} b_{F,n} \\ & + R_D x_{R,c} b_{R,n} + R_B y_{B,c} b_{B,n} - H_n \nu_c R_n, \quad c = 1, ..., n_c, \end{aligned} \tag{2.82}$$

with holdup H_n, stoichiometric coefficient ν_c and rate of formation R_n. The energy balance remains unchanged, since the reaction enthalpy is included in the enthalpy of formation of the reactive species. An additional constraint for the diameter with respect to the required

holdup in the reactive section is also added to the column model:

$$D_{col} \geq \sqrt{\frac{4H_n}{\pi H_{tray}}} \quad n = 2, ..., N_T - 1. \tag{2.83}$$

2.3.5 Extractive distillation column

For an extractive distillation column, the mass balances (Equation 2.48) and energy balances (Equation 2.49) for each column tray are substituted by

$$\begin{aligned} L_n x_{n,c} + V_n y_{n,c} = L_{n-1} x_{n-1,c} + V_{n+1} y_{n+1,c} + F z_{F,c} b_{F,n} + E z_{E,c} b_{E,n} \\ + R_D x_{R,c} b_{R,n} + R_B y_{B,c} b_{B,n}, \quad c = 1, ..., n_c, \end{aligned} \tag{2.84}$$

and

$$\begin{aligned} L_n h_{L,n} + V_n h_{V,n} = L_{n-1} h_{L,n-1} + V_{n+1} h_{V,n+1} + F h_F b_{F,n} + E h_E b_{E,n} \\ + R_D h_{L,R} b_{R,n} + R_B h_{V,B} b_{B,n}. \end{aligned} \tag{2.85}$$

Hereby, E, z_E and h_E are the flow rate, composition and enthalpy of the entrainer stream. The closure relation and additional constraints

$$\sum_{n=1}^{N_T} b_{E,n} = 1, \tag{2.86}$$

$$\sum_{k=1}^{n} b_{B,k} + b_{E,n+1} \leq 1, \quad n = 1, ..., N_T - 1, \tag{2.87}$$

$$\sum_{k=n}^{N_T} b_{R,k} + b_{E,n-1} \leq 1, \quad n = 2, ..., N_T, \tag{2.88}$$

$$\sum_{k=1}^{n} b_{E,k} + b_{R,n+1} \leq 1, \quad n = 1, ..., N_T - 1, \tag{2.89}$$

$$\sum_{k=n}^{N_T} b_{E,k} + b_{B,n-1} \leq 1, \quad n = 2, ..., N_T, \tag{2.90}$$

ensure that the entrainer feed is located below the reflux from the condenser and above the boil-up stream.

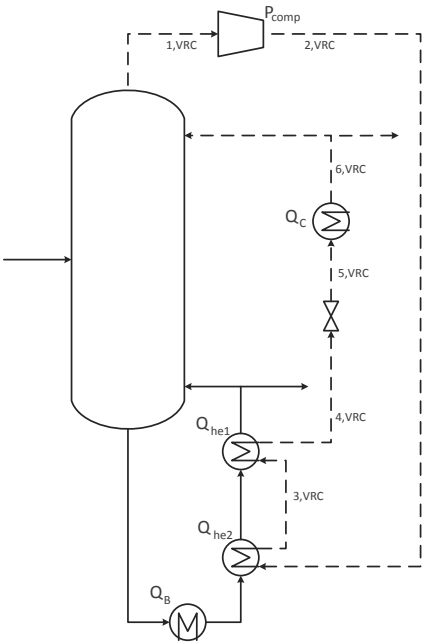

Figure 2.6: Basic configuration for a vapor recompression column.

2.3.6 Vapor recompression column

The basic configuration for a vapor recompression column (VRC), as described by Harwardt and Marquardt (2012), is shown in Figure 2.6. The compressor outlet temperature is modeled by means of a modified isentropic pressure-temperature relationship

$$T_{2,VRC} = T_{1,VRC}\left(1 + \frac{1}{\eta_{comp}}\left(\left(\frac{p_{2,VRC}}{p_{1,VRC}}\right)^{\frac{\kappa-1}{\kappa}} - 1\right)\right). \tag{2.91}$$

The isentropic efficiency of the compression η_{comp} is assumed to be 0.72, the isentropic exponent κ to be 1.165. The VRC model also includes energy balances for the compressor with a power duty P_{comp}

$$0 = (h_{1,VRC} - h_{2,VRC})V_{comp} + P_{comp}, \tag{2.92}$$

the cooler of the superheated vapor stream with heat stream $Q_{he,1}$

$$Q_{he,1} = (V_{3,VRC}h_{V,3,VRC} + L_{3,VRC}h_{L,3,VRC}) - (V_{4,VRC}h_{V,4,VRC} + L_{4,VRC}h_{4,L,VRC}), \tag{2.93}$$

the condenser of the vapor stream with the heat stream $Q_{he,2}$

$$Q_{he,2} = (V_{2,VRC}h_{V,2,VRC}) - (V_{3,VRC}h_{V,3,VRC} + L_{3,VRC}h_{L,3,VRC}), \tag{2.94}$$

a balance which describes the decompression in the valve

$$0 = (V_{4,VRC}h_{V,4,VRC} + L_{4,VRC}h_{4,3,VRC}) - (V_{5,VRC}h_{V,5,VRC} + L_{5,VRC}h_{5,L,VRC}), \tag{2.95}$$

and a balance which describes the total condensation

$$0 = (V_{5,VRC}h_{V,5,VRC} + L_{5,VRC}h_{5,L,VRC}) - (V_{6,VRC}h_{V,6,VRC}). \tag{2.96}$$

The energy balances for the condenser (Equation 2.55) and for the reboiler (Equation 2.57) have to be substituted by

$$0 = V_{n+1}h_{V,n+1} - (D + R_D)h_{L,n} + Q_c + P_{comp} - Q_{he,1} - Q_{he,2}, \quad n = 1, \tag{2.97}$$

and

$$0 = L_{n+1}h_{L,n+1} - Bh_{L,n} - R_Bh_{V,n} + Q_B + Q_{he,1} + Q_{he,2}, \quad n = N_T. \tag{2.98}$$

Although the heat exchanger he1 and he2 are described by two models, they are represented by a single unit of equipment with the heat transfer area

$$A_{hx} = \frac{Q_{he,1}}{\Delta T_{he,1} k} + \frac{Q_{he,2}}{\Delta T_{he,2} k}. \tag{2.99}$$

The investment cost for the column are increased by the cost for the compressor C_{comp} which is determined by the power requirement for compression:

$$C_{comp} = \frac{MS-index_{today}}{MS-index_{1969}} \$23000 \left(\frac{P_{comp}[hp]}{100hp} \right)^{0.77} (MPF + MF - 1). \tag{2.100}$$

The material pressure factor MPF is 1.0 for a centrifugal compressor driven by an electric motor, the module factor MF is 3.11.

2.3.7 Solution procedure

In order to optimize a complete reaction-separation process comprising several units, the unit models are connected by streams with variable flow rates and compositions. The objective function

$$\min \ TAC = C_{op} + f_c \, C_{cap} \tag{2.101}$$

is specified to minimize the cumulated total annualized operating and capital cost of all units in the process. It includes operating cost C_{op} and capital cost C_{cap}. The capital charge factor $f_c = 0.14$ accounts for a depreciation time of about 8 years including interest.

Figure 2.7 illustrates the solution strategy for the resulting optimization problem which is of discrete-continuous nature due to discrete decisions relating to, e.g., the number of trays of the distillation columns, and to continuous decisions like energy duties and flow rates. Although the reformulation of the optimization problem by means of NCC and the utilization of external functions (cf. Section 2.3.3) improve the robustness of the optimization runs, still a suitable initialization procedure is necessary to provide a feasible starting point. This initialization is carried out in several steps, because, according to our experience, a stepwise initialization of the optimization problem with gradually refined models helps both robustness and efficiency, although more optimization problems have to be solved. During initialization, the shortcut models for the units are consecutively substituted by rigorous models with a fixed number of stages (in case of distillation columns) or volume elements (in case of tubular reactors) to provide good initial values for the following rigorous process optimization. After each of these replacements the process is optimized by minimizing operating cost, only to adjust the previously computed operating point

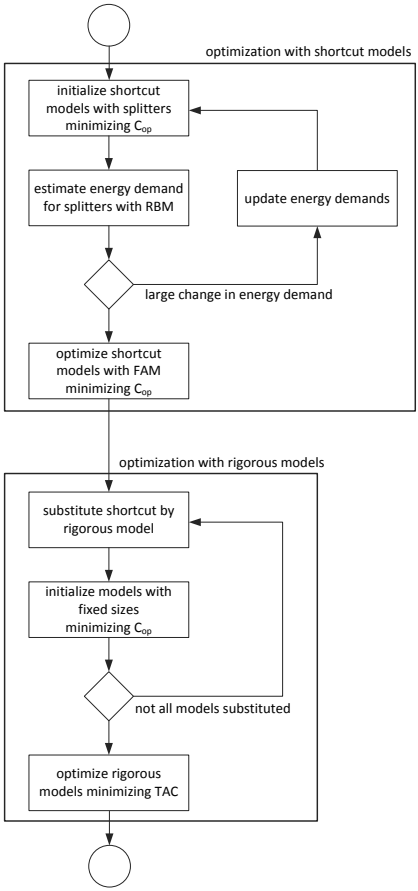

Figure 2.7: Solution strategy for optimization of integrated reaction-separation processes.

with the help of the rigorous models. After the last shortcut model has been substituted, the initialization procedure is completed and the process optimization problem minimizing total annualized cost and adjusting all degrees of freedom simultaneously can be robustly performed. Because of the systematic model refinement and initialization, this last step of the solution strategy will converge quickly to a local optimal solution of good quality of the MINLP problem.

2.4 Illustrative example: ETBE synthesis

In this section, the proposed framework is illustrated by the industrially relevant case study of ethyl tert-buthyl ether (ETBE) production. The fuel additive ETBE is commercially produced by a reversible reaction of isobutene (IB) and ethanol (EtOH) with a strong acidic macroporous ion exchange resin in liquid phase at 10 bar. Since the undesired dimerization and isomerization side-reactions can be suppressed by means of an ethanol excess of at least 4 mol-% (Thiel, Sundmacher and Hoffmann, 1997), an ethanol recycle is considered in the flowsheet variants. Additionally, one of the process feeds, the one containing IB, is usually not pure but contains a number of impurities, which are further taken into account in a lumped n-butane (nBa) fraction (Ryll, Blagov and Hasse, 2006). Due to two binary azeotropes, one on the nBA/EtOH edge and one on the ETBE/EtOH edge, the mixture exhibits a (non-reactive) distillation boundary (cf. Figure 2.8), which is qualitatively corresponding to a reactive separation boundary. It prevents the separation of the reactor outlet into the product and unconverted raw materials by simple distillation and further complicates the recycle strategy of the process. In the following, we will show how the utilization of the proposed framework supports the development of a new and innovative process for this production problem. The presentation follows the workflow in Figure 2.1.

2.4.1 Variant generation

Since automatic flowsheet generation procedures for integrated reaction-separation processes are not available yet (cf. Section 2.1), several conventional combinations of reactor networks and distillation columns without additional separating agents have been generated using heuristics (Douglas, 1988). Figure 2.9 shows these initial flowsheet candidates for an ETBE process. Alternative 1.1, which is a simple conventional variant combining a reactor network (R1) and a single distillation column (C1), serves as a starting point. Since the distillation boundaries restrict the separation, some ETBE is recycled with the not yet converted raw materials and the inert nBa. To avoid the accumulation of nBa in the process, some of the recycle containing the raw materials and ETBE has to be purged.

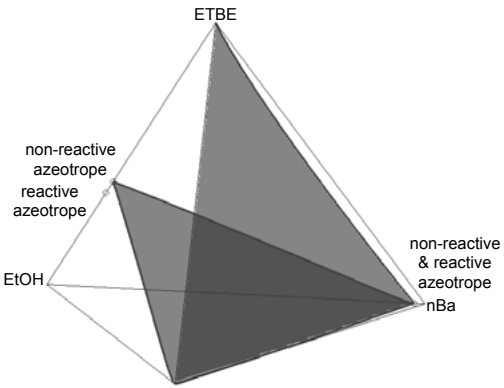

Figure 2.8: Vapor-liquid diagram for the quaternary system of isobutene - n-butane - ethanol - ETBE at 8 bar with non-reactive separation boundaries.

To overcome the limitations of the distillation boundary and to prevent the purging of the raw materials and ETBE, two variants with better recovery are added to the variant tree. Alternative 1.2 consists of one reactor network (R1) and three distillation columns. In a first column (C2) the IB/nBa and EtOH/ETBE mixtures are separated. In a second column (C3) ETBE and the EtOH/ETBE azeotrope are separated and the azeotrope is recycled. A third column (C4) separates nBa and IB, which is also recycled. Alternative 1.3 includes a fourth column (C5) to overcome the ETBE/EtOH azeotrope by pressure-swing distillation to allow for recycling of pure EtOH rather than the azeotrope. Improving the reaction yield of the process is possible by introducing a second reactor network to transform the unconverted raw material and to avoid the accumulation of the inert nBa in the first reactor network. Therefore, alternative 2.1, which represents the industrially used Oxeno-process, and alternative 2.2, which represents the industrially used Hüls-process (Ullmann, 2001), are also added to the variant tree. Alternative 2.1 consists of two reactor networks and two distillation columns. Hereby, a first column (C1) separates ETBE from the reactor effluent. In contrast to alternative 1.1, where the mixture containing the unconverted raw material, nBa and ETBE (due to the separation boundary), is recycled, this mixture is fed to a second reactor network (R2) in alternative 2.1. Subsequently, nBa is separated from the second reactor network's effluent and the remaining mixture is recycled. The separation strategy of alternative 2.2 is slightly different. A first column (C7) separates an EtOH/ETBE mixture from the reactor effluent. In an additional column (C8) this mixture is further separated into ETBE and the EtOH/ETBE azeotrope, which is recycled.

Although the utilized methods also allow the optimization of the column pressures, they are fixed at 8 bar for all alternatives (but the pressure-swing column (C5) in alternative 1.3, which is operated at 1 atm). Since higher pressures would increase the reboiler temperatures above the temperature of the available 10 bar steam and lower pressures would increase the ETBE concentration in the recycle streams, these degrees of freedom have been fixed to increase the robustness of the optimization problems.

2.4.2 Optimization with shortcut models

Using the proposed shortcut-based evaluation method (cf. Section 2.2) the optimal operating points of the process variants can be found by minimizing the operating cost $C_{op} = C_{Raw} + C_{Cat} + C_{Sep}$, which includes the cost of raw material C_{Raw}, the cost of catalyst C_{Cat}, and the cost of separation C_{Sep}. It is evaluated for the process constraints given in Table 2.1 and the cost factors given in Table 2.2.

Table 2.1: Process constraints (adapted from Thiel et al. (1997) and Praefke et al. (2007)).

ETBE capacity	34.5 mol/s
ETBE stream purity	$\geq$ 99 mol%
n-Butane stream purity	$\leq$ 1 mol% isobutene
ethanol excess in reactor	$\geq$ 4 mol%
reactor temperature	293 K $\leq T_R \leq$ 363 K

Table 2.2: Cost factors for economic potential (adapted from Sundmacher et al. (1995) and Kossack et al. (2007)).

C_{ETBE}	69.92 \$/kmol
C_{EtOH}	38.29 \$/kmol
C_{IB}	4.55 \$/kmol
C_{Steam}	15.85 \$/t
$C_{CoolingWater}$	0.05 \$/t
$C_{Electricity}$	50 \$/MWh
$C_{Catalyst}$	3.06 \$/kg
T_{Steam}	527 K
$T_{CoolingWater}$	288 K
annual operation time	8000 h
catalyst lifetime	8000 h
catalyst density	1.515 kg/l
catalyst porosity	0.36

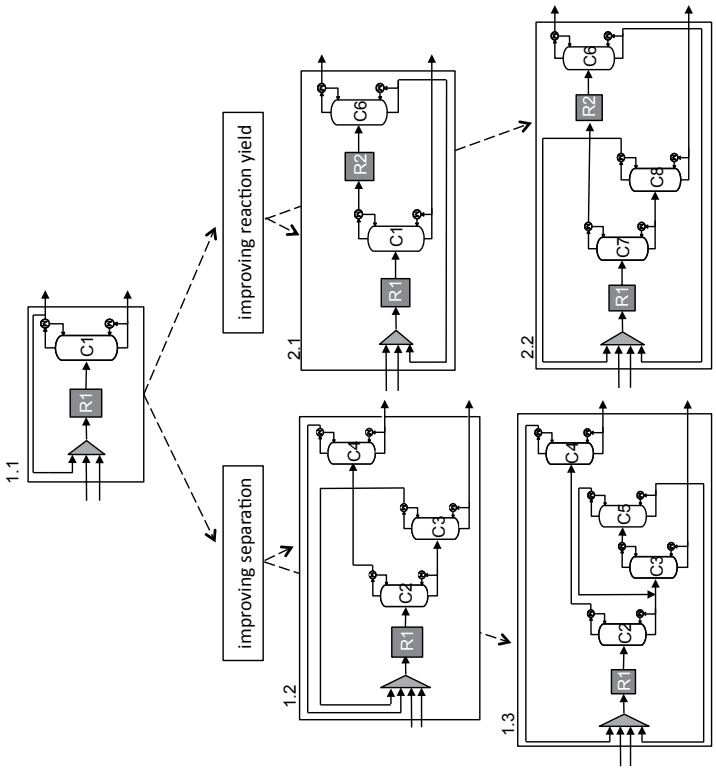

Figure 2.9: Initial flowsheet candidates for ETBE production process.

Table 2.3: Coefficients for the calculation of heat capacity $c_{p,c}$ (taken from Jensen and Datta (1995) and Palczewska-Tuliânska (1997)).

	$K_{1,c}$	$K_{2,c}$	$K_{3,c}$	$K_{4,c}$	$K_{5,c}$
ETBE	40.418	0.7532	-0.001053	1.8066E-06	0
IB	35.44	0.802	-0.003124	5.045E-06	0
EtOH	29.01	0.2697	-0.0005658	2.079E-06	0
nBa	-164.2166	5.482195	-0.0401624	0.00012947	-1.513E-07

As mentioned before, the cost of separation are approximated by the FAM (cf. Section 2.2.2). For calculating the cost of catalyst we assume that the volumes of the reaction devices of the reactor shortcut model (cf. Section 2.2.1) are filled with macroporous ion exchange resign. For all optimization runs, reaction kinetic data are taken from Thiel et al. (1997) and the VLE is modeled using UNIFAC with parameters taken from the ASPEN® APV73 database. The coefficients for the calculation of the heat capacities are given in Table 2.3. Table 2.4 shows the results obtained from the optimization procedure presented in Section 2.2.3.

Table 2.4: Optimization results using shortcut models: Cost contributions for process alternatives displayed in Figure 2.9.

	C_{Raw} $[10^6\$/a]$	C_{Cat} $[10^6\$/a]$	C_{Sep} $[10^6\$/a]$	C_{Op} $[10^6\$/a]$
alternative 1.1	54.1	2.2	2.2	58.5
alternative 1.2	49.2	0.1	1.9	51.2
alternative 1.3	49.2	0.1	1.9	51.2
alternative 2.1	49.3	2.1	1.5	52.9
alternative 2.2	49.3	2.1	1.5	52.9

Alternative 1.1 shows the highest operating cost, as unconverted raw material has to be purged to avoid the accumulation of the inert nBa. In the two-stage alternatives 2.1 and 2.2 this unconverted raw material is transformed in a second reactor network to reduce the operating cost. However, the purity requirement of the nBa stream leaving the process, which suppresses the catalyst poisoning in the following processing steps, constrains the conversion of IB and leads to higher catalyst cost compared to the single-stage alternatives 1.2 and 1.3 with multiple columns and a different recycle strategy. At the optimal operating point the more complicated alternatives 1.3 and 2.2 simplify to the alternatives 1.2 and 2.1 as the additional columns separating the ETBE/EtOH azeotrope (C5 and C8) do not improve the operating cost.

In addition to an assessment of the cost contributions, an analysis of the device connectivity of the reactor shortcut results allows to identify the optimal reactor network for all process alternatives. Since the reaction devices show similar residence times and are

arranged in a sequence without sidestreams the optimal reactor network for all alternatives is identified to constitute of a single PFR.

2.4.3 Revision of the process variants

Based on the results of the shortcut evaluation, alternative 1.1 shows the highest operating cost. Hence, this alternative is discarded. Alternatives 1.3 and 2.2 are also discarded as their additional columns do not improve the operating cost. A promising approach to improve the ETBE process are hybrid separation processes, which have been investigated in literature. A pervaporation-distillation hybrid process and an extraction-distillation hybrid process have been identified as most promising alternatives (Yee, Mohamed and Tan, 2013). Both are focusing on the separation of the azeotropic EtOH/ETBE mixture. The results of the shortcut evaluation already show that breaking the azeotrope by pressure-swing distillation is not economically attractive since the possible cost reduction for recycling pure EtOH does not compensate the energy cost for the additional column (C5) of alternative 1.3. Further studies show that even if the energy cost for C5 are set to zero the economic potential does not increase in case pure EtOH is recycled. Therefore, the sole potential of such a hybrid separation process is the energy cost reduction of the column separating ETBE and the EtOH/ETBE azeotrope. However, the energy cost of the process are dominated by columns C2 and C4, which are not influenced by the hybrid separation processes. Nevertheless, the energy cost for column C4 can be reduced by heat integration. As the temperature difference of the distillate and bottom products is less than 10 K, vapor recompression appears promising (Harwardt and Marquardt, 2012).

Alternatively, the process cost may be reduced by reactive distillation. The large internal recycle in column C2, which causes its high energy cost, can help to overcome the kinetic restriction of the low reaction rate to possibly result in lower catalyst cost. The reactive distillation column might also be more energy-efficient since heat generated by the exothermic reaction can compensate the reboiler heat input (Daniel and Jobson, 2007). Therefore, two additional variants are added to the variant tree: alternative 1.4, which extends variant 1.2 by including VRC for column C4 (C9) and alternative 1.5, which incorporates VRC for column C4 and replaces column C2 by a reactive distillation column (C10). Though the novel process variants could be optimized with shortcut models to determine a bound on operating cost, the alternatives shown in the revised variant tree in Figure 2.10 are directly selected for rigorous optimization. Initialization information can be deduced from the results obtained for alternative 1.2.

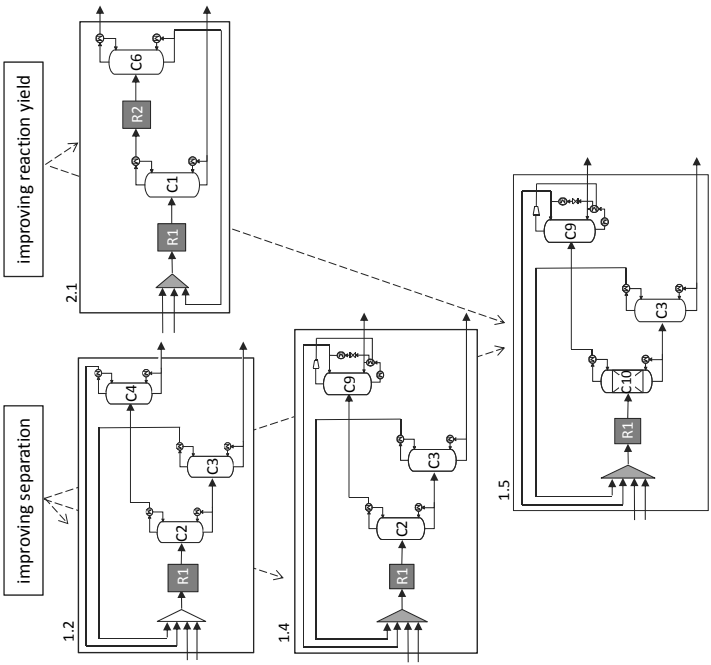

Figure 2.10: Revised flowsheet candidates for ETBE production process after shortcut optimization.

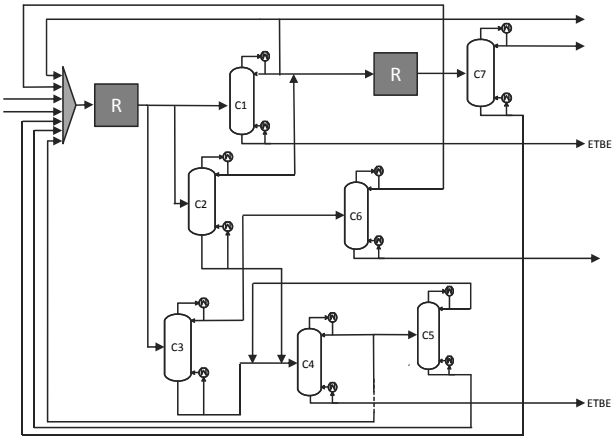

Figure 2.11: Superstructure for ETBE process.

2.4.4 Optimization of a process superstructure with shortcut models

In literature, different process alternatives are often aggregated to one process superstructure which is consequently optimized with shortcut models to identify the optimal process structure (see, e.g., Gassner and Maréchal, 2009a;b). However, as mentioned in Section 1.1.3, modeling for superstructure optimization requires always a trade-off between complexity of the superstructure and the solvability of the problem. Therefore, to improve solvability, often simple shortcut models are utilized to optimize superstructures embedding multiple process alternatives. Such a superstructure for an ETBE process, which embeds the process alternatives displayed in Figure 2.9, is shown in Figure 2.11.

The solution of such a superstructure with several units and recycles is challenging. Since no optimal solution for the superstructure shown in Figure 2.11 could be found utilizing the shortcut models presented in Section 2.2 the models for the reactor networks are simplified to equilibrium reactors in the following optimization run. This simplification reduces the degrees of freedom of this complex optimization problem to the flow rates of the process feeds and the split factors of the superstructure nodes. To allow for discarding of individual columns within the superstructure, the energy demand for the columns are evaluated for a fixed feed flow rate and the specified separation tasks for each column listed in Table 2.5. This ensures that the FAM equations do not become singular. However, the concentrations of the individual species are variable. For approximating the cost for separation the energy demands for each column (calculated for the fixed feed flow rates) are scaled with the real

feed flow rate and add up.

Table 2.5: Overview on separation tasks of individual columns in superstructure.

Column	Feed	Distillate	Bottom
C_1	IB/nBa/EtOH/ETBE	IB/nBa/EtOH	ETBE
C_2	IB/nBa/EtOH/ETBE	IB/nBa/EtOH/ETBE	EtOH/ETBE
C_3	IB/nBa/EtOH/ETBE	IB/nBa	EtOH/ETBE
C_4	EtOH/ETBE	EtOH/ETBE	ETBE
C_5	EtOH/ETBE	EtOH/ETBE	EtOH
C_6	IB/nBa	IB	nBa
C_7	nBa/EtOH/ETBE	nBa	EtOH/ETBE

Table 2.6 shows the optimization results and Figure 2.12 the optimal structure for the ETBE process obtained by optimization of the superstructure using the initialization procedure described in Section 2.2. This structure consists of two reactor networks and six distillation columns. The only unit of the superstructure that is not used in the optimal process structure is the distillation column for breaking the ETBE/EtOH azeotrope (C5) since it does not improve the operating cost. The operating cost for this structure are lower than for all alternatives displayed in Figure 2.9. However, it has to be noted that the cost of catalyst has been discarded from the objective function used for optimizing the superstructure. The utilized equilibrium reactor model does not allow an estimation of this cost factor. This reveals one of the drawbacks of superstructure optimization. Since often simple models are utilized to improve the solvability of the problem, important cost factors may not be estimated as accurately as possible. Another drawback is that the results of the superstructure optimization reveals only the structure with minimum operating cost but allows no conclusions on other structures. However, other process structures might have comparable operating cost and should therefore not be discarded in this design step. For this case study, alternative 2.1 has comparable operating cost if the cost of catalyst are not taken into account. However, this alternative consists of a significant smaller number of units and therefore will most probably reveal smaller investment cost. In addition, based on the information gained during the shortcut evaluation novel process variants could be developed and selected for rigorous optimization. All in all, the better solvability of the smaller problems, the resulting possibility to use more sophisticated shortcut models and the additional information gained during the evaluation of the different flowsheet alternatives lead to the conclusion that the evaluation of the different process variants should be favored over the optimization of a superstructure embedding all alternatives.

Table 2.6: Optimization results using shortcut models: Cost contributions for process superstructure displayed in Figure 2.12.

	C_{Raw} $[10^6\$/a]$	C_{Cat} $[10^6\$/a]$	C_{Sep} $[10^6\$/a]$	C_{Op} $[10^6\$/a]$
superstructure	49.5	–	1.0	50.4

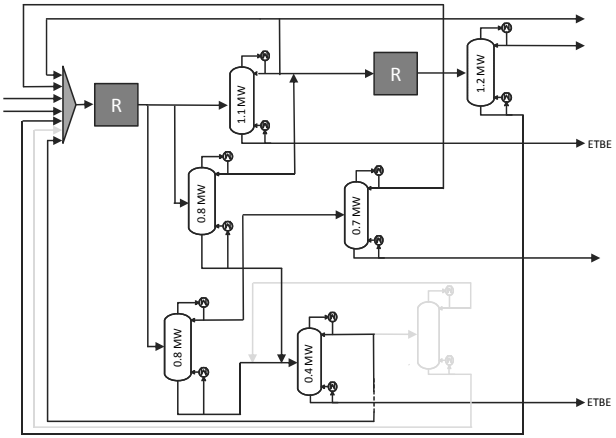

Figure 2.12: Optimal structure for ETBE process and energy demands for columns obtained by superstructure optimization. The unused streams and unit of the superstructure are displayed in gray.

2.4.5 Optimization with rigorous models

The goal of rigorous optimization is to identify the cost-optimal production process. Detailed specifications of the units, such as the numbers of column trays, reactor dimensions, and heat exchanger areas are determined for each instance in the updated tree of alternatives shown in Figure 2.10. The efficient solution strategy introduced in Section 2.3.7 allows the robust solution of this challenging optimization problem. The economic objective reflecting the total annualized cost includes the operating as well as the investment cost for the reaction and separation units. As the analysis of the device connectivity of the reactor shortcut results revealed the optimal reactor system to be a PFR (cf. Section 2.4.2), the corresponding model presented in Section 2.3.1 is used for the rigorous optimization of all variants. The model presented in Section 2.3.3 is utilized for the simple distillation columns. For the VRC column C9 the model presented in Section 2.3.6 is utilized. It extends the column model for simple distillation to include the necessary equations for the compressor and additional heat exchangers. For the reactive column C10 the rigorous

Table 2.7: Optimization results using rigorous models: Cost contributions for process alternatives displayed in Figure 2.10.

	C_{Raw} [10^6\$/a]	C_{Reac} [10^6\$/a]	C_{Sep} [10^6\$/a]	TAC [10^6\$/a]
alternative 1.2	51.1	1.0	2.6	54.7
alternative 1.4	51.0	0.3	2.5	53.8
alternative 1.5	51.0	0.3	2.5	53.8
alternative 2.1	51.2	4.4	1.3	56.9

column model presented in Section 2.3.4 is employed for rigorous optimization. This model integrates the reaction rates into the balance equations of the model presented in Section 2.3.3. The liquid hold-ups on each tray are treated as additional degrees of freedom.

Based on the rigorous optimization results for the previously selected variants (cf. Table 2.7) the cost-optimal process with total annualized cost of $53.8 \cdot 10^6$\$/a is alternative 1.4, which is illustrated in more detail in Figure 2.13. This revised alternative outperforms alternative 1.2 which showed the lowest operating cost for the optimization with shortcut models (cf. Table 2.4). In contrast to a previous study on the ETBE process (Daniel and Jobson, 2007), which utilizes the boundary value method and assumes chemical equilibrium, the reactive distillation column C10 of alternative 1.5 does not improve the economic potential of the process. The unfavored endothermic reverse reaction dominates the overall reaction rate on all trays since the enforced EtOH excess in the reactor to prevent the formation of side products, the purity constraint of the nBa stream to prevent catalyst poisoning in the following processing step and, in addition, the high volatility of IB lead to low IB concentrations in the liquid phase on the column trays. Consequently, the hold-ups for all trays of column C10 are set to zero although the reactive azeotrope on the ETBE/EtOH edge would allow a slightly higher ETBE recovery (cf. Figure 2.8). Therefore, alternative 1.5 (w/ reactive distillation) simplifies to alternative 1.4 (w/o reactive distillation). This is even the case when different reactor conversions are used as starting points for the rigorous optimization to reduce the possibility of local minima.

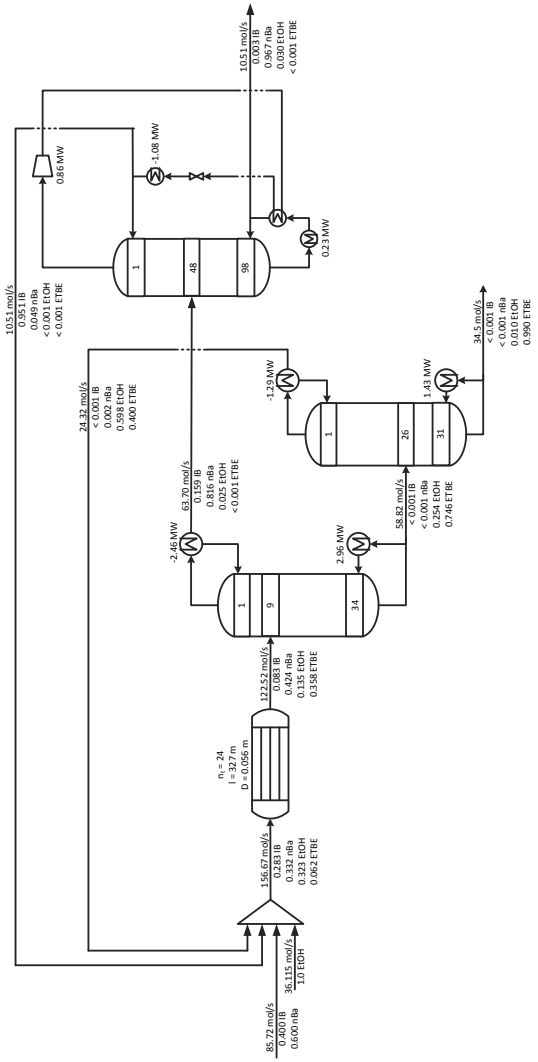

Figure 2.13: Cost-optimal flowsheet for the ETBE process.

2.5 Illustrative example: Allyl chloride production

The previous section has shown how the proposed framework facilitates the design of an optimal flowsheet structure, when distillation boundaries impede separation. In this section we will shift the focus to the design of a suitable reactor network for a reaction scheme with side- and consecutive reactions. As stated in Section 1.1.1, the different design methods for reactor networks all have their weaknesses which complicate their utilization for the design of reaction/separation processes. Attainable region approaches, e.g., require a given reactor feed concentration, which is often not known in the early design phase. Superstructure approaches can, in principle, be utilized if the structure of a reactor network is not known a priori. However, these highly complex MINLP problems are difficult to set up and solve (cf. Sections 1.1.3 and 2.4.4). In this section, we will show how the proposed framework can facilitate the identification of a suitable structure of a reactor network embedded into a flowsheet with separation units. As illustrative example serves the case study of allyl chloride production.

2.5.1 Variant generation

Allyl chloride is an intermediate in the production of chemicals like esters and salines. The key reaction for its production is the non-catalytic chlorination of propylene (C_3H_6) with chlorine (Cl_2) in the vapor phase

$$C_3H_6 + Cl_2 \xrightarrow{R_1} C_3H_5Cl + HCl, \tag{2.102}$$

which forms the desired product allyl chloride (C_3H_5Cl) and the byproduct hydrogen chloride (HCl). In a consecutive reaction allyl chloride reacts with chlorine to form 1,3-dichloropropene ($C_3H_4Cl_2$) and hydrogen chloride:

$$C_3H_5Cl + Cl_2 \xrightarrow{R_2} C_3H_4Cl_2 + HCl. \tag{2.103}$$

The selectivity of the system is limited by the parallel reaction of propylene with chlorine which forms the side-product 1,2-dichloropropane ($C_3H_6Cl_2$):

$$C_3H_6 + Cl_2 \xrightarrow{R_3} C_3H_6Cl_2. \tag{2.104}$$

The reaction kinetics of the system can be described by the non-isothermal van de Vusse reaction scheme (Pahor et al., 2001)

$$\mathrm{A} \xrightarrow{R_1} \mathrm{B} \xrightarrow{R_2} \mathrm{C}, \tag{2.105}$$

$$2\,\mathrm{A} \xrightarrow{R_3} \mathrm{D}, \tag{2.106}$$

with the rate equations

$$R_1 = k_1\ x_{\mathrm{C_3H_6}}\ x_{\mathrm{Cl_2}}, \tag{2.107}$$

$$R_2 = k_2\ x_{\mathrm{C_3H_5Cl}}\ x_{\mathrm{Cl_2}}, \tag{2.108}$$

$$R_3 = k_3\ {x_{\mathrm{C_3H_6}}}^2\ x_{\mathrm{Cl_2}}. \tag{2.109}$$

The reaction rate constants k_r, $r = 1, 2, 3$, are described by the Arrhenius equation

$$k_r = k_{r,0} \exp\left(\frac{-E_{a,r}}{R_g T}\right), \tag{2.110}$$

where $k_{r,0}$ is the pre-exponential factor, $E_{a,r}$ the activation energy of each reaction, R_g the ideal gas constant and T the temperature. Table 2.8 lists the activation energies, pre-exponential factors and heat of reactions for the allyl-chloride reactions used for all optimization runs. The pressure of the reaction is assumed to be 1 bar.

Table 2.8: Activation energies $E_{a,r}$, pre-exponential factors $k_{r,0}$ and heat of reactions $\Delta H_{R,r}$ for the allyl chloride reactions.

reaction	$E_{a,r}\ \left[\frac{kJ}{mol}\right]$	$k_{r,0}\ \left[\frac{mol}{m^3 s}\right]$	$\Delta H_{R,r}\ \left[\frac{kJ}{mol}\right]$
(1)	66.3	$1.5 \cdot 10^9$	-113
(2)	99.4	$4.4 \cdot 10^{11}$	-128
(3)	33.1	$1 \cdot 10^5$	-183

Figure 2.14 shows an initial flowsheet candidate for an allyl chloride production process, which has been generated using heuristics (Douglas, 1988). This candidate consists of one reactor network and three distillation columns. The first column (C1) separates the low boiling hydrogen chloride from the reactor network effluent. A part of the hydrogen chloride can be recycled to the reactor network, the rest is purged. The pressure of this column is set to 13 bar. As mentioned in Section 2.4.1, the utilized methods in principle allow for the optimization of the column pressures. However, these degrees of freedom have been fixed to increase the robustness of the optimization problems, since higher pressures would increase the reboiler temperature above the temperature of the available 10 bar steam and lower pressures would decrease the condenser temperature below the temperature of the

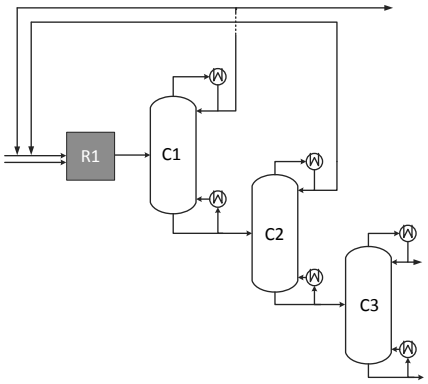

Figure 2.14: Initial flowsheet candidate for allyl-chloride production process.

available cooling water. The second column (C2) separates the non-converted propylene and chlorine, which are recycled to the reactor network, its pressure is also set to 13 bar. The third column (C3) separates the allyl chloride from the high boiling side products 1,3-dichloropropene and 1,2-dichloropropane, its pressure is set to 1 bar.

2.5.2 Optimization with shortcut models

Using the shortcut models and solution procedure presented in Section 2.2, the optimal operating point of the process variant can be found by minimizing the operating cost $C_{op} = C_{Raw} + C_{Sep}$, which includes the cost of raw material C_{Raw} and the cost of separation C_{Sep}. It is evaluated for the process constraints and cost factors given in Table 2.9. The VLE is modeled using UNIFAC with parameters taken from the ASPEN® APV73 database. The coefficients for the calculation of the heat capacity are given in Table 2.10.

Table 2.11 shows the results of the shortcut evaluation. At the optimal operating point 83% of the propylene are converted in the reactor. Chlorine is added in a small excess (chlorine to propylene ratio of 1.03) to improve the selectivity towards allyl chloride. Additionally, a large amount of hydrogen chloride is recycled to the reactor network, since the higher separation cost for this recycle are more than compensated by the improved selectivity due to the lower concentrations of propylene and chlorine. In contrast to the ETBE case study, an analysis of the device connectivity of the reactor shortcut results for this case study does not allow to deduce the optimal reactor system. At the optimal operating point the reaction devices vary in a wide range in their residence time and are in many cases interconnected. We will show in Section 2.5.4 how the stepwise solution presented in Section 2.3 can facilitate the identification of an appropriate reactor network.

Table 2.9: Process constraints and cost factors for economic potential (adapted from Pahor et al., 2001).

allyl chloride capacity	7.56 mol/s
allyl chloride stream purity	$\geq$ 99 mol%
reactor temperature	320 K $\leq T_R \leq$ 460 K
$C_{C_3H_6}$	21.55 \$/kmol
C_{HCl}	7.8 \$/kmol
C_{Steam}	15.85 \$/t
$C_{CoolingWater}$	0.05 \$/t
T_{Steam}	527 K
$T_{CoolingWater}$	288 K
annual operation time	8000 h

Table 2.10: Coefficients for the calculation of heat capacity $c_{p,c}$.

	$K_{1,c}$	$K_{2,c}$	$K_{3,c}$	$K_{4,c}$	$K_{5,c}$
HCl	29157	9048	2093.8	-107	120
propylene	43852	150600	1398.8	74754	616.46
chlorine	29142	9176	949	10030	425
allyl chloride	143710	1677.7	103130	0.00012947	769.64
1,3-dichloropropene	52989	96580	583.6	86298	1965.6
1,2-dichloropropane	78658	174290	1715.7	126270	765

2.5.3 Revision of the process variant

According to heuristics (Douglas, 1988) the light key component hydrogen chloride is separated in the first column in the initial flowsheet alternative. One part of the recovered hydrogen chloride is recycled to the reactor, the other part is purged. The results of the shortcut evaluation have shown that, at the optimal operating point, the main part of hydrogen chloride is recycled to the reactor network together with the unconverted propylene and chlorine. Therefore, it is possible to use a partial vapor-liquid condenser for the second column and to remove the first column from the flowsheet since it is not necessary to ensure a sharp split between hydrogen chloride and propylene and chlorine. The liquid stream of the partial condenser contains some amount of hydrogen chloride which is recycled to the reactor network together with propylene and chlorine. The vapor stream, which mainly consists of hydrogen chloride, is partly recycled to the reactor network or purged out. Consequently this stream can be used to adjust the hydrogen chlorine concentration within the reactor network which makes the first column superfluous. The revised flowsheet candidate is shown in Figure 2.15.

Table 2.11: Optimization results using shortcut models: Cost contributions for process alternative displayed in Figure 2.14.

C_{Raw} $[10^6\$/a]$	C_{Sep} $[10^6\$/a]$	C_{Op} $[10^6\$/a]$
6.84	0.12	6.96

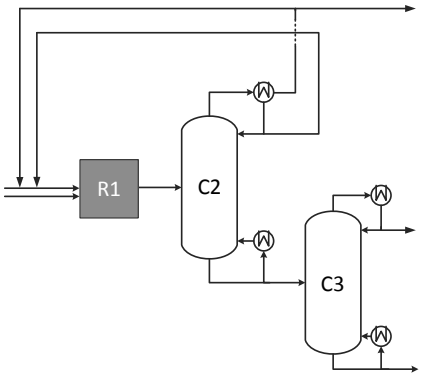

Figure 2.15: Revised flowsheet candidate for allyl-chloride production process.

2.5.4 Optimization with rigorous models

Using the rigorous optimization models and solution procedure presented in Section 2.3, detailed specifications of the entire reaction and separation units of the revised flowsheet candidate are determined. The economic objective function hereby includes the operating as well as the investment cost for the reaction and separation units. As mentioned in Section 2.5.2, an analysis of the device connectivity of the reactor shortcut results does not allow to identify the optimal reactor network. Therefore, the stepwise solution strategy presented in Section 2.3.7 is adapted to facilitate the identification of a suitable reactor network.

As stated in Section 2.2, the shortcut evaluation results serve as performance bounds for the operating cost. During initialization of the rigorous models, the shortcut models of the single units are consecutively substituted by rigorous models with fixed sizes (cf. Section 2.3.7). After each of these replacements the process is optimized by minimizing operating cost, only to adjust the operating point previously computed with shortcut models by means of the rigorous models. As one step of the initialization procedure an alternative with rigorous models for the distillation columns and the reactor shortcut models is optimized. For this case study, this initialization step furthermore facilitates the identification of a suitable reactor network. By minimizing the sum of C_{op} and the

investment cost of the distillation columns, a performance bound for the reactor network can be conduced. Consequently, different reactor networks can be benchmarked against this bound. In a first run we benchmark two flowsheet variants with different (simple) reactor networks, a single CSTR and a single PFR, to evaluate their process performance.

Table 2.12: Optimization results using rigorous column models and alternative reactor models.

	C_{Raw} $[10^6\$/a]$	C_{Sep} $[10^6\$/a]$	C_{Reac} $[10^6\$/a]$	TAC $[10^6\$/a]$
reactor shortcut	6.87	0.32	-	7.19
CSTR	7.05	0.51	0.54	8.10
PFR	7.01	0.30	0.15	7.46

Table 2.12 shows the results of the optimization with rigorous column and alternative reactor models. The process alternative with a PFR outperforms the alternative with a CSTR in raw material cost, separation cost, and cost for the reactor. The separation systems of both processes are structurally identical. Since the boiling temperatures of all components of the gaseous mixture are widely spread and no azeotropes are present, the separation is not expensive in either case. The separation cost for the CSTR alternative are higher, since more hydrogen chloride is recycled to improve the selectivity towards allyl chloride. The reaction rates in a CSTR are determined by its outlet composition. Therefore, a high dilution is necessary to suppress the consecutive reaction of allyl chloride to 1,3-dichloropropene. However, this high dilution leads to a low reaction rate for the allyl chloride formation and results in a large reactor volume. The residence time of the CSTR is almost 60 times higher compared to the residence time of the PFR. Consequently, the cost for the CSTR are also higher than for the PFR. A shortcut evaluation with side-streams to the reactor network has shown that a DSR does not lead to a decrease of the operating cost. Consequently, a reactor network consisting of at least two reactors is necessary to reduce the TAC. However, it is unlikely that the additional investment cost for a second reactor are compensated by decreasing raw material cost. Therefore, no further alternative reactor network is evaluated in this work, although there is still a gap between the TAC of the PFR alternative and the alternative with the reactor shortcut. Based on the results of the rigorous optimization the alternative with a PFR, which is shown in Figure 2.16, is selected as cost-optimal process.

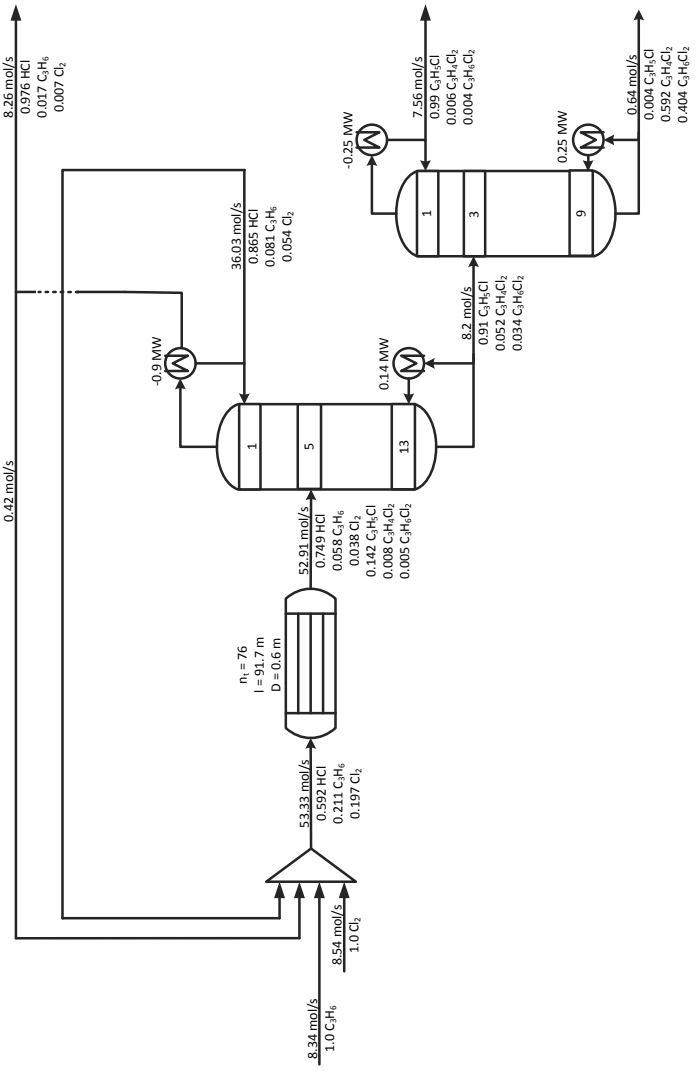

Figure 2.16: Cost-optimal flowsheet for the allyl chloride process.

2.6 Conclusions

When reviewing classical design methods for conceptual design of reaction-separation processes, it becomes obvious that no single method for process design is capable of solving all problems associated to the design of integrated reaction and separation processes. This is partly due to the large number of continuous and discrete degrees of freedom, the coupling of reaction and separation units in a flowsheet and the strongly nonlinear unit models. Therefore, a design framework which combines different design methods is proposed in this chapter and applied to two complex case studies. In this framework the process design task is separated into three distinct steps. In the first step, possible process variants are generated. Consequently, the generated alternatives are evaluated with the help of shortcut models in the second step. In previous publications either equilibrium reactor models and thermodynamically sound distillation shortcuts (see, e.g., Kossack et al., 2007) or kinetically controlled reactor models and correlations for the distillation of ideal mixtures (see, e.g., Hentschel et al., 2014) have been coupled. Equilibrium reactor models do not allow to determine the cost of catalyst and the optimal conversion for reaction schemes with consecutive and/or side reactions. Simple distillation shortcuts, e.g., the Fenske-Underwood-Gilliland correlations, may be inaccurate for azeotropic mixtures. In order to estimate all important cost factors as accurately as possible, in this work a kinetically-controlled reactor shortcut is coupled with the pinch-based FAM. The aggregation of these efficient shortcut models in one NLP problem facilitates the optimization-based evaluation of several process alternatives within a few minutes of computational time. Based on these results some of the flowsheet candidates can be discarded and new candidates are added to the variant tree taking into account the knowledge gained from the first evaluation step. The results of the shortcut calculation are further used for an efficient initialization of the rigorous optimization models. The relaxation of the binary variables by NCCs and the utilization of external equations significantly increase the robustness of the rigorous optimization calculations. Nevertheless, a suitable initialization is necessary to provide a feasible starting point. To this end, the shortcut models for the units are consecutively substituted by rigorous models to provide good initial values for the following rigorous process optimization. After each of these replacements the process is optimized to minimize operating cost only adjusting the operating point computed previously with shortcut models by means of rigorous models. Finally, the process optimization problem minimizing total annualized cost and adjusting all degrees of freedom simultaneously is solved robustly within a few hours computational time. Since a number of feasible pro-

cesses are already eliminated, only a few optimization runs are necessary in the final step. The whole process design framework constitutes a procedure of incremental refinement and successive initialization to allow for a systematic generation and evaluation of complex reaction-separation processes. The time for developing new and innovative processes can be significantly reduced and the quality of the result is improved at the same time.

3 Systematic variant generation for catalytic processes

In industrial practice heuristics play an important role for conceptual process design. Well-known heuristic rules for the design of general chemical processes have been proposed by Douglas (1988), for example. In this hierarchical approach, the very large and complex design task is decomposed into a number of smaller problems that are much better to solve (cf. Section 1.1.3). While these rules have been adapted to the design for, e.g., energy processes (Upadhye et al., 2011), the design of catalytic processes has not gotten appropriate attention yet. Reasons are the additional decisions related to the catalyst which further complicate the generation of suitable process variants.

Catalyst-based processes account for about 60% of chemicals production. Catalysts are used in the production of over 7000 compounds worth over $3 trillion globally (Senkan, 2001). Therefore, a systematic procedure to facilitate the design of catalytic processes is necessary. In principle, the framework presented in Chapter 2 provides a systematic tool to design catalytic processes. Within this framework, possible process candidates are evaluated and consequently optimized to identify the best process. The framework also helps to identify the steps within a process that are the most expensive providing insight into how cost can be reduced and guiding where future research efforts should be directed. The main challenge in the current version of the framework is that the generation of alternative flowsheet variants still requires expert knowledge and experience in order to come up with good alternatives and as such the approach is not completely systematic. As mentioned in Section 2.1, automatic variant generation methods are not applicable to general reaction-separation processes yet and for catalytic processes even heuristics are lacking. Therefore, to allow the design of a catalytic butadiene telomerization process in Chapter 4, necessary extension of the heuristic rules proposed by Douglas (1988) for the design of catalytic telomerization processes are presented in this chapter.

Especially for catalytic processes, the necessary insight into the reaction cannot be generated fully *in silico*, but requires laboratory experiments to determine important process parameters. Laboratory chemists can spend significant effort on improving a reaction with their 'favorite' catalyst which could turn out to be not economical, e.g., due to high catalyst

degeneration. Therefore, a systematic process design methodology should also serve as a research tool in planning and guiding laboratory experiments. In this chapter, a procedure for the generation of catalytic process variants is presented which integrates laboratory experiments into the design procedure. Together with the shortcut evaluation and rigorous optimization methodology presented in Chapter 2, this procedure can be used for the systematic design of catalytic processes. The procedure follows the key steps of the heuristic proposed by Douglas (1988). They are consequently reviewed in the following sections, but for a more comprehensive presentation of the technical details we refer to the Douglas' monograph. To facilitate the design of a catalytic telomerization process in Chapter 4, the individual steps are extended where necessary to include the decisions related to the catalyst. Additionally, a further step is integrated into the design methodology which forms the connection between process design and laboratory experiments and facilitates the identification of reaction kinetic models for the previously identified catalysts. The insight gained during the experiments can be used to revise the process variants. Additionally, the kinetic models can be utilized for subsequent shortcut evaluation and rigorous optimization.

3.1 Batch vs. continuous

The first decision towards the generation of process variants relates to the mode of operation, wether a batch or a continuous production is preferred. The most common guideline that helps to indicate when a batch process may be favored over a continuous process is based on the production rate. Plants having a capacity of more than 5000 t/a should usually be operated in continuous mode, plants having a capacity of less than 500 t/a should be operated in batch mode. However, the development of compact and microreactor systems has started to break with this tradition (Lapkin and Plucinski, 2009). Continuous processes are also more and more considered for fine chemical and pharma processes (Valera, Quaranta, Moran, Blacker, Armstrong, Cabral and Blackmond, 2010, Colberg, Koenig, Leahy and Poechlauer, 2013). Therefore, for catalytic processes having a capacity of less than 5000 t/a both modes of operation should be evaluated to find the best process. Since the evaluation might include a wide range of criteria beside cost, in some cases a detailed life cycle analysis (LCA) of the process with both modes of operation might be necessary to allow a vital comparison of the batch and continuous process (Falß, Tomaiuolo, Perazzo, Hodgson, Yaseneva, Zakrzewski, Guido, Lapkin, Woodward and Meadows, 2016).

3.2 Input/output structure

In the second step, the input/output structure of process flows is considered by taking into account the balance envelope for the entire process. The decisions at this stage are the selection of raw materials, products and, for complex synthesis routes, the reaction pathway from raw material to product. For simple synthesis routes, the process economic potential at this step is calculated based on the reaction stoichiometry and is primarily the difference between the revenue from the product and the raw material cost

$$\Phi = \text{product revenue} - \text{raw material cost}. \tag{3.1}$$

The cost for catalyst cannot be included in the economic potential at this step, since the required amount of catalyst cannot be assessed from the reaction stoichiometry. For many alternative reaction pathways, rapid screening methods like the reaction network flux analysis (RNFA) (Voll and Marquardt, 2012) or the process network flux analysis (PNFA) (Ulonska, Skiborowski, Mitsos and Viell, 2016) can be used for an automated evaluation.

3.3 Recycle structure

In the third step, more details are added to the process. The process is separated into reaction and separation sections while recycle streams are introduced in the flowsheet. In general, there exist different reasons for introducing recycle streams. In cases of, e.g., equilibrium-limited reactions, the excess of one reactant can be used to shift the reaction equilibrium into a favorable region, with the excess reactant recycled back from the product stream. For exothermic reactions, a diluent can be used to reduce the concentration of the reactants and help to remove the heat of reaction. However, in most cases, the recycle back to the reactor leads to an increase in capital and operational cost of the subsequent separation subsystem. Therefore, a trade off between decreasing the cost for reaction and increasing the cost for separation has to been found. Different reactor networks may be used, if sets of reactions take place at different conditions (different temperatures or pressures), or if they require different catalysts. However, additional reactor networks will increase the investment cost of the process.

For catalytic processes special attention has to be placed on the catalyst which also should be assessed in this step. Hereby, the selection of a catalyst and the type of immobilization is interlinked, and thus in many cases fixing one decision can mean that the range of options for the other decision is significantly reduced. With many options available, there are by definition a very large number of hypothetically possible process options, which cannot be assessed completely by model-based studies yet (Nørskov, Bligaard, Ross-

meisl and Christensen, 2009). Although many of these variants can readily be dismissed as unfeasible, a proper assessment of the various whole process options is important to ensure that innovative opportunities are not missed. At the start of process development the selection of a catalyst is typically focused on the performance of a range of catalytic options in small-scale screening tests, preferably in high throughput devices (Senkan, 2001). The lead options are selected based on a limited range of selection criteria. Hintermair, Franciò and Leitner (2011) propose three general catalyst selection criteria with the following priorities:

1. Selectivity
2. Activity and Robustness
3. Availability and Cost

From an industrial perspective, selectivity to the desired product is particularly important, as higher selectivity can result in a reduction in waste and downstream processing requirements. While low catalyst activity may be overcome by optimized reaction conditions or extended contact times (e.g., by recycle of unconverted raw materials), there is no alternative to maximum selectivity. However, it is important that a broader range of techno-economic criteria is considered to ensure that the selected catalysts can meet the overall process requirements. Therefore, activity and robustness as well as availability and cost of the catalyst should also be considered since they affect the process economics. The immobilization approach has to be assessed simultaneously since it affects the selectivity, activity and robustness of the catalyst. Alternative immobilization approaches can be captured in the form of a decision tree from which viable options may be selected based on expert knowledge and literature data. An example of such a decision tree for metal-ligand based catalysts for telomerization reactions is shown in Figure 3.1. This decision tree captures two levels of detail for immobilization - catalyst phase, and general approach to immobilization - but further levels of detail could be employed for other types of catalyst which explores, e.g., the nature of different catalyst supports or the influence of the solvent. For the design of different catalytic processes different decision trees may be constructed for other types of catalyst. The viability of the different approaches should be assessed against the existing experimental and literature data. The result of this step is consequently a first sketch of a flowsheet with a recycle structure as well as a set of promising catalysts. Since the design of the separation system and the subsequent evaluation of the flowsheets require profound insight into the reaction behavior, the selected catalysts are experimentally investigated in the next step.

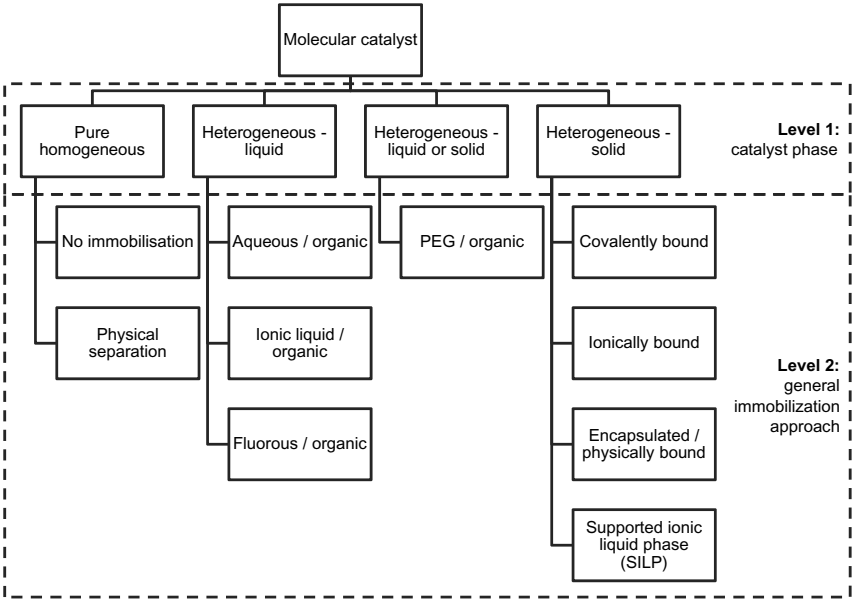

Figure 3.1: Decision tree for immobilization of molecular metal-ligand based catalysts.

3.4 Model-based kinetic investigation

For catalytic processes, the cost for the catalyst is often a major factor of the operational cost. Therefore, special attention has to be paid to determine the optimal reaction conditions and especially the optimal catalyst loading. Model-based conceptual design methods can be used to identify the optimal operating point of a process if reaction kinetic models are available (cf. Section 2.2). Coupled cluster theory and density functional theory recieve increasing interest for the estimation of rate constants for individual reaction steps (see, e.g., Metcalfe, Simmie and Curran, 2010, Freund and Sundmacher, 2011a). However, model-based kinetic investigations of catalytic reactions constitute still an essential part of fundamental mechanistic studies (Blackmond, 2005, Marquardt, 2005). Such studies not only provide insight regarding the evolution of the concentration of the reactants, but also allow for a better understanding of the reaction mechanism and for the determination of reaction rate and equilibrium constants. However, the analysis of experimental data in multi-step catalytic reactions is often complicated due to the complexity of the reaction rate law; therefore, simplified reaction kinetic models are often desired to represent concentration data. For such complex reaction systems, dynamic parameter estimation problems

are often formulated to estimate the unknown parameters in the rate models (Bard, 1974). The structure of the reaction kinetic model embedded in this parameter estimation problem is postulated using a priori knowledge on possible reaction mechanisms. The model is fitted to experimental data by adjusting the unknown model parameters such that the deviation between the concentrations predicted by the model and the measured concentration data is minimized. This so-called simultaneous model identification is capable to handle reaction systems of arbitrary complexity. However, if an incorrect model structure is assumed (i.e., if some of the kinetic laws are structurally wrong), an erroneous overall model prediction is obtained and the model error might be difficult to attribute to a particular model-part. To overcome these well known problems, Marquardt and co-workers suggested an alternative methodology, the so-called incremental model identification (IMI for short), which decomposes the model identification problem into a sequence of properly chosen steps (see Mhamdi and Marquardt (2013) or Marquardt (2013) for a tutorial overview). For catalytic reactions, the particular stepwise problem decomposition strategy proposed by Brendel, Bonvin and Marquardt (2006) can be adapted as follows to allow an analysis of the underlying catalytic reaction mechanism:

In a first step, the time-variant reaction fluxes for the various species are estimated from the noisy experimental concentration data. While the reaction flux is often estimated by simple finite difference approximations from concentration data measured at adjacent sampling points (Blackmond, 2005), the ill-posedness of this inverse problem and the resulting amplification of the errors present in the concentration data is well-known (Tikhonov and Arsenin, 1977). Special care has to be taken, in particular, if only a limited number of error-prone data points are available in each of the experiments. In this work, we employ a filter-based approach (Tikhonov and Arsenin, 1977) to estimate the reaction fluxes, which successfully controls the amplification of the measurement errors in the concentration data (Mhamdi and Marquardt, 1999). The individual reaction rates are then calculated from the estimated reaction fluxes using the generalized inverse of the stoichiometry matrix. Subsequently, the reaction rates and the concentration data are correlated by nonlinear regression using a set of candidate reaction rate model structures. The most suitable model structure is selected in a subsequent step from the list of candidates ranked by means of Akaike weights (Burnham and Anderson, 2002), and graphically evaluated by reaction progress kinetic analysis (Blackmond, 2005). The value of the Akaike weights hereby correspond to the probability that one model is the best from a set of models. In a second step, a parameter estimation problem is set up and solved for the most promising model structure identified in the previous step. This way, statistically sound parameter values and their corresponding confidence intervals can be obtained. Throughout this analysis, profound insight can be accumulated which can be used to elucidate a possible underlying

reaction mechanism. Furthermore, the insight can be used in the next step to facilitate the design of a suitable separation system.

3.5 Separation system

Based on the insight into the reaction behavior gained in the previous step, the separation system is subsequently designed. To determine the general structure of the separation system, Douglas (1988) considers in the first instance the phase of the reactor effluent stream. For vapor-liquid reactions he proposes three possibilities:

- If the reactor effluent is a liquid, only a liquid separation system is needed. Possible separation units are distillation, extraction, or adsorption columns.
- If the reactor effluent is a two-phase mixture, the reactor can be used as a phase splitter. The liquid is sent to a liquid separation system and the vapor usually to a vapor recovery system. However, if the rector effluent stream contains only a small amount of vapor, the stream is directly sent to a liquid separation system.
- If the reactor effluent is all vapor, it is cooled to cooling water temperature to achieve a phase split or to completely condense the stream. The condensed liquid is sent to a liquid recovery system, and the vapor is sent to a vapor recovery system.

Afterwards, the recycle structure can be revised based on the insight gained in the previous step and, e.g., knowledge-based approaches can be used to design the individual liquid separation (Barnicki and Fair, 1990) and/or vapor recovery systems (Barnicki and Fair, 1992). For processes with complex reaction networks and/or strongly non-ideal phase behavior the integration of the concept of elementary process functions (cf. Section 1.1.3) into the design procedure can also help to identify innovative process concepts (Freund and Sundmacher, 2011a;b;c;d, Sundmacher, 2015).

For homogeneous catalytic systems, special attention has to be paid to the separation of the catalyst from the reaction product and any reaction solvent. This problem arises because the most common separation method, distillation, requires elevated temperatures unless the product is very volatile. Most homogeneous catalysts are thermally sensitive, usually decomposing below 150 $°C$. The thermal stress caused by product distillation even at reduced pressure will therefore decompose the often expensive catalyst. A number of innovative solutions to the problem of separation of catalyst from products in homogeneous catalytic processes have been proposed by Cole-Hamilton (2003). The question of which of these solutions should be included into the flowsheet has once more to be assessed against the existing experimental and literature data.

3.6 Conclusions

The framework presented in Chapter 2 allows, in principle, the systematic design of general chemical processes. The central challenge of the framework is the variant generation, since this step still requires expert knowledge and experience and as such the approach is not completely systematic. Heuristics systematically decompose the complex design task into a number of smaller problems. However, to the author's knowledge no heuristic for the design of catalytic processes has been proposed in literature yet. To allow the design of a catalytic telomerization process in Chapter 4, a procedure for the variant generation for catalytic telomerization processes is presented in this chapter. This systematic procedure follows the key steps of the heuristic proposed by Douglas (1988) but is extended towards the decisions related to the catalyst where necessary for the telomerization reaction. Furthermore, an additional step is added (cf. Section 3.4) to integrate laboratory experiments into the procedure. Integrating experiments with conceptual process design can give guidance of economical attractive catalysts and a range of economic reaction conditions and consequently help to design better processes. The result of this procedure is a set of alternative flowsheet variants which can subsequently be evaluated using the shortcut evaluation and rigorous optimization procedure presented in Sections 2.2 and 2.3.

4 Systematic design of a butadiene telomerization process

Most chemical products can be obtained from a limited range of basic chemicals, which are mainly produced by large-scale petrochemical processes. Amongst these basic chemicals, 1-octene is an important representative, serving as intermediate in the production of a broad range of end products. Apart from its most common application in the production of linear low density polyethylene, it also functions as a precursor for plasticizer alcohols, corrosion inhibitors, solvents, and nonvolatile herbicides (Jackstell, Gómez Andreu, Frisch, Selvakumar, Zapf, Klein, Spannenberg, Röttger, Briel, Karch and Beller, 2002). The production by traditional synthesis routes, such as Fischer-Tropsch synthesis or the oligomerization of ethylene, covers most of the worldwide demand of 1-octene. However, both synthesis routes require expensive workup to fulfill the high purity demands of the following processing steps. This is due to the broad product spectrum of both processes, resulting from the unselective nature of the reactions. In contrast, the patented reaction cascade shown in Figure 4.1 including the telomerization of butadiene with methanol allows the production of 1-octene with high selectivity (Bohley, Jacobsen, Pelt, Schaart, Schenk and van Oeffelen, 1992).

In the first step, the telomerization of 1,3-butadiene with methanol (MeOH) produces the telomer 1-methoxy-2,7-octadiene (1-MODE) with high chemoselectivity (Behr, Becker, Beckmann, Johnen, Leschinski and Reyer, 2009). In the following reaction, the telomer is completely hydrogenated to the respective 1-methoxyoctane. Finally, pure 1-octene is obtained by thermal cracking of 1-methoxyoctane followed by distillation to remove the by-product methanol (Krissmann, Roettger, Borgmann, Kaemper, Nierlich, Kaizik, Knippenberg and Malzkorn, 2008). Another major advantage of this reaction cascade, besides the high chemoselectivity, is the possible utilization of a C_4-stream from naphtha crackers as cheap and easily available butadiene source (Bohley et al., 1992). However, only one industrial application of this production route to 1-octene is known, an industrial scale plant run by Dow Chemicals (Tschan, Launay, Hagen, Benet-Buchholz and van Leeuwen, 2011). The process came on stream in Tarragona 2007 and its key step is the homogeneously catalyzed butadiene telomerization. The established homogenous catalyst is based

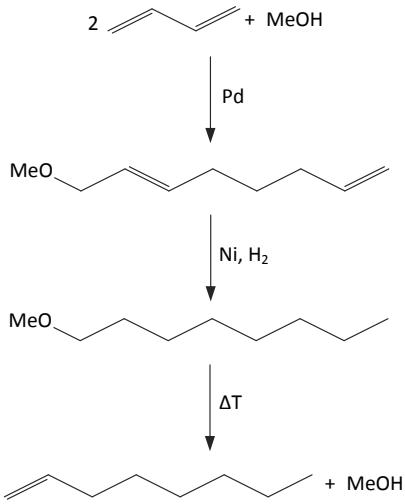

Figure 4.1: Reaction steps of 1-octene production.

on palladium (Pd) modified with a triphenylphosphine (TPP) ligand (Jacobsen, Pelt and Schaart, 1991). The bottleneck of this process is the high cost for catalyst regeneration, since the catalyst is inactive at the end of the reaction and has to be reactivated before recycling.

To assess the economic viability of this reaction route for replacing classical processes for the production of 1-octene, such as Fischer-Tropsch synthesis and the oligomerization of ethylene, a conceptual design study is performed in this chapter. Since the cost for catalyst dominate the operating cost for the industrial process, the choice of catalyst is explicitly considered in this design study. Therefore, in Section 4.1 promising flowsheet variants are generated utilizing the heuristic procedure presented in Chapter 3. These alternatives are consequently evaluated by means of shortcut calculations (Section 4.2) and rigorous optimization (Section 4.3) using the procedures presented in Chapter 2. In Section 4.4, we summarize first results on pilot plant experiments for a novel butadiene telomerization process before we close with a summary and conclusions of the design study in Section 4.5.

4.1 Variant generation

The reaction cascade relying on the telomerization of butadiene with methanol allows the production of 1-octene with high selectivity and has the potential to replace classical processes for the production of 1-octene, such as Fischer Tropsch synthesis and the

oligomerization of ethylene. However, the challenge is to identify which process options are likely to be viable on an industrial scale based only on limited amounts of lab experiments and literature data. Using the heuristic approach described in Chapter 3, in the following alternative flowsheet variants for a telomerization process are generated.

4.1.1 Batch vs. continuous

At first, the decision to be made is whether to design a continuous or a batch process. For the butadiene telomerization process, the desired product capacity is 25 mol/s which corresponds to 100,000 t/a. Consequently, the large volume of the processed materials suggests the use of a continuous process.

4.1.2 Input/output structure

At this second step, the input/output structure of the flowsheet is specified and the economic potential of the process based on the reaction stoichiometry is assessed. As mentioned in Section 3.2, the input/output structure includes only reactants, products and byproducts. Figure 4.2 shows the input-output flow diagram of the butadiene telomerization process. Since the reaction cascade relying on the telomerization of butadiene allows the utilization of crude C_4 from naphtha crackers as cheap and easily available butadiene source (Bohley et al., 1992), a crude C_4-stream is chosen as process input. Its composition is listed in Table 4.1. The second input to the process is a stream containing the second reactant MeOH. Outputs are a raffinate-I stream (the C_4-cut without the converted butadiene), the desired product 1-MODE and possible by-products.

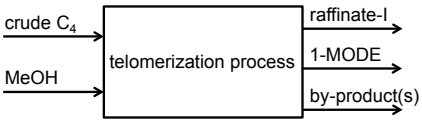

Figure 4.2: Input/output structure of the butadiene telomerization process.

Table 4.1: Composition of the crude C_4-stream in mole fractions.

$x_{isobutane}$	$x_{isobutene}$	$x_{n-butene}$	$x_{butadiene}$	$x_{n-butane}$
0.03	0.25	0.20	0.45	0.07

Table 4.2 summarizes the cost factors for the first economic assessment. This assessment does not include the cost for catalyst, since this cost factor is not assessable based on the

reaction stoichiometry. The economic potential of the butadiene telomerization process following the reaction scheme shown in Figure 4.1 is $\Phi = 30 \cdot 10^6$ \$/a. The largest portion of the production cost is due to MeOH, since the crude C_4-stream from a steam cracker is a cheap butadiene source. However, MeOH is recovered in the thermal cracking step of the reaction cascade (cf. Figure 4.1) and does therefore not affect the cost for 1-octene. Assuming a recovery rate for MeOH of 90%, an evaluation of this reaction cascade results in an economic potential of $\Phi = 42 \cdot 10^6$ \$/a for a 1-octene production process. This suggests that this reaction cascade is an economic attractive route for 1-octene production and that the input/output structure displayed in Figure 4.2 should consequently be further investigated.

Table 4.2: Cost factors for economic potential.

C_{MeOH}	21 \$/kmol
$C_{crude C_4}$	6 \$/kmol
C_{1-MODE}	68 \$/kmol
1-MODE capacity	25 mol/s
annual operation time	8000 h

4.1.3 Recycle structure

After the economic potential of the process has been assessed in the previous step, at this third step more details are added to the process by selecting a suitable catalyst and an immobilization strategy and by introducing recycle streams in a first flowsheet. In the case of the telomerization reaction, two possible catalysts have been identified. One is based on Pd modified with TPP and already used in the industrially process patented by Dow (Bohley et al., 1992). The other catalyst is based on Pd modified with 1,3-dimesitylimidazol-2-ylidene (IMes) (Jackstell et al., 2002). This monocarbene-palladium complex is more selective than the standard Pd/TPP catalyst and can, in principle, be continuously separated and recycled since it remains active at the end of the reaction (Roettger, Beller, Jackstell, Klein and Wiese, 2002).

Based on literature data (Jackstell et al., 2002, Clement, Routaboul, Grotevendt, Jackstell and Beller, 2008, Hausoul, Parvulescu, Lutz, Spek, Bruijnincx, Weckhuysen and Klein Gebbink, 2010, Völkl et al., 2015) the key variables for catalyst selection proposed by Hintermair et al. (2011) (cf. Section 3.3) have been assessed. This analysis is presented in Table 4.3. As a result of this analysis, Pd/IMes appears to offer a better overall performance profile, especially if the impact of the higher selectivity to 1-MODE on the whole process is considered. The disadvantages, however, are the higher cost and the lack

of commercial availability of the new Pd/IMes catalyst. At this stage, therefore, neither catalyst can be unequivocally ruled out.

Table 4.3: Assessment of viable catalyst options for butadiene telomerization.

Criteria	Pd/TPP	Pd/IMes
Selectivity	84.5% to product 1-MODE, 93% to 1-MODE & by-product 3-methoxy-1,7-octadiene (3-MODE) combined.	$\geq$ 97.5% to 1-MODE, $\geq$ 99 % to 1- & 3-MODE combined.
Activity	Higher initial activity than Pd/IMes, but reaction does not reach complete conversion.	Lower initial activity, but activity maintained to full conversion.
Robustness	Catalyst degradation apparently faster than for Pd/IMes.	Lower level of catalyst degradation under standard operating conditions.
Availability	Ligand readily available on industrial scale.	Ligand currently not commercially available on industrial scale.
Cost	TPP ligand significantly cheaper than IMes ligand.	IMes ligand synthesis more complex than TPP ligand, cost likely to be higher.

Alternative immobilization approaches for metal-ligand based catalysts like Pd/TPP and Pd/IMes have been captured in the form of a decision tree which is shown in Figure 3.1. This decision tree captures two levels of detail for immobilization (catalyst phase, and general approach to immobilization) to be used to select viable immobilization options based on expert knowledge and literature data. In the case of butadiene telomerization, all of the process components are present in a single liquid phase under the standard reaction conditions, and no solvent is necessary since MeOH serves as solvent. This means that all of the immobilization approaches listed in Figure 3.1 can at least be considered. In general, it is known that Pd/TPP and Pd/IMes can be applied successfully to this reaction in liquid phase (Jackstell et al., 2002, Clement et al., 2008, Hausoul et al., 2010), but there are no existing reports on the use of solid-phase catalysts. Despite, a recent assessment of the mechanism of butadiene telomerization (Völkl et al., 2015) suggests that there is no intrinsic barrier to the use of a solid-phase supported analogue of either Pd/TPP or Pd/IMes. The impact of different approaches to the immobilization of homogeneous catalysts on the butadiene telomerization process has been assessed against the existing

experimental data from literature (Jackstell et al., 2002, Clement et al., 2008, Hausoul et al., 2010, Völkl et al., 2015), with the results being summarized in Table 4.4. The viability of the different approaches is scored using a simple High/Medium/Low scale. This analysis indicates that the liquid phase approach without immobilization has the highest level of viability, based on existing data. The biphasic ionic liquid-organic system would introduce a number of complexities into the process, notably some degree of ligand modification to ensure that no catalyst leaching occurs, and identification of an ionic liquid that is compatible with the overall process. Thus, it is ranked with low viability. Finally, two further approaches involving solid-phase supported catalysts could be viable, but would require additional experimental tests to assess the impact of solid-phase catalysts on the reaction performance, as such data is currently not available.

The resulting block diagrams for the most viable Pd/TPP and Pd/IMes processes are displayed in Figure 4.3. Both block diagrams include the possibility to recycle unconverted butadiene and MeOH. For the PD/IMes catalyst, the diagram also includes a possible catalyst recycle which requires the recovery of the catalyst in the separation system. Due to catalyst deactivation, the Pd/TPP catalyst has to be recovered at the end of the process and reactivated in a separate batch process. It prevents the continuous recycle of the catalyst. This step is not included in the flowsheet but in the cost for this catalyst.

Table 4.4: Immobilization options considered for butadiene telomerization.

Phase	Immobilization	Comments	Viability
Liquid	None	Downstream separation of spent catalyst - current scenario	High
	Aqueous / organic biphasic	Reaction not compatible with water.	Low
	Ionic liquid / organic biphasic	Technique previously demonstrated for butadiene telomerization (Magna, Chauvin, Niccolai and Basset, 2003). However, different ionic liquids have been screened and tested in laboratory experiments for Pd/TPP and Pd/IMes and catalyst leaching has been observed (Völkl, Geburtig, Kiermaier, Wasserscheid and Haumann, 2016). Therefore, ligands may require modification to ensure full immobilization of catalyst.	Medium / Low

	Fluorous solvent / organic biphasic	Unproven for large-scale industrial applications. Ligand will require modification to enable immobilization in fluorous phase.	Low
Liquid / solid	PEG / organic	Unproven for large-scale industrial applications. Ligand will require modification to enable PEG immobilization.	Low
Solid	Covalently bound	Covalently bound TPP ligands are commercially available (e.g. Johnson Matthey FibreCat® 1001). Supported IMes ligands have been reported in literature (Martinez, Krinsky, Penafiel, Castillon, Loponov, Lapkin, Godard and Claver, 2015), but are not available commercially at present. Impact of solid support on catalyst activity and robustness is not known.	Medium
	Ionically bound	No known commercially available ionically bound TPP or IMes ligands. Impact of solid support on catalyst activity and robustness is not known.	Low
	Encapsulated / physically bound	Encapsulated Pd catalysts with TPP ligands are commercially available (e.g. Reaxa Pd-EnCat TPP30). No encapsulated IMes catalysts are currently commercially available. Impact of encapsulation on catalyst activity and robustness not known.	Medium
	Supported Ionic Liquid Phase (SILP)	May be feasible, but most commonly operated with supercritical fluid mobile phase which is unlikely to be viable for this process.	Low

4.1.4 Model-based kinetic investigation

In cooperation with the Institute of Chemical Reaction Engineering at the University of Erlangen-Nuremberg a kinetic study for the previously identified homogeneous Pd/TPP

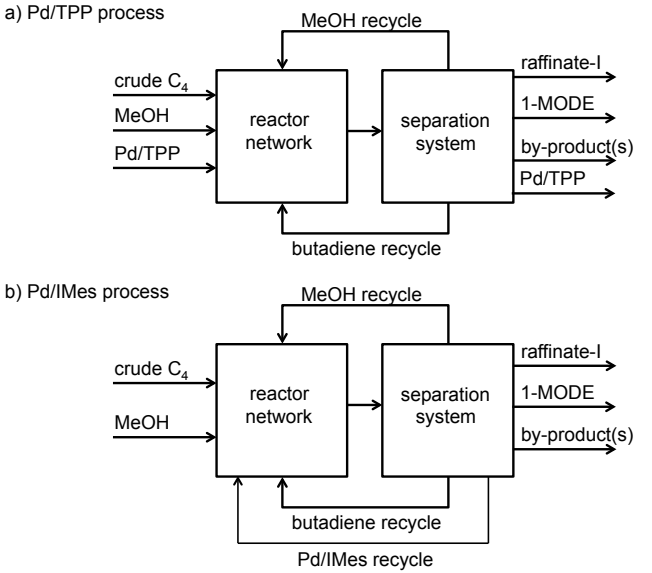

Figure 4.3: Recycle structure for the butadiene telomerization process with a) the Pd/TPP and b) the Pd/IMes catalyst.

and Pd/IMes catalysts was performed. Hereby, the catalysts' activity with a crude C_4 feed to pure 1,3-butadiene feed was compared. For the Pd/TPP system, the initial reaction rate was higher for pure 1,3-butadiene compared to crude C_4 (cf. Figure 4.4), which is most likely caused by the dilution effect. In contrast, the conversion for the Pd/IMes system increased when the crude C_4 feed was used instead of pure 1,3-butadiene. Due to the complexity of this multi-parameter system the exact influence of each individual component could not be determined independently in experiments. Therefore, a model-based experimental analysis is applied to further shed light on this complex system.

Pd/TPP catalyst

As mentioned in Section 3.4, the first step of the applied model-based experimental analysis is the calculation of the individual reaction rates from experimental data. Although the stoichiometric matrix of the reactions

$$\mathrm{Pd_{pre}} + 2\mathrm{B} \xrightarrow{R_0} \mathrm{Pd_{act}} \tag{4.1}$$

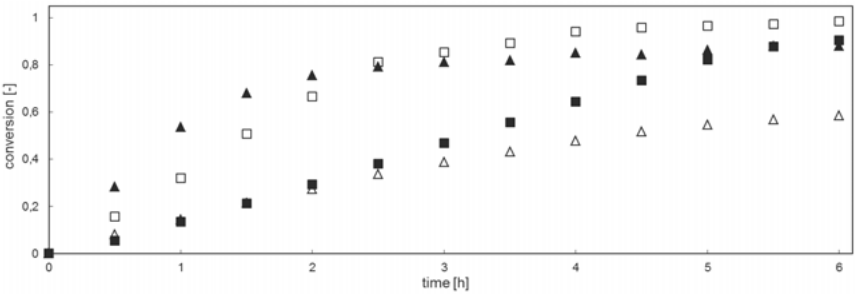

Figure 4.4: Exemplary conversion profiles for experiments with pure 1,3-butadiene (solid symbols) and crude C_4 (open symbols) catalyzed by Pd/TPP (triangles) and Pd/IMes (squares). Experimental conditions: 70 $°C$, 15 bar, $butadiene : MeOH = 0.5$, $butadiene : Pd = 40000$, $ligand : Pd = 4$, $butadiene : base = 400$. Experimental data are taken from Völkl et al. (2015).

$$2\,\mathrm{B} + \mathrm{M} + \mathrm{Pd_{act}} \xrightarrow{R_1} \mathrm{P} + \mathrm{Pd_{act}} \tag{4.2}$$

$$2\,\mathrm{B} + \mathrm{Pd_{act}} \xrightarrow{R_2} \mathrm{D} + \mathrm{Pd_{act}} \tag{4.3}$$

(with B for butadiene, M for methanol, P for the main-product 1-MODE, D for the side-product 3-MODE, $\mathrm{Pd_{pre}}$ for the catalyst precursor and $\mathrm{Pd_{act}}$ for the activated catalyst) is regular (Brendel et al., 2006), the reaction rate R_0 for catalyst activation cannot be deduced from the available measurements due to the following two reasons not covered by the structural argument ensuring identifiability: (i) the catalyst activation occurs in the first few minutes of the reaction, where only few measured data points are available; (ii) the influence of this reaction on the 1,3-butadiene concentration is quite low due to small catalyst concentrations. The experimental errors are dominating the concentration measurements, such that this reaction rate is not accessible from the data in the suggested experimental setting. Consequently, it is assumed in the following, that the catalyst has already been activated at the start of the reaction. Hence, the competition between the first (Eq. 4.1) and the other two reactions (Eqs. 4.2 and 4.3) for B during the very first minutes of the reaction is neglected.

Mechanistic cycles reported for similar reactions in literature can serve as a good starting point for deriving kinetic model candidates. For the telomerization reaction considered here, two different catalytic cycles can be found in literature, the dipalladium-bisally mechanism (Keim, 1968, Behr, Ilsemann, Keim, Krueger and Tsay, 1986) and the Jolly mechanism (Jolly, Mynott, Raspel and Schick, 1986). Assuming that the order of each

reaction step corresponds strictly to the stoichiometry and the Bodenstein approximation of quasi-stationary behavior of reaction intermediates, the model structures

$$R_1 = [\mathrm{Pd_{act}}]\frac{K_1^{Dipa}[\mathrm{M}][\mathrm{B}]^2}{1 + K_2^{Dipa}[\mathrm{M}]}, \tag{4.4}$$

$$R_2 = [\mathrm{Pd_{act}}]\frac{K_3^{Dipa}[\mathrm{B}]^2}{1 + K_4^{Dipa}[\mathrm{M}]} \tag{4.5}$$

and

$$R_1 = [\mathrm{Pd_{act}}]\frac{K_1^{Jolly}[\mathrm{M}][\mathrm{B}]^2}{1 + K_2^{Jolly}[\mathrm{B}]^2 + K_3^{Jolly}[\mathrm{B}]^4}, \tag{4.6}$$

$$R_2 = [\mathrm{Pd_{act}}]\frac{K_4^{Jolly}[\mathrm{M}][\mathrm{B}]^2(1 + K_5^{Jolly}[\mathrm{B}]^2)}{1 + K_6^{Jolly}[\mathrm{B}]^2 + K_7^{Jolly}[\mathrm{B}]^4} \tag{4.7}$$

have been derived for the dipalladium-bisally (Equations 4.4 and 4.5) and the Jolly mechanism (Equations 4.6 and 4.7) respectively, using the procedure reported by Chern (2000). These rate equations are mechanistically correct since they do not apply any simplyfing assumptions on the micro-kinetic level. The parameters in these rate equations are complex nonlinear functions of the reaction rate constants of the elementary reactions postulated in the reaction mechanism. Both model structures show a first-order dependency of the reaction rates, R_1 for the main and R_2 for the side reactions, on the catalyst concentration, but a more complex dependency on the reactants' concentrations.

A drawback of such mechanistically motivated model structures is that they are often not identifiable. The identifiability of a model refers to the question whether the model parameters of a given model structure can be determined uniquely from the available set of (perfect) experimental data. The mechanistic models are shown not to be identifiable using the procedure reported by McLean and McAuley (2012) and the parameter identifiability test presented by Quaiser and Mönnigmann (2009). Since no additional measurements are possible, identifiability can only be restored by model reduction. Following the procedure reported by McLean and McAuley (2012) the identifiable reduced models

Table 4.5: Results of incremental model identification for Pd/TPP.

	rate equations	Akaike weights
Jolly mechanism	(4.6), (4.7)	0.015
reduced Jolly mechanism	(4.10), (4.11)	0.814
dipalladium mechanism	(4.4), (4.5)	0.02
reduced dipalladium mechanism	(4.8), (4.9)	0.15
empirical	(4.12), (4.13)	0.001

$$R_1 = [\mathrm{Pd_{act}}]K_1^{Dipa}[\mathrm{M}][\mathrm{B}]^2, \tag{4.8}$$

$$R_2 = [\mathrm{Pd_{act}}]K_3^{Dipa}[\mathrm{B}]^2 \tag{4.9}$$

and

$$R_1 = [\mathrm{Pd_{act}}]\frac{K_1^{Jolly}[\mathrm{M}][\mathrm{B}]^2}{1 + K_2^{Jolly}[\mathrm{B}]^2}, \tag{4.10}$$

$$R_2 = [\mathrm{Pd_{act}}]K_4^{Jolly}[\mathrm{M}][\mathrm{B}]^2 \tag{4.11}$$

were derived for the dipalladium (Equations 4.8 and 4.9) and the Jolly mechanism (Equations 4.10 and 4.11), respectively. These model structures will be used in the subsequent IMI. For comparison, we also consider the empirical model

$$R_1 = K_1^{Emp}[\mathrm{Pd_{act}}]^{K_2^{Emp}}[\mathrm{B}]^{K_3^{Emp}}[\mathrm{M}]^{K_4^{Emp}}, \tag{4.12}$$

$$R_2 = K_5^{Emp}[\mathrm{Pd_{act}}]^{K_6^{Emp}}[\mathrm{B}]^{K_7^{Emp}}[\mathrm{M}]^{K_8^{Emp}}, \tag{4.13}$$

where the reaction orders are treated as model parameters. The parameters of this model can also be shown to be non-identifiable.

Table 4.5 shows the results of the IMI for the Pd/TPP catalyst. The models for the reduced Jolly and the reduced dipalladium mechanisms result in Akaike weights which are at least an order of magnitude higher than those of the other three models. Hence, one of the mechanistically motivated, reduced models will most likely qualify as the best model in the sense of Akaike's Information Criterion (AIC). This is consistent with the finding that only these models are identifiable. The lower Akaike weights of the empirical and non-reduced models can be explained by the presence of (additional) non-identifiable parameters.

To allow a graphical inspection by reaction progress kinetic analysis (Blackmond, 2005)

of the two favorable models identified by IMI, the rates for the main reactions were normalized to provide new functions, which only depend on one substrate concentration. For the reduced Jolly mechanism, the rate R_1 of the main reaction is normalized by the catalyst and the methanol concentrations to provide a new function depending only on butadiene concentration:

$$\frac{R_1}{[\mathrm{Pd_{act}}][\mathrm{M}]} = \frac{K_1^{Jolly}[\mathrm{B}]^2}{1 + K_2^{Jolly}[\mathrm{B}]^2} = f_1([\mathrm{B}]). \tag{4.14}$$

Likewise, the rate R_1 for the reduced dipalladium mechanism is normalized by the catalyst concentration and by the square of the butadiene concentration to provide a new function depending only on the methanol concentration:

$$\frac{R_1}{[\mathrm{Pd_{act}}][\mathrm{B}]^2} = K_1^{Dipa}[\mathrm{M}] = g_1([\mathrm{M}]). \tag{4.15}$$

An evaluation of the model structures' validity for the reduced Jolly and dipalladium mechanisms is possible, if the normalized reaction rates are plotted as a function of butadiene or methanol, respectively. These plots are shown in Figure 4.5.

The experimental data for experiments with different initial conditions show a much better match with the reduced Jolly mechanism at the top than with the reduced dipalladium mechanism at the bottom. Hence, this graphical analysis confirms the ranking results of the IMI. Still, the normalized reaction rates do not align completely for the reduced Jolly mechanism (Figure 4.5, top). The deviations, especially at the beginning of the experiments with crude C_4[1], can be explained by the neglected catalyst activation reaction and by experimental errors (cf. Völkl et al., 2015).

[1]The reaction progresses from right to left, because reactant concentration decreases over the course of the reaction.

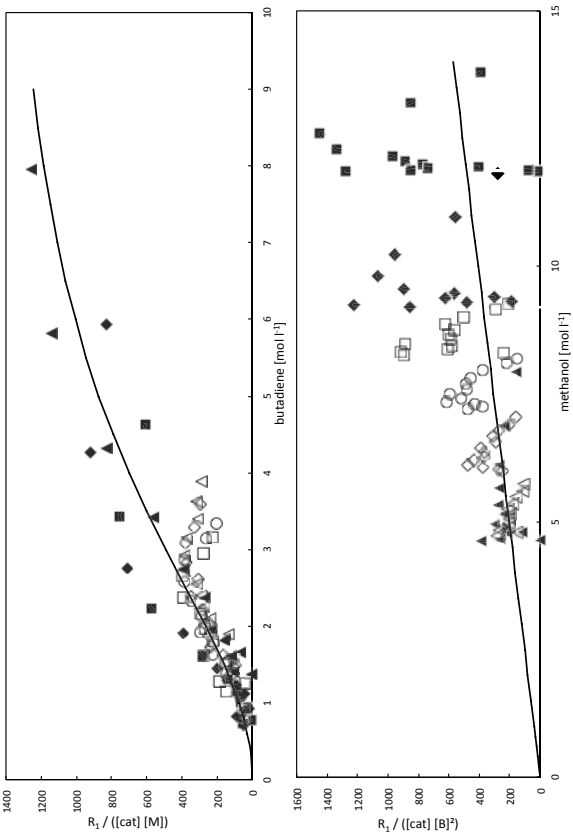

Figure 4.5: Normalized measured reaction rates and identified rate equations (line) for Pd/TPP; reduced Jolly mechanism (top); reduced dipalladium mechanism (bottom). Solid symbols refer to experiments with pure 1,3-butadiene, open symbols to experiments with crude C_4.

A simultaneous parameter estimation has been performed for the more promising reduced Jolly mechanism to obtain statistically sound parameter values and to calculate their corresponding confidence intervals. The parameter estimation is constrained by a dynamic model for the batch experiments consisting of the following mass balance equations:

$$\frac{d[\mathrm{Pd_{pre}}]}{dt} = -R_0 \tag{4.16}$$

for the Pd-precursor concentration,

$$\frac{d[\mathrm{Pd_{act}}]}{dt} = R_0 \tag{4.17}$$

for the active catalyst concentration,

$$\frac{d[\mathrm{B}]}{dt} = -2R_1 - 2R_2 \tag{4.18}$$

for the butadiene concentration,

$$\frac{d[\mathrm{M}]}{dt} = -R_1 \tag{4.19}$$

for the methanol concentration,

$$\frac{d[\mathrm{P}]}{dt} = R_1 \tag{4.20}$$

for the 1-MODE concentration,

$$\frac{d[\mathrm{D}]}{dt} = R_2 \tag{4.21}$$

for the dimer concentration and

$$R_0 = K_0[\mathrm{Pd_{pre}}][\mathrm{B}]^2 \tag{4.22}$$

as rate equation for catalyst activation

$$R_1 = [\mathrm{Pd_{act}}]\frac{K_1^{Jolly}[\mathrm{M}][\mathrm{B}]^2}{1 + K_2^{Jolly}[\mathrm{B}]^2} \tag{4.23}$$

$$R_2 = [\mathrm{Pd_{act}}]K_4^{Jolly}[\mathrm{M}][\mathrm{B}]^2 \tag{4.24}$$

Table 4.6: Parameter values and confidence intervals for Pd/TPP after simultaneous correction step.

parameter	estimated value	95% confidence interval
K_0	0.75	0.23
K_1^{Jolly}	66.1	1.6
K_2^{Jolly}	0.03	0.002
K_4^{Jolly}	3.19	0.3

as rate equations for product formation according to the reduced Jolly mechanism.

The resulting parameter estimates and their confidence intervals are shown in Table 4.6. The uncertainties represented by the confidence intervals are less than 10% of the nominal parameter values, except in case of parameter K_0. As discussed before, a reliable estimation of this parameter is difficult, since the reaction rate of the catalyst activation cannot be suitably accessed by the available measurements. For the main reaction, the model exhibits second-order dependency in butadiene and first-order in methanol at moderate to low butadiene concentrations. This is in agreement with the slow reaction progress towards the end of the reaction, especially for the experiments with crude C_4 (cf. Figure 4.6). At very high butadiene concentrations, the expression $K_2^{Jolly}[B]^2$ is much larger than 1 meaning that the reaction only depends on the methanol concentration in this range of butadiene concentration. This aligns with the approximately linear butadiene consumption (zero order dependency) in the first hour of the reaction for all experiments.

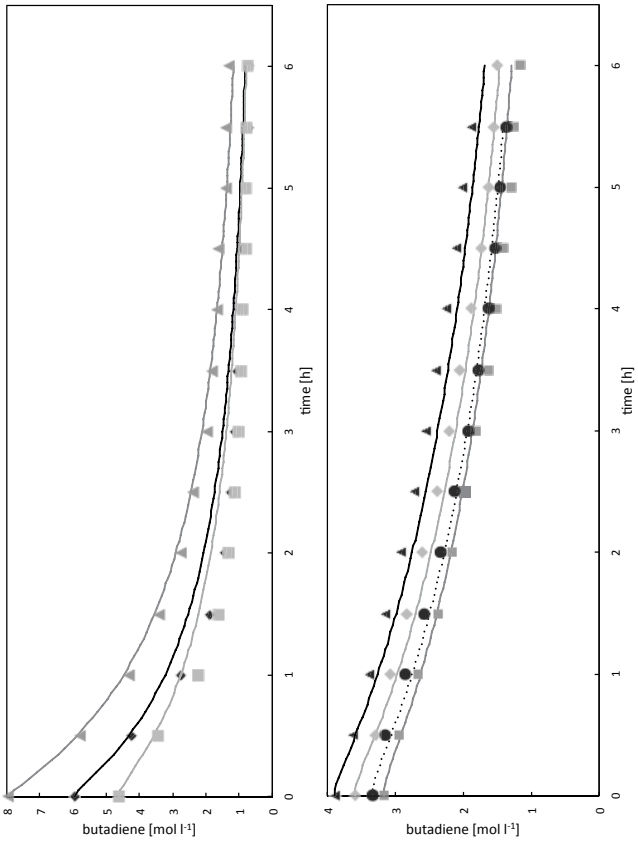

Figure 4.6: Results of simultaneous parameter estimation for the Pd/TPP with the model for reduced Jolly mechanism. Top: experiments with pure 1,3-butadiene, bottom: experiments with crude C_4.

Pd/IMes catalyst

The systematic identification approach presented above has also been applied to the Pd/IMes catalyst. Since the amount of side-product is very small in this case, the rate for the side reaction is set to zero for all model candidates and IMI is performed for the rate equation of the main reaction only.

Table 4.7 shows the results of the IMI for the Pd/IMes catalyst. Here, the unidentifiable, empirical model yields the highest Akaike weight, while the Akaike weights for all models resulting from mechanistic considerations are at least an order of magnitude lower. In contrast to the Pd/TPP catalyzed reaction, the penalization of the (additional) non-identifiable parameters of the empirical model is more than compensated by the better match with the experimental data. This is consistent with graphical findings from reaction progress kinetic analysis (Blackmond, 2005) shown in Figure 4.7, which reveals that neither the normalized reaction rates for the reduced Jolly mechanism nor for the reduced dipalladium mechanism fall on top of each other. It consequently can be concluded that the reaction with the Pd/IMes catalyst does not follow the kinetic mechanism observed for Pd/TPP. Therefore, a completely different dependency on the concentrations of the involved components has been derived and studied in further experiments.

By variation of the base concentration, a strong influence on the reaction rate was observed resembling a first-order dependency in the base concentration. This strong influence was already discussed in the literature (Tschan, Garcia-Suarez, Freixa, Launay, Hagen, Benet-Buchholz and van Leeuwen, 2010). In contrast, a change of the butadiene concentration did not show an effect on the reaction rate meaning that the telomerization reaction with the Pd/IMes catalyst is of zeroth order in the butadiene concentration. For the methanol variation, the observed behavior was completely different. The reaction rate decreased with increasing methanol, meaning that methanol shows a negative effect on the telomerization reaction. One possible reason for this might be that the nucleophilicity of the base changes with changing methanol concentration. The methoxide anion of the base will possibly be a much better nucleophile at lower concentration of the protic solvent methanol. An alternative is that there is an equilibrium between bound methoxide and

Table 4.7: Results of incremental model identification for Pd/IMes.

	rate equation	Akaike weights
Jolly mechanism	(4.6)	0.019
reduced Jolly mechanism	(4.10)	0.054
dipalladium mechanism	(4.4)	≤ 0.001
reduced dipalladium mechanism	(4.8)	≤ 0.001
empirical	(4.12)	0.926

bound methanol, either through displacement of bound methoxide by methanol or by protonation of bound methoxide by methanol (these are kinetically indistinguishable). If only the methoxide complex can carry the mechanistic cycle, this would also give a first-order dependency on base and a dependency on methanol of order -1.

The utilized model-based experimental analysis strategy does not allow to consider reaction steps which occur outside the catalytic cycle. Thus, the aspects and dependencies worked out in the experiments have to be incorporated directly into the catalytic cycle. Based on the experimental data, it is concluded that the Pd/IMes catalyst requires the presence of the base to proceed the reaction. The bound methoxy is not strong enough to attack the allyl-group in an intramolecular fashion, but rather activates this part of the carbon chain for intermolecular attack by another methoxide under release of the bound methoxide. Thus, without a strong base, the reaction would stop at this point. In addition, methanol was shown to have a negative influence. To account for this, we considered the nucleophilicity of the base to be represented in the adapted mechanism as a function of the protic methanol (cf. Figure 4.8).

With this formal modification of the Jolly mechanism, a kinetic model could be derived applying the procedure described by Chern (2000) and assuming all reactions except the product release to be reversible. The resulting rate equations

$$R_1 = [\mathrm{Pd_{act}}]\frac{K_1^{adJolly}[\mathrm{B}]^2[\mathrm{KO}]}{1 + K_2^{adJolly}[\mathrm{B}]^2[\mathrm{M}][\mathrm{KO}] + K_3^{adJolly}[\mathrm{B}]^2[\mathrm{KO}] + K_4^{adJolly}[\mathrm{B}]^2[\mathrm{M}] + K_5^{adJolly}[\mathrm{B}]^2 + K_6^{adJolly}[\mathrm{KO}]} \tag{4.25}$$

for the adapted Jolly mechanism and the reduced, identifiable model

$$R_1 = [\mathrm{Pd_{act}}]\frac{K_1^{adJolly}[\mathrm{B}]^2[\mathrm{KO}]}{1 + K_4^{adJolly}[\mathrm{B}]^2[\mathrm{M}] + K_6^{adJolly}[\mathrm{KO}]} \tag{4.26}$$

incorporate the dependency on the base concentration [KO]. They are subsequently utilized for an additional IMI.

Table 4.8 shows the results of IMI for the Pd/IMes catalyst with the models derived from the adapted Jolly mechanism. Based on the Akaike weights, the new derived models outperform the empirical model. This once more encourages the derivation of mechanistically motivated models for catalytic reactions. The reduced model derived from the adapted Jolly mechanism, the parameters of which are all identifiable, shows the highest Akaike weight. A graphical analysis by reaction progress analysis for this rate equation is not possible, since the reaction rates cannot be normalized to result in a function depending only on one reactant concentration. This fact underlines the advantages of the analytical approach of IMI over the graphical approach followed by reaction progress analysis.

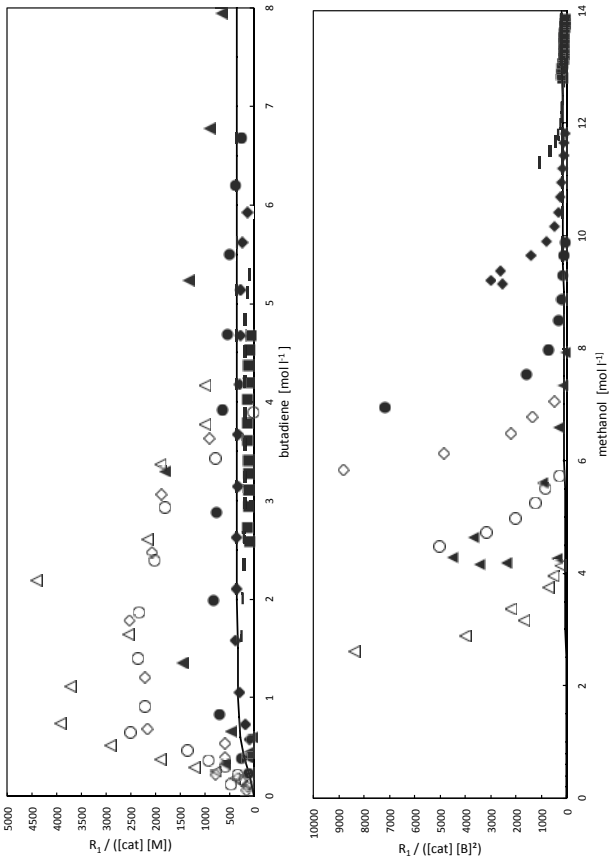

Figure 4.7: Normalized measured reaction rates and identified rate equations (line) for Pd/IMes; reduced Jolly mechanism (top); reduced dipalladium mechanism (bottom). Solid symbols refer to experiments with pure 1,3-butadiene, open symbols to experiments with crude C_4.

Table 4.8: Results of incremental model identification for Pd/IMes with models derived from the adapted mechanism.

	rate equation	Akaike weights
Jolly mechanism	(4.6)	< 0.001
reduced Jolly mechanism	(4.10)	< 0.001
dipalladium mechanism	(4.4)	< 0.001
reduced dipalladium mechanism	(4.9)	< 0.001
empirical	(4.12)	0.001
adapted Jolly mechnism	(4.25)	0.048
reduced adapted Jolly mechanism	(4.26)	0.951

Again, a simultaneous parameter estimation with the dynamic model for the batch experiments presented above is executed with the following rate equations for the reduced model derived from the adapted Jolly mechanism:

$$R_0 = K_0[B]^2[Pd_{pre}], \tag{4.27}$$

$$R_1 = [Pd_{act}]\frac{K_1^{adJolly}[B]^2[KO]}{1 + K_4^{adJolly}[B]^2[M] + K_6^{adJolly}[KO]}. \tag{4.28}$$

The confidence intervals of the estimated parameters are shown in Table 4.9 together with their nominal values. The confidence intervals are once more less than 10% of the nominal value, except for K_0 as expected according to the analysis above. At high to moderate butadiene concentrations, the model gives a zero-order dependency in butadiene, a first-order dependency in base and a negative influence of methanol (cf. Figure 4.9). Only at very high base concentrations, the reaction is independent of the base concentration. At the end of the reaction, when the butadiene concentration is low, the Pd/IMes catalyzed telomerization is of second-order in butadiene. It has to be noted that the model does not fully align with the experimental data which reveals that the heuristic modification of the Jolly mechanism is not sufficient to describe all effects of the base. However, no mechanistically modified mechanism showed a better result in further studies.

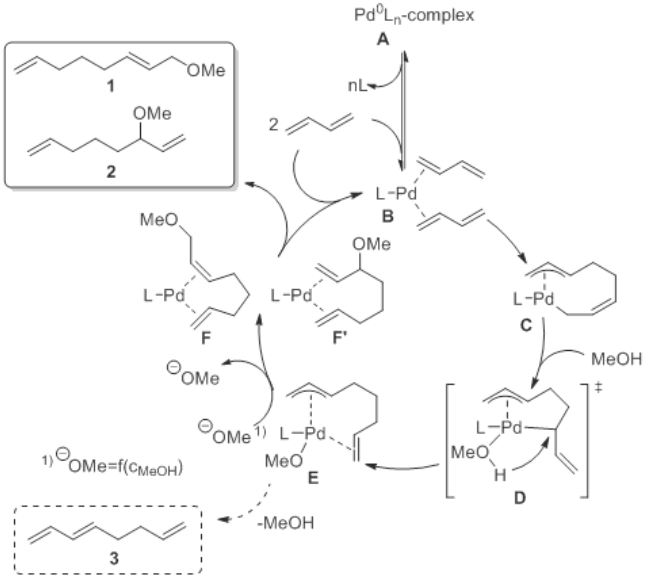

Figure 4.8: Adapted Jolly mechanism for the Pd/IMes catalyst.

Table 4.9: Parameter values and confidence intervals for Pd/IMes after simultaneous correction step.

parameter	estimated value	95% confidence interval
K_0	620	> 1000
$K_1^{adJolly}$	50.3e6	41e4
$K_4^{adJolly}$	19.3	1.6
$K_6^{adJolly}$	3417	292

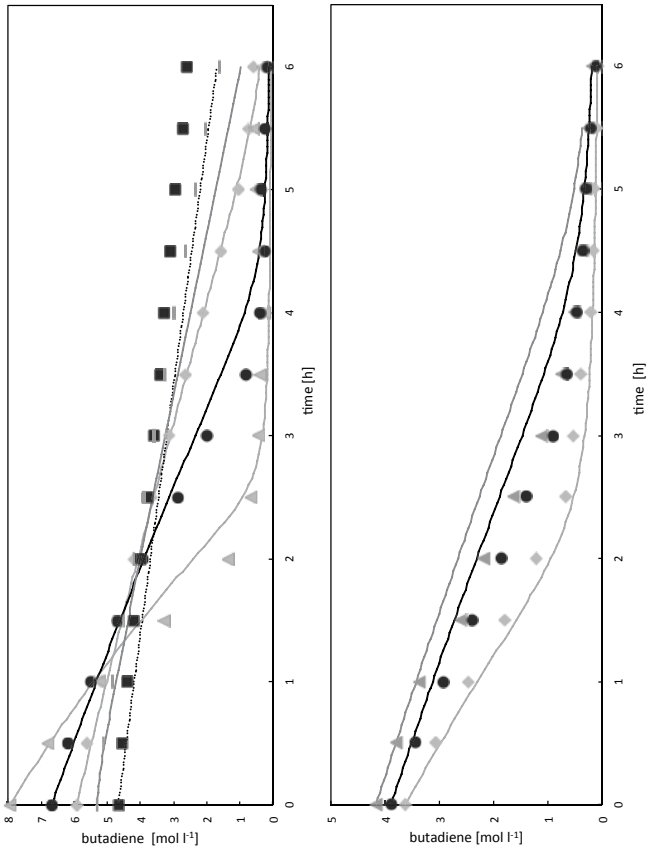

Figure 4.9: Results of the simultaneous parameter estimation for Pd/IMes with the reduced model for the adapted Jolly mechanism. Top: experiments with pure 1,3-butadiene, bottom: experiments with crude C_4.

4.1.5 Separation system

Having carried out an assessment of the kinetic behavior of the two identified catalysts, at this step the recycle structure is revisited and the separation system of the process is designed. Figure 4.10 shows a flowsheet for the telomerization process catalyzed by Pd/TPP which is based on the Dow process as described by Krissmann et al. (2008). Hereby, crude C_4, MeOH and the Pd/TPP catalyst (streams 1-3) are mixed with the recyles (streams 13 and 17) and fed to the reactor (stream 4). The reactor effluent (stream 5) is fed to a distillation column which separates the C_4/MeOH-mixture (stream 7) from the telomers (stream 6). The telomers are consequently separated into a 1-MODE rich stream (stream 9) and a stream containing the by-product 3-MODE (stream 8). Since an excess of butadiene can be used to increase the reaction rate especially at the end of the reaction (cf. Section 4.1.4), a butadiene recovery system is included in the flowsheet. Due to the azeotropic behaviour of the C_4 cut, separation by simple distillation is not possible. Therefore, the C_4/MeOH mixture (stream 7) is passed to an extractive distillation column. As suggested by Kroper, Weitz and Wagner (1962), N-methylpyrrolidone (NMP) is used as entrainer to separate the 1,3-butadiene from the remaining C_4/MeOH-mixture (stream 11). A distillation column is used to separate NMP (stream 12) and 1,3-butadiene (stream 13), which is recycled to the reactor. Subsequently, a further extractive distillation column is used to allow the recovery of potential excess MeOH, which also can be used to increase the reaction rate. The remaining C_4 cut (raffinate-I) leaves the process (stream 15). Water is used as entrainer for this separation as suggested by Krissmann et al. (2008). It is recovered in a last distillation column and purified MeOH (stream 17) is recycled to the reactor.

The main problem of the Pd/TPP process is the catalyst degradation which leads to high cost for catalyst and separation of the unconverted reactants. Therefore, a different catalyst based on Pd modified with IMes has been identified as alternative option. Figure 4.11 shows a process tailored for the Pd/IMes catalyst. Hereby, crude C_4, the Pd/IMes catalyst, and the necessary base (streams 1-3) are mixed with the recycles (streams 8 and 14) and fed to the reactor (stream 5). Since an excess of MeOH would lead to a decrease of the reaction rate (cf. Section 4.1.4), the recycle structure for this process is revisited. The MeOH recycle is removed from the flowsheet since an excess of MeOH would decrease the catalyst activity and consequently increase the operating cost of the Pd/IMes process. Furthermore, the MeOH feed is not mixed with the other reagents, but fed to the reactor by sidestreams (stream 4). The Pd/IMes catalyst remains active at the end of the reaction. Therefore, it is possible to use the high molecular weight of the catalyst to retain it with a nanofiltration membrane while permeating the resting mobile phase. Consequently, a membrane module is inserted in the Pd/IMes process to partly recover and recycle the

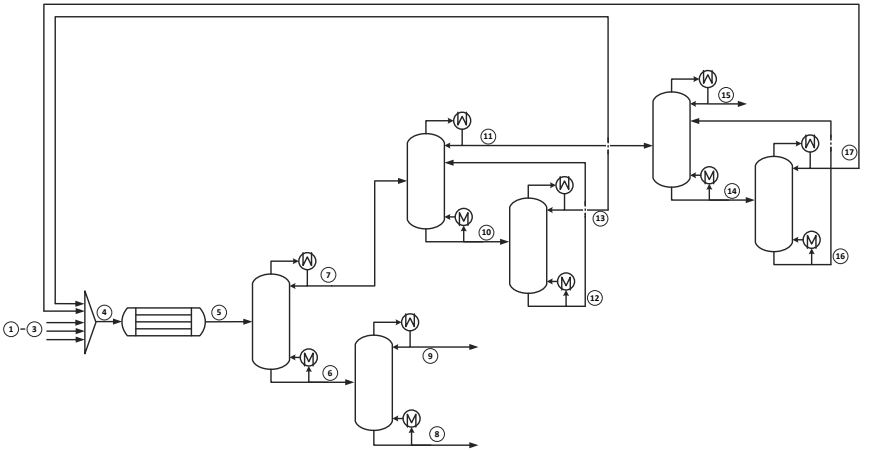

Figure 4.10: Flowsheet for Pd/TPP process.

catalyst (stream 8). The permeate (stream 7) is fed to a distillation column which separates the C_4 cut (stream 10) from the product 1-MODE and the remaining catalyst (stream 9). Due to the higher selectivity of the catalyst, no further purification is necessary. Similar to the Pd/TPP process, the C_4 cut is passed to an extractive distillation column, where NMP is used as entrainer to recover an 1,3-butadiene excess from the remaining raffinate-I (stream 12). Subsequently, a distillation column is used to recover NMP (stream 13) from 1,3-butadiene (stream 14), which is recycled to the reactor.

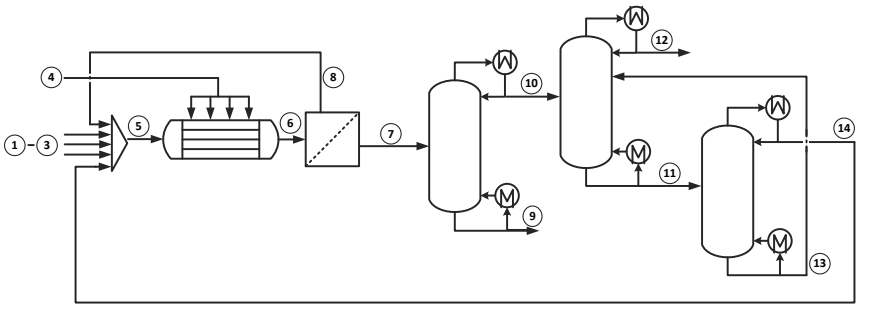

Figure 4.11: Flowsheet for Pd/IMes process.

4.2 Optimization with shortcut models

After designing flowsheet candidates for a Pd/TPP and a Pd/IMes process, these flowsheets are consequently economically evaluated with the help of shortcut models in this step. The iterative procedure described in Section 2.2 is employed to allow the evaluation of the flowsheet candidates with low computational effort. The optimal operating point of the process variant is found by minimizing the economic objective function $C_{Op} = C_{Raw} + C_{Cat} + C_{Sep}$ with the additional cost factors and process constraints given in Table 4.10. The objective function reflects the operational cost of the process and consists of the cost of raw material loss, C_{Raw}, the cost of catalyst, C_{Cat}, and the energy cost for separation, C_{Sep}. For the evaluation of both alternatives, the reaction kinetic models derived in Section 4.1.4 are utilized while the VLE is modeled using UNIFAC with parameters taken from the ASPEN® APV73 database. For the Pd/IMes process, the membrane module is modeled as a splitter. The split factors for the retentate are set to 90% for the catalyst and 10% for the remaining stream. These split factors could be achieved in laboratory experiments for a single membrane and it is supposed that a membrane cascade can even exceed these ratios (Maschmeyer, 2014).

Table 4.10: Additional cost factors and process constraints for economic evaluation.

$C_{Pd/TPP}$	600 \$/mol
$C_{Pd/IMes}$	6000 \$/mol
C_{Base}	23 \$/mol
C_{Steam}	28 \$/MWh
reactor residence time	$\leq$ 10 h
raffinate-I purity	$\leq$ 5mol% water
raffinate-I purity	$\leq$ 1mol% MeOH
1-MODE purity	$\geq$ 99%

The optimization results obtained by utilization of the iterative shortcut evaluation methodology described in Section 2.2 are shown in Table 4.11. For the Pd/TPP process, only 17% of the 1,3-butadiene fed to the reactor is converted at the optimal operating point (cf. Table 4.12). Additionally, MeOH is fed to the reactor in a MeOH to 1,3-butadiene ratio of 1.4 to further increase the catalyst activity. This leads to high separation cost to recover the unconverted raw material, but results in a turnover number (TON) for the Pd/TPP catalyst of $5.3 \cdot 10^5$. However, the high separation cost to recover the unconverted 1,3-butadiene and MeOH as well as the high cost for catalyst are restricting the process economics. For the Pd/IMes process, the 1,3-butadiene conversion is increased by 12% to 29% compared to the Pd/TPP process (cf. Table 4.13). This leads to lower cost for separation as less unconverted raw material has to be recycled. As mentioned

before, MeOH is fed to the reactor stoichiometrically. This further reduces the cost for separation and leads to a simpler distillation sequence since no unconverted MeOH needs to be recycled. Compared to the Pd/TPP system, the TON of the Pd/IMes catalyst is significantly increased by the catalyst recycle, with a calculated value of $4.7 \cdot 10^6$. All in all, the Pd/IMes process shows a reduction of more than 75% operational cost compared to the Pd/TPP process. Considering the economic potential for a 1-octene production process of $\Phi = 42 \cdot 10^6$ \$/a calculated in Section 4.1.2, the low operational cost of the Pd/IMes process of $C_{Op} = 4.0 \cdot 10^6$ \$/a shows the potential of this process.

Table 4.11: Results of shortcut evaluation for the Pd/TPP and the Pd/IMes processes.

	C_{Raw} [10^6\$/a]	C_{Cat} [10^6\$/a]	C_{Sep} [10^6\$/a]	C_{Op} [10^6\$/a]
Pd/TPP process	0.6	8.1	8.0	16.7
Pd/IMes process	0	1.6	2.4	4.0

Table 4.12: Flow rate and mole fraction table for Pd/TPP process after shortcut evaluation.

	N $[mol/s]$	$x_{isobutane}$	$x_{isobutene}$	$x_{n-butene}$	$x_{butadiene}$	$x_{n-butane}$	$x_{methanol}$	x_{water}	x_{NMP}	x_{3-Mode}	x_{1-Mode}	x_{cat}
1	119.373	0.03	0.25	0.2	0.45	0.07	0	0	0	0	0	0
2	25	0	0	0	0	0	1	0	0	0	0	0
3	4.7e-5	0	0	0	0	0	0	0	0	0	0	1
4	423.717	0.008	0.07	0.056	0.35	0.02	0.495	0	0	0	0	1.11e-6
5	371.859	0.01	0.08	0.064	0.254	0.022	0.497	0	0	0.005	0.067	1.26e-6
6	26.859	0	0	0	0	0	0	0	0	0.069	0.931	17.5e-6
7	344.999	0.01	0.087	0.066	0.274	0.024	0.535	0	0	0	0	0
8	25	0	0	0	0	0	0	0	0	0	1	18.8e-6
9	1.859	0	0	0	0	0	0	0	0	1	0	0
10	203.898	0	0	0	0	0	0.905	0.095	0	0	0	0
11	160.262	0.022	0.186	0.149	0.59	0.052	0	0	0	0	0	0
12	19.324	0	0	0	0	0	0	1	0	0	0	0
13	184.737	0	0	0	0	0	1	0	0	0	0	0
14	212.757	0	0	0	0.445	0	0	0	0.556	0	0	0
15	65.655	0.055	0.455	0.364	0	0.127	0	0	0	0	0	0
16	118.203	0	0	0	0	0	0	0	1	0	0	0
17	94.606	0	0	0	1	0	0	0	0	0	0	0

Table 4.13: Flow rate and mole fraction table for Pd/IMes process after shortcut evaluation.

	N $[mol/s]$	$x_{isobutane}$	$x_{isobutene}$	$x_{n-butene}$	$x_{butadiene}$	$x_{n-butane}$	$x_{methanol}$	x_{NMP}	x_{1-Mode}	x_{cat}	x_{base}
1	111.107	0.03	0.25	0.2	0.45	0.07	0	0	0	0	0
2	25	0	0	0	0	0	1	0	0	0	0
3	5.33e-6	0	0	0	0	0	0	0	0	1	0
4	9.9e-4	0	0	0	0	0	0	0	0	0	1
5	156.666	0.024	0.197	0.158	0.549	0.055	0	0	0.018	0.68e-6	7.02e-6
6	131.667	0.028	0.234	0.188	0.273	0.066	0	0	0.211	0.81e-6	8.35e-6
7	118.501	0.028	0.234	0.188	0.273	0.066	0	0	0.211	0.05e-6	8.35e-6
8	13.167	0.028	0.234	0.188	0.273	0.066	0	0	0.211	7.7e-6	8.35e-6
9	25	0	0	0	0	0	0	0	1	0.702e-6	8.896e-5
10	93.501	0.036	0.297	0.238	0.346	0.083	0	0	0	0	0
11	132.575	0	0	0	0.244	0	0	0.756	0	0	0
12	61.109	0.055	0.455	0.364	0	0.127	0	0	0	0	0
13	100.224	0	0	0	0	0	0	1	0	0	0
14	32.392	0	0	0	1	0	0	0	0	0	0

4.3 Optimization with rigorous models

The results of the shortcut evaluation have shown that the Pd/IMes process significantly outperforms the Pd/TPP process in terms of operating cost. Consequently, the Pd/IMes process should be optimized with rigorous models to get more precise cost information. In order to accurately describe the highly non-ideal separation characteristics of membranes, a complex mass-transfer model is required (Melin and Rautenbach, 2007). The identification of such a model is, to date, only possible by postulating a specific model structure and identifying parameters from time-consuming experiments (Lutze and Gorak, 2013). Since such a membrane model is currently not available for the Pd/IMes separation, only the column sequence is optimized following the models and procedure presented in Section 2.3. This way, the feasibility of the splits is checked and more precise cost information for the columns are obtained at this stage of the process design.

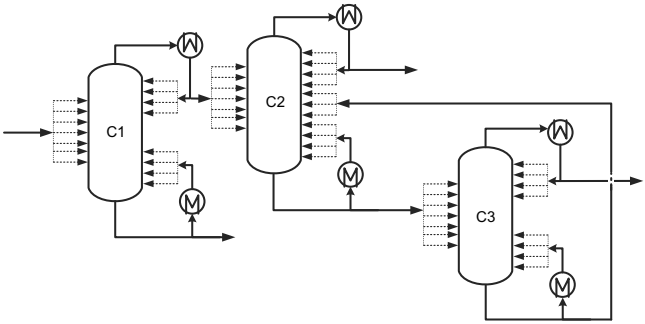

Figure 4.12: Column sequence for Pd/IMes process.

The results for the rigorous optimization of the column sequence superstructure displayed in Figure 4.12 are shown in Table 4.14. For this calculation, the feed to the column sequence has been set to the value obtained by the shortcut evaluation (cf. Table 4.13). Since the TAC include the investment cost for the columns, the operating cost is slightly increased compared to the results for the shortcut evaluation. Nevertheless, the results are within reasonable limits and all splits are feasible. Therefore, it can be concluded that the Pd/IMes catalyzed process outperforms the Pd/TPP process in terms of TAC and should be further investigated in pilot-scale experiments.

Table 4.14: Detailed column configurations for Pd/IMes process

	column 1	column 2	column 3
TAC $[10^6\$/a]$	0.5	1.5	1.7
operating cost $[10^6\$/a]$	0.4	1.2	1.5
investment cost $[10^6\$/a]$	0.1	0.3	0.2
reboiler duty $[MW]$	1.8	5.3	6.9
condenser duty $[MW]$	1.9	0.9	1.2
number of trays	9	73	3
fresh feed tray	7	49	3
entrainer feed tray	-	1	-
entrainer / fresh feed ratio	-	1.9	-
diameter $[m]$	3.2	2.3	2.3

4.4 Pilot plant experiments

Within the EU project SYNLFOW [2], a long-term pilot plant experiment for the Pd/IMes process was performed at Evonik Industries (Maschmeyer, 2014). They observed that the initial catalyst loading was deminishing by more than 90% within 1000 h process time. Since the membrane showed a good retention of the catalyst in previous experiments (cf. Section 4.1.5) they concluded that the catalyst precipitated during the experiment. Therefore, the Pd/IMes process without immobilization but with downstream separation of the catalyst by a membrane is not stable. Consequently, different immobilization approaches for the catalyst have to be investigated in order to design an economic attractive and stable butadiene telomerization process.

The use of ionic liquids as catalyst immobilization phase in telomerization reactions has already been reported by Magna et al. (2003). However, the catalyst recycling of the homogeneous catalyst by the use of ionic liquids is complicated significantly since the MeOH acts as strong phase-transfer agent. Consequently, the application of a biphasic reaction system for catalyst immobilization requires the appropriate choice of the ionic liquid. Völkl et al. (2016) conducted an *in silico* screening of 960 different ionic liquids with COSMO-RS (Klamt and Eckert, 2000). However, Pd/TPP as well as Pd/IMes showed only poor immobilization efficiencies in the experiments with the selected ionic liquids. The determined leaching was in the range of up to 50% of the initial Pd content. However, Völkl et al. (2016) showed that for the threefold sulfonated derivative of the TPP ligand (TPPTS) the leaching of the Pd catalyst could be lowered by a factor of four. Despite its lower activity, the Pd/TPPTS catalyst turned out to be stable for more than 200 h in continuous experiments. The measured Pd-leaching was found to be only between 20 and

[2] http://www.synflow.eu

200 $ppm\ h^{-1}$ of the initial Pd content which corresponds to an amount of less than 3 ppm Pd in the exit stream. A threefold sulfonated derivative of the IMes ligand (IMesTS) might combine the better reaction performance of Pd/IMes with the high immobilization stability of Pd/TPPTS. It should therefore be synthesized and tested in laboratory experiments to investigate its potential for a butadiene telomerization process.

4.5 Conclusions

The telomerization of 1,3-butadiene with methanol is the key step of the commercial route developed by Dow Chemicals to produce 1-octene. The main problem of the commercially used process is the catalyst degradation which leads to high cost for catalyst and separation. In this chapter, a conceptual design study for a butadiene telomerization process is presented. In this design study, the heuristic variant generation methodology presented in Chapter 3 and the optimization-based evaluation methods presented in Chapter 2 are combined. Therefore, the - often neglected - impact of the catalyst selection on the process economics can be assessed.

Within the study, laboratory experiments are integrated to facilitate the process design. The thorough model identification procedure employed in this study also demonstrates that the derivation of mechanistically motivated models for catalytic reactions should be preferred over blindly relying on postulated empirical models. Furthermore, this study shows that kinetic reaction progress analysis is a valuable tool, but is clearly limited in case of complex reaction mechanisms. Still, it can be a valuable tool also in these cases if it is combined with thorough model identification methodologies. In this sense, the procedures for elucidating mechanisms in complex chemical reactions and reaction kinetic modeling described in this work are of a more general nature and should be considered to better understand and optimize other catalytic reaction systems.

As a result of the design study, a novel process is designed and evaluated. This homogeneously catalyzed Pd/IMes process significantly outperforms the process with the commercially used Pd/TPP catalyst in terms of raw material and catalyst cost, as well as energy demand for separation. The operational cost for this process are more than 75% lower compared to the commercially used process. However, this process showed to be not stable in pilot plant experiments due to catalyst precipitation. Consequently, alternative immobilization strategies should be investigated in future work.

First laboratory experiments have shown that a threefold sulfonated derivative of the Pd/TPP catalyst could be run stable for more than 200 h. If a threefold sulfonated derivative of the Pd/IMes catalyst shows the same low leaching a novel Pd/IMesTS catalyzed process might have the potential to replace classical processes for the production of 1-octene, such as Fischer Tropsch-synthesis or the oligomerization of ethylene, and should be further investigated.

5 Conclusions and final thoughts

In industrial practice, conceptual process design is typically conducted by repetitive simulation studies, which require detailed design specifications in an early design phase. Guided by heuristics, these iterative solution procedures result in high manual effort and, in addition, no guarantee concerning the quality of the solution can be given. Various authors have therefore suggested the use of surrogate models, which do not require detailed specifications. Others have developed methods for the optimization-based process design by means of superstructure optimization. Marquardt et al. (2008) proposed a framework for an optimization-based design of hybrid separation processes, which combines shortcut and rigorous evaluation steps. This framework has been successfully demonstrated for conceptual design of various processes (see, e.g., Krämer et al., 2011).

In this thesis, the process design framework of Marquardt et al. (2008) is extended towards the optimization-based design of reaction-separation processes. For this purpose, powerful shortcut and rigorous evaluation methods for reactor networks and reaction-separation processes are proposed. It is important to emphasize that all of these methods are developed to be computationally efficient in order to allow an optimization-based design and analysis of large-scale processes. As a consequence, cost-optimal process solutions can be obtained with considerably less effort compared to the use of tedious repetitive simulation studies. It also has to be stressed that the performance of all methods is validated by large-scale industrial case studies. Thus, it is shown that the process design framework can contribute decisively towards the sustainable solution of today's challenging design problems in chemical engineering.

After classical design methods for reactor networks, separation systems and reaction-separation processes are reviewed in Chapter 1, the extension of the framework to reaction-separation processes is presented in Chapter 2. The necessary extensions of both, the shortcut evaluation methodology for the pre-selection of flowsheets and the rigorous optimization procedure integrate existing and new approaches. After all of these advancements, the process optimization problem minimizing total annualized cost and adjusting all degrees of freedom simultaneously is solved robustly within a few hours computational time. In addition, the time for developing new and innovative processes can be significantly reduced and the quality of the result is improved at the same time.

The limitations of the framework is that the generation of alternative flowsheet variants still requires expert knowledge and experience in order to come up with good alternatives and as such the approach is not completely systematic. Especially for catalytic processes, the necessary insight into the reaction cannot be generated fully *in silico*, but requires laboratory experiments to determine important process parameters. To support this process, an extension of the well known heuristic proposed by Douglas (1988) for the generation of catalytic process variants is presented in Chapter 3. In this procedure, some decisions related to the catalyst are explicitly addressed and laboratory experiments are integrated into the design procedure.

In Chapter 4, the industrial case study for telomerization of 1,3-butadiene with methanol is addressed in order to demonstrate the capabilities of the extended process synthesis framework. This reaction is the key step of a novel route for 1-octene production. To allow the utilization of the optimization-based design methods proposed in Chapter 2, two literature-known palladium catalysts for the telomerization of 1,3-butadiene with methanol are selected by the heuristic procedure presented in Chapter 3 and investigated by model-based experimental analysis. Based on the results a novel process for telomerization of 1,3-butadiene is designed and evaluated. This novel process significantly outperforms the current process in terms of raw material and catalyst cost, as well as energy demand for separation. The operational cost for this process are more than 75% lower compared to the commercially used process demonstrating the potential of careful conceptual design. However, the process shows to be not stable in long term pilot plant experiments. Consequently, a novel catalyst needs to be derived which might have the potential to replace classical processes for the production of 1-octene, such as Fischer Tropsch synthesis or the oligomerization of ethylene, and should be further investigated.

5.1 Open research topics

While this thesis presents a comprehensive methodology for the optimization-based design of reaction-separation processes, it also provides a foundation for further extensions. The two most important topics, according to the authors' assessment, are briefly illustrated in the following subsections.

Integration of model-based experimental analysis and process design

Reliable models for reaction and separation phenomena are the backbone of the model-based process design methodology presented in this thesis. These models are often unknown in the early design phase and need to be determined. Thus, data from laboratory experiments - often statistically designed - are used to identify a suitable model struc-

ture and to estimate its parameters. As model identification and process optimization are typically executed sequentially, the region of confidence of the resulting models might not match the relevant operating points of the process. Therefore, the model might not be suitable to reliably design the process, it can leave the designer with significant uncertainty concerning the predicted process performance and can complicate the decision making. To avoid this problem, optimal experiments should be designed for proper model identification, such that the uncertainty in the predicted process performance is minimized. Therefore, a new problem formulation for optimal experiment design (OED), which minimizes the confidence in the process design (τ) rather than the uncertainty in the model used in process design (σ), should be developed to overcome this limitation and embedded in a novel workflow for integrated model identification and process optimization (cf. Figure 5.1 and Recker et al., 2013). Through a simple case study, Recker et al. (2013) showed the potential in improving the process uncertainty by coupling process optimization and model identification. This example motivates the development of a systematic methodology that integrates process optimization and model identification through the propagation of process uncertainty into the latter.

Distributed flowsheet optimization

An effective way to increase robustness of the rigorous optimization is to decrease the number of equations of the flowsheet model. Although the number of equations of some unit models can be reduced, e.g., by utilizing a collocation method (cf. Section 2.3.1) or external functions (cf. Section 2.3.3) a more sophisticated optimization approach is desirable to simplify the industrial utilization of the model-based process design methodology presented in this thesis. A promising approach for such a more sophisticated optimization approach, which is currently used, e.g., for model-predictive control (Scheu and Marquardt, 2011), is the distributed optimization by sensitivity-based coordination (Scheu, Busch and Marquardt, 2010). Within this approach, the overall problem is solved by solving a sequence of subproblems, which are connected with one another via a communicator. The vigorous communication between the subsystems is realized by an adaption of the objective function of each subsystem, such that the subproblems can be solved independently from each other. This approach is in principle applicable to many fields of application. However, the nonlinearities encountered by recycle streams hinder the direct application to distributed flowsheet optimization even for simple problems. Nevertheless, such a distributed flowsheet optimization approach could simplify the application of the model-based process design methodology presented in this thesis to large-scale industrial processes and should be further investigated.

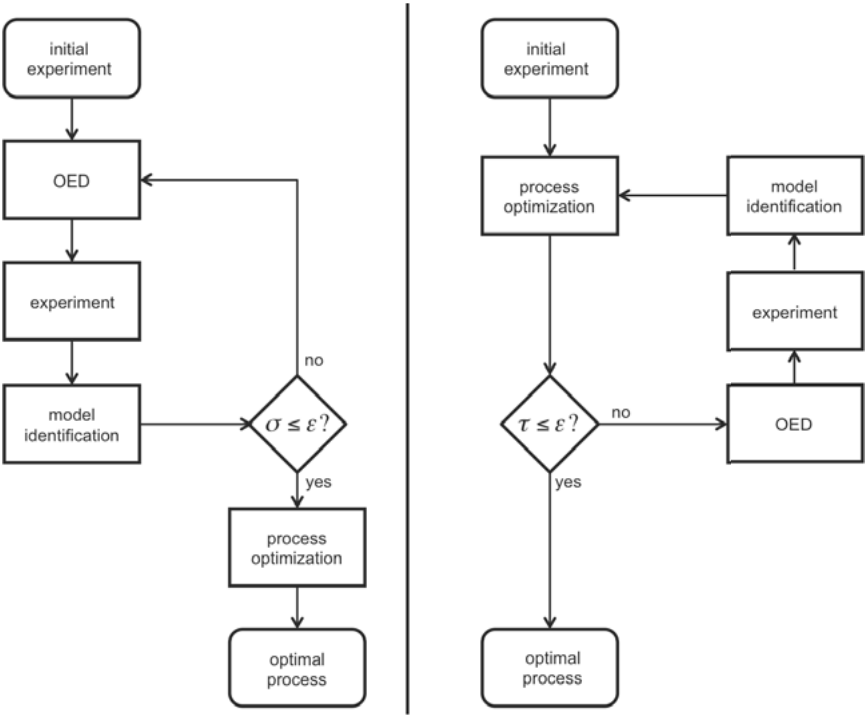

Figure 5.1: Left: sequential model identification and process optimization; right: envisioned integrated model identification and process optimization.

Bibliography

Abraham, T. and Feinberg, M. (2004): Kinetic bounds on attainability in the reactor synthesis problem, *Industrial & Engineering Chemistry Research* **43**(2), 449–457.

Aris, R. (1961): *The Optimal Design of Chemical Reactors*, Elsevier, Burlington.

Babi, D. K., Holtbruegge, J., Lutze, P., Gorak, A., Woodley, J. M. and Gani, R. (2015): Sustainable process synthesis–intensification, *Computers & Chemical Engineering* **81**, 218 – 244.

Balakrishna, S. and Biegler, L. (1993): A unified approach for the simultaneous synthesis of reaction, energy, and separation systems, *Industrial & Engineering Chemistry Research* **32**(7), 1372–1382.

Bard, Y. (1974): *Nonlinear Parameter Estimation*, Academic Press, New York.

Barnicki, S. D. and Fair, J. R. (1990): Separation system synthesis: a knowledge-based approach. 1. Liquid mixture separations, *Industrial & Engineering Chemistry Research* **29**(3), 421–432.

Barnicki, S. D. and Fair, J. R. (1992): Separation system synthesis: a knowledge-based approach. 2. Gas/vapor mixtures, *Industrial & Engineering Chemistry Research* **31**(7), 1679–1694.

Bauer, M. (1997): *Synthese und Optimierung nichtidealer Rektifizierprozesse*, Fortschritt-Berichte VDI: Reihe 3, Nr. 496, VDI-Verlag, Düsseldorf.

Bausa, J. (2001): *Shortcut-methods for Conceptual Design and Thermodynamic Analysis of Distillation Processes*, Fortschritt-Berichte VDI: Reihe 3, Nr. 692, VDI-Verlag, Düsseldorf.

Bausa, J., von Watzdorf, R. and Marquardt, W. (1998): Shortcut methods for nonideal multicomponent distillation: I. Simple columns, *AIChE Journal* **44**(10), 2181–2198.

Behr, A., Becker, M., Beckmann, T., Johnen, L., Leschinski, J. and Reyer, S. (2009): Telomerization: advances and applications of a versatile reaction, *Angewandte Chemie International Edition* **48**(20), 3598–3614.

Behr, A., Ilsemann, G. V., Keim, W., Krueger, C. and Tsay, Y. H. (1986): Octadienyl-bridged bimetallic complexes of palladium as intermediates in telomerization reactions of butadiene, *Organometallics* **5**(3), 514–518.

Biegler, L. T., Grossmann, I. E. and Westerberg, A. W. (1997): *Systematic Methods for Chemical Process Design*, Prentice Hall, Old Tappan.

Bilous, O. and Amundson, N. R. (1956): Optimum temperature gradients in tubular reactors: I. General theory and methods, *Chemical Engineering Science* **5**(2), 81–92.

Blackmond, D. G. (2005): Reaction progress kinetic analysis: a powerful methodology for mechanistic studies of complex catalytic reactions, *Angewandte Chemie International Edition* **44**(28), 4302–4320.

Blagov, S. and Hasse, H. (2002): Topological analysis of vapor–liquid equilibrium diagrams for distillation process design, *Physical Chemistry Chemical Physics* **4**(6), 896–908.

Bohley, R., Jacobsen, G., Pelt, H., Schaart, B., Schenk, M. and van Oeffelen, D. (1992): Process for producing 1-octene. WO 92/10450.

Brendel, M., Bonvin, D. and Marquardt, W. (2006): Incremental identification of kinetic models for homogeneous reaction systems, *Chemical Engineering Science* **61**(16), 5404–5420.

Brooke, A., Kendrick, D., Meeraus, A. and Raman, R. (2005): *GAMS, A User's Guide*, GAMS Development Corporation: Washington, DC.

Brüggemann, S. (2005): *Rapid Screening of Conceptual Design Alternatives for Distillation Processes*, Fortschritt-Berichte VDI, Nr. 841, VDI-Verlag, Düsseldorf.

Burnham, K. P. and Anderson, D. R. (2002): *Model Selection and Multimodel Inference: a Practical Information-theoretic Approach*, Springer Science & Business Media, New York.

Caballero, J. A. and Grossmann, I. E. (2008): An algorithm for the use of surrogate models in modular flowsheet optimization, *AIChE Journal* **54**(10), 2633–2650.

Carey, G. and Finlayson, B. A. (1975): Orthogonal collocation on finite elements, *Chemical Engineering Science* **30**(5), 587–596.

Chern, J.-M. (2000): General rate equations and their applications for cyclic reaction networks: Single-cycle systems, *Industrial & Engineering Chemistry Research* **39**, 4100–4105.

Clement, N. D., Routaboul, L., Grotevendt, A., Jackstell, R. and Beller, M. (2008): Development of palladium–carbene catalysts for telomerization and dimerization of 1, 3-dienes: From basic research to industrial applications, *Chemistry–A European Journal* **14**(25), 7408–7420.

Colberg, J., Koenig, S., Leahy, D. and Poechlauer, P. (2013): Go with the flow, *Innovations in Pharmaceutical Technology* **46**, 52–55.

Cole-Hamilton, D. J. (2003): Homogeneous catalysis – new approaches to catalyst separation, recovery, and recycling, *Science* **299**(5613), 1702–1706.

Cozad, A., Sahinidis, N. V. and Miller, D. C. (2014): Learning surrogate models for simulation-based optimization, *AIChE Journal* **60**(6), 2211–2227.

Cremaschi, S. (2015): A perspective on process synthesis: Challenges and prospects, *Computers & Chemical Engineering* **81**, 130–137.

Daniel, G. and Jobson, M. (2007): Conceptual design of equilibrium reactor-reactive distillation flowsheets, *Industrial & Engineering Chemistry Research* **46**(2), 559–570.

Denbigh, K. G. (1944): Velocity and yield in continuous reaction systems, *Transactions of the Faraday Society* **40**, 352–373.

Deuflhard, P. and Bornemann, F. (1994): *Numerische Methoden II: Integration gewöhnlicher Differentialgleichungen*, De Gruyter, Berlin.

Doherty, M. F. and Malone, M. F. (2001): *Conceptual Design of Distillation Systems*, McGraw-Hill, Boston.

Douglas, J. M. (1988): *Conceptual Design of Chemical Processes*, McGraw-Hill, New York.

Dowling, A. W. and Biegler, L. T. (2015): A framework for efficient large scale equation-oriented flowsheet optimization, *Computers & Chemical Engineering* **72**, 3–20.

Fahmi, I. and Cremaschi, S. (2012): Process synthesis of biodiesel production plant using artificial neural networks as the surrogate models, *Computers & Chemical Engineering* **46**, 105–123.

Falß, S., Tomaiuolo, G., Perazzo, A., Hodgson, P., Yaseneva, P., Zakrzewski, J., Guido, S., Lapkin, A., Woodward, R. and Meadows, R. E. (2016): A continuous process for Buchwald-Hartwig amination at micro-, lab-, and mesoscale using a novel reactor concept, *Organic Process Research & Development* **20**(2), 558–567.

Feinberg, M. (2000a): Optimal reactor design from a geometric viewpoint–III. Critical CFSTRs, *Chemical Engineering Science* **55**(17), 3553–3565.

Feinberg, M. (2000b): Optimal reactor design from a geometric viewpoint. Part II. Critical sidestream reactors, *Chemical Engineering Science* **55**(13), 2455–2479.

Feinberg, M. (2002): Toward a theory of process synthesis, *Industrial & Engineering Chemistry Research* **41**(16), 3751–3761.

Feinberg, M. and Ellison, P. (2001): General kinetic bounds on productivity and selectivity in reactor- separator systems of arbitrary design: Principles, *Industrial & Engineering Chemistry Research* **40**(14), 3181–3194.

Feinberg, M. and Hildebrandt, D. (1997): Optimal reactor design from a geometric viewpoint–I. Universal properties of the attainable region, *Chemical Engineering Science* **52**(10), 1637–1665.

Fox, J. A., Hildebrandt, D., Glasser, D. and Patel, B. (2013): A graphical approach to process synthesis and its application to steam reforming, *AIChE Journal* **59**(10), 3714–3729.

Franke, M., Gorak, A. and Strube, J. (2004): Design and optimization of hybrid separation processes, *Chemie Ingenieur Technik* **76**(3), 199–210.

Freund, H. and Sundmacher, K. (2008): Towards a methodology for the systematic analysis and design of efficient chemical processes: Part 1. From unit operations to elementary process functions, *Chemical Engineering and Processing: Process Intensification* **47**(12), 2051–2060.

Freund, H. and Sundmacher, K. (2011a): Process Intensification, 1. Fundamentals and Molecular Level, *Ullmann's Encyclopedia of Industrial Chemistry*, Wiley-VCH, Weinheim.

Freund, H. and Sundmacher, K. (2011b): Process Intensification, 2. Phase Level, *Ullmann's Encyclopedia of Industrial Chemistry*, Wiley-VCH, Weinheim.

Freund, H. and Sundmacher, K. (2011c): Process Intensification, 3. Process Unit Level, *Ullmann's Encyclopedia of Industrial Chemistry*, Wiley-VCH, Weinheim.

Freund, H. and Sundmacher, K. (2011d): Process Intensification, 4. Plant Level, *Ullmann's Encyclopedia of Industrial Chemistry*, Wiley-VCH, Weinheim.

Gassner, M. and Maréchal, F. (2009a): Methodology for the optimal thermo-economic, multi-objective design of thermochemical fuel production from biomass, *Computers & Chemical Engineering* **33**(3), 769–781.

Gassner, M. and Maréchal, F. (2009b): Thermo-economic process model for thermochemical production of synthetic natural gas (sng) from lignocellulosic biomass, *Biomass and Bioenergy* **33**(11), 1587–1604.

Gross, B. and Roosen, P. (1998): Total process optimization in chemical engineering with evolutionary algorithms, *Computers & Chemical Engineering* **22**, S229–S236.

Grossmann, I., Caballero, J. and Yeomans, H. (1999): Mathematical programming approaches to the synthesis of chemical process systems, *Korean Journal of Chemical Engineering* **16**(4), 407–426.

Guthrie, K. (1969): Data and techniques for preliminary capital cost estimating, *Chemical Engineering* **76**(6), 114–142.

Hagen, J. (2004): *Chemiereaktoren - Auslegung und Simulation*, Whiley-VCH, Weinheim.

Harwardt, A. (2013): *Systematic Design of Separations for Processing of Biorenewables*, Fortschritt-Berichte VDI: Reihe 3, Nr. 936, VDI-Verlag, Düsseldorf.

Harwardt, A., Kraemer, K., Rüngeler, B. and Marquardt, W. (2011): Conceptual design of a butyl-levulinate reactive distillation process by incremental refinement, *Chinese Journal of Chemical Engineering* **19**(3), 371–379.

Harwardt, A. and Marquardt, W. (2012): Heat-integrated distillation columns: Vapor recompression or internal heat integration?, *AIChE Journal* **58**(12), 3740–3750.

Hausoul, P. J., Parvulescu, A. N., Lutz, M., Spek, A. L., Bruijnincx, P. C., Weckhuysen, B. M. and Klein Gebbink, R. J. (2010): Facile access to key reactive intermediates in the pd/pr3-catalyzed telomerization of 1, 3-butadiene, *Angewandte Chemie* **122**(43), 8144–8147.

Hentschel, B., Peschel, A., Freund, H. and Sundmacher, K. (2014): Simultaneous design of the optimal reaction and process concept for multiphase systems, *Chemical Engineering Science* **115**, 69 – 87.

Hintermair, U., Franciò, G. and Leitner, W. (2011): Continuous flow organometallic catalysis: new wind in old sails, *Chemical Communications* **47**(13), 3691–3701.

Horn, F. (1961): C1. Optimale Temperatur- und Konzentrationsverläufe , *Chemical Engineering Science* **14**(1), 77 – 88.

Horn, F. (1964): Attainable and non-attainable regions in chemical reaction techniques, *in* R. Jottrand (ed.), *Chemical Reaction Engineering. Proceedings of the Third European Symposium*, Pergamon Press, Oxford, pp. 293 – 303.

Ismail, S. R., Pistikopoulos, E. and Papalexandri, K. (1999): Synthesis of reactive and combined reactor/separation systems utilizing a mass/heat exchange transfer module, *Chemical engineering science* **54**(13), 2721–2729.

Ismail, S. R., Proios, P. and Pistikopoulos, E. N. (2001): Modular synthesis framework for combined separation/reaction systems, *AIChE Journal* **47**(3), 629–649.

Jackstell, R., Gómez Andreu, M., Frisch, A., Selvakumar, K., Zapf, A., Klein, H., Spannenberg, A., Röttger, D., Briel, O., Karch, R. and Beller, M. (2002): A highly efficient catalyst for the telomerization of 1, 3-dienes with alcohols: First synthesis of a monocarbenepalladium (0)–olefin complex, *Angewandte Chemie International Edition* **41**(6), 986–989.

Jacobsen, G. B., Pelt, H. L. and Schaart, B. J. (1991): Continuous process for the telomerization of conjugated dienes. WO 91/09822.

Jaksland, C. A., Gani, R. and Lien, K. M. (1995): Separation process design and synthesis based on thermodynamic insights, *Chemical Engineering Science* **50**(3), 511–530.

Jensen, K. L. and Datta, R. (1995): Ethers from ethanol. 1. Equilibrium thermodynamic analysis of the liquid-phase ethyl tert-butyl ether reaction, *Industrial & Engineering Chemistry Research* **8**, 392–399.

Jolly, P., Mynott, R., Raspel, B. and Schick, K. (1986): Intermediates in the palladium-catalyzed reactions of 1, 3-dienes. The reaction of (. eta. 1,. eta. 3-octadiendiyl) palladium complexes with acidic substrates, *Organometallics* **5**(3), 473–481.

Kallrath, J. (2000): Mixed integer optimization in the chemical process industry: Experience, potential and future perspectives, *Chemical Engineering Research and Design* **78**(6), 809–822.

Kauchali, S., Rooney, W., Biegler, L., Glasser, D. and Hildebrandt, D. (2002): Linear programming formulations for attainable region analysis, *Chemical Engineering Science* **57**(11), 2015–2028.

Keim, W. (1968): Bimetallische π-Allylkomplexe von Nickel und Palladium, *Angewandte Chemie* **80**(22), 968–969.

Kirkwood, R., Locke, M. H. and Douglas, J. (1988): A prototype expert system for synthesizing chemical process flowsheets, *Computers & Chemical Engineering* **12**(4), 329–343.

Klamt, A. and Eckert, F. (2000): COSMO-RS: a novel and efficient method for the a priori prediction of thermophysical data of liquids, *Fluid Phase Equilibria* **172**(1), 43–72.

Kokossis, A. C. and Floudas, C. A. (1990): Optimization of complex reactor networks–I. Isothermal operation, *Chemical Engineering Science* **45**, 595 – 614.

Kokossis, A. C. and Floudas, C. A. (1991): Synthesis of isothermal reactor-separator-recycle systems, *Chemical engineering science* **46**(5), 1361–1383.

Kokossis, A. C. and Floudas, C. A. (1994): Optimization of complex reactor networks–II. Nonisothermal operation, *Chemical Engineering Science* **49**(7), 1037 – 1051.

Kossack, S. (2010): *A Systematic Synthesis Framework for the Conceptual Design of Distillation Processes*, Fortschritt-Berichte VDI, Nr. 914, VDI-Verlag, Düsseldorf.

Kossack, S., Refinius, A., Brüggemann, S. and Marquardt, W. (2007): Konzeptioneller Entwurf von Reaktions-Destillations-Prozessen mit Näherungsverfahren, *Chemie Ingenieur Technik* **79**(10), 1601–1612.

Krämer, K. (2012): *Optimization-based Synthesis of Hybrid Separation Processes*, Fortschritt-Berichte VDI, Nr. 934, VDI-Verlag, Düsseldorf.

Krämer, K., Harwardt, A., Bronneberg, R. and Marquardt, W. (2011): Separation of butanol from acetone-butanol-ethanol fermentation by a hybrid extraction-distillation process, *Computers & Chemical Engineering* **35**, 949–963.

Krämer, K., Kossack, S. and Marquardt, W. (2009): Efficient optimization-based design of distillation processes for homogenous azeotropic mixtures, *Industrial & Engineering Chemistry Research* **48**(14), 6749–6764.

Krissmann, J., Roettger, D., Borgmann, C., Kaemper, K., Nierlich, F., Kaizik, A., Knippenberg, U. and Malzkorn, R. (2008): Method for producing 1-octene from crack-C4. US Patent 7,368,621.

Kroper, H., Weitz, H. M. and Wagner, U. (1962): New butadiene recovery process, *Hydrocarbon Processing & Petroleum Refiner* **41**(11), 191–196.

Lapkin, A. A. and Plucinski, P. K. (2009): Engineering Factors for Efficient Flow Processes in Chemical Industries, *in* S. V. Luis and E. Garcia-Verdugo (eds), *Chemical Reactions and Processes under Flow Conditions*, The Royal Society of Chemistry, pp. 1–43.

Linke, P. and Kokossis, A. (2003): Attainable reaction and separation processes from a superstructure-based method, *AIChE Journal* **49**(6), 1451–1470.

Liu, G., Jobson, M., Smith, R. and Wahnschafft, O. M. (2004): Shortcut design method for columns separating azeotropic mixtures, *Industrial & Engineering Chemistry Research* **43**(14), 3908–3923.

Lutze, P. and Gorak, A. (2013): Reactive and membrane-assisted distillation: recent developments and perspective, *Chemical Engineering Research and Design* **91**(10), 1978–1997.

Lutze, P., Román-Martinez, A., Woodley, J. M. and Gani, R. (2012): A systematic synthesis and design methodology to achieve process intensification in (bio) chemical processes, *Computers & Chemical Engineering* **36**, 189 – 207.

Luyben, W. (2010): Heuristic design of reaction/separation processes, *Industrial & Engineering Chemistry Research* **49**(22), 11564–11571.

Luyben, W. L. (2011): Heuristic design of reaction/separation processes with two recycles, *Industrial & Engineering Chemistry Research* **50**(8), 4788–4795.

Magna, L., Chauvin, Y., Niccolai, G. P. and Basset, J.-M. (2003): The importance of imidazolium substituents in the use of imidazolium-based room-temperature ionic liquids as solvents for palladium-catalyzed telomerization of butadiene with methanol, *Organometallics* **22**, 4418–4425.

Marquardt, W. (2005): Model-based experimental analysis of kinetic phenomena in multiphase reactive systems, *Chemical Engineering Research and Design* **83**(6), 561–573.

Marquardt, W. (2013): Identification of Kinetic Models by Incremental Refinement, *in* U. Gähde, S. Hartmann and J. H. Wolf (eds), *Models, Simulations, and the Reduction of Complexity*, De Gruyter, Berlin, pp. 187–220.

Marquardt, W., Harwardt, A., Recker, S., Viell, J. and Voll, A. (2012): Bio-based value chains of the future - an opportunity for process systems engineering, *in* I. A. Karimi and R. Srinivasan (eds), *11th International Symposium on Process Systems Engineering*, Vol. 31 of *Computer Aided Chemical Engineering*, Elsevier, pp. 19 – 28.

Marquardt, W., Kossack, S. and Kraemer, K. (2008): A framework for the systematic design of hybrid separation processes, *Chinese Journal of Chemical Engineering* **16**(3), 333–342.

Martinez, A., Krinsky, J. L., Penafiel, I., Castillon, S., Loponov, K., Lapkin, A., Godard, C. and Claver, C. (2015): Heterogenization of Pd-NHC complexes onto a silica support and their application in Suzuki-Miyaura coupling under batch and continuous flow conditions, *Catalysis Science & Technology* **5**, 310–319.

Maschmeyer, D. (2014): Personal communication, Evonik Industries AG, Marl.

McLean, K. A. and McAuley, K. B. (2012): Mathematical modelling of chemical processes-obtaining the best model predictions and parameter estimates using identifiability and estimability procedures, *The Canadian Journal of Chemical Engineering* **90**(2), 351–366.

Melin, T. and Rautenbach, R. (2007): *Membranverfahren: Grundlagen der Modul- und Anlagenauslegung*, Springer-Verlag, Berln.

Metcalfe, W. K., Simmie, J. M. and Curran, H. J. (2010): Ab initio chemical kinetics of methyl formate decomposition: The simplest model biodiesel, *The Journal of Physical Chemistry A* **114**(17), 5478–5484.

Mhamdi, A. and Marquardt, W. (1999): An inversion approach for the estimation of reaction rates in chemical reactors, *European Control Conference ECC'99, Karlsruhe*.

Mhamdi, A. and Marquardt, W. (2013): Incremental Identification of Distributed Parameter Systems, *in* S. Pushpavanam (ed.), *Control and Optimization of Process Systems, Advances in Chemical Engineering*, Elsevier, Amsterdam, pp. 51–106.

Nørskov, J. K., Bligaard, T., Rossmeisl, J. and Christensen, C. H. (2009): Towards the computational design of solid catalysts, *Nature chemistry* **1**, 37–46.

Pahor, B., Kravanja, Z. and Iri Bedenik, N. (2001): Synthesis of reactor networks in overall process flowsheets within the multilevel minlp approach, *Computers & Chemical Engineering* **25**(4-6), 765–774.

Palczewska-Tuliânska, M. (1997): *Solid and liquid heat capacity data collection: C1 - C33 compounds*, DECHEMA, Frankfurt am Main.

Papalexandri, K. P. and Pistikopoulos, E. N. (1996): Generalized modular representation framework for process synthesis, *AIChE Journal* **42**(4), 1010–1032.

Peschel, A., Freund, H. and Sundmacher, K. (2010): Methodology for the design of optimal chemical reactors based on the concept of elementary process functions, *Industrial & Engineering Chemistry Research* **49**(21), 10535–10548.

Praefke, J., Rix, A., Santiago Fernandez, S., Grompling, M., Hoper, F., Peters, U., Leistner, J., Nierlich, F. and Rottger, D. (2007): Process for preparing ethyl tert-butyl ether from technical mixtures of c4 hydrocarbons. US patent 2007/0203369 A1.

Quaiser, T. and Mönnigmann, M. (2009): Systematic identifiability testing for unambiguous mechanistic modeling–application to jak-stat, map kinase, and nf-κb signaling pathway models, *BMC systems biology* **3**(1), 1–21.

Recker, S., Kerimoglu, N., Harwardt, A., Tkacheva, O. and Marquardt, W. (2013): On the integration of model identification and process optimization, *in* A. Kraslawski and I. Turunen (eds), *23rd European Symposium on Computer Aided Process Engineering*, Vol. 32 of *Computer Aided Chemical Engineering*, Elsevier, pp. 1021 – 1026.

Recker, S. and Marquardt, W. (2012): A nonlinear programming approach to conceptual design of reaction-separation systems, *in* I. D. L. Bogle and M. Fairweather (eds), *Proceedings of the 22nd European Symposium on Computer Aided Process Engineering*, Vol. 30 of *Computer Aided Chemical Engineering*, Elsevier, pp. 592 – 596.

Recker, S., Skiborowski, M., Redepenning, C. and Marquardt, W. (2014): Systematic and optimization-based design of integrated reaction-separation processes, *in* M. R. Eden, J. D. Siirola and G. P. Towler (eds), *Proceedings of the 8th International Conference on Foundations of Computer-Aided Process Design*, Vol. 34 of *Computer Aided Chemical Engineering*, Elsevier, pp. 417 – 422.

Recker, S., Skiborowski, M., Redepenning, C. and Marquardt, W. (2015): A unifying framework for optimization-based design of integrated reaction-separation processes, *Computers & Chemical Engineering* **81**, 260–271.

Redepenning, C., Recker, S. and Marquardt, W. (2016): Pinch-based shortcut method for the conceptual design of isothermal extraction columns, *AIChE Journal, in press* .

Rios, L. M. and Sahinidis, N. V. (2013): Derivative-free optimization: A review of algorithms and comparison of software implementations, *Journal of Global Optimization* **56**(3), 1247–1293.

Roettger, D., Beller, M., Jackstell, R., Klein, H. and Wiese, K.-D. (2002): Verfahren zur Telomerisation von nicht cyclischen Olefinen. DE 101 28 144 A1.

Roetzel, W. and Spang, B. (2013): C3: Typische Werte von Wärmedurchgangskoeffizienten, *VDI-Wärmeatlas*, Springer, pp. 85–90.

Rooney, W., Hausberger, B., Biegler, L. and Glasser, D. (2000): Convex attainable region projections for reactor network synthesis, *Computers & Chemical Engineering* **24**(2-7), 225–229.

Ryll, O., Blagov, S. and Hasse, H. (2006): Thermodynamic analysis of multicomponent distillation-reaction processes for conceptual process design, *Institution of Chemical Engineers Symposium Series* **152**, 100–110.

Ryll, O., Blagov, S. and Hasse, H. (2012): Inf/inf-analysis of homogeneous distillation processes, *Chemical Engineering Science* **84**, 315–332.

Ryll, O., Blagov, S. and Hasse, H. (2013): Inf/inf-analysis of heterogeneous distillation processes, *Chemical Engineering Science* **104**, 374–388.

Ryll, O., Blagov, S. and Hasse, H. (2014): Thermodynamic analysis of reaction-distillation processes based on piecewise linear models, *Chemical Engineering Science* **109**, 284 – 295.

Schembecker, G., Dröge, T., Westhaus, U. and Simmrock, K. H. (1995): Readpert–development, selection and design of chemical reactors, *Chemical Engineering and Processing: Process Intensification* **34**(3), 317–322.

Scheu, H., Busch, J. and Marquardt, W. (2010): Nonlinear distributed dynamic optimization based on first order sensitivities, *Proceedings of the American Control Conference 2010*, pp. 1574–1579.

Scheu, H. and Marquardt, W. (2011): Sensitivity-based coordination in distributed model predictive control, *Journal of Process Control* **21**(5), 715 – 728.

Schweiger, C. and Floudas, C. (1999): Synthesis of optimal chemical reactor networks, *Computers & Chemical Engineering* **23**, 47–50.

Senkan, S. (2001): Combinatorial heterogeneous catalysis - a new path in an old field, *Angewandte Chemie International Edition* **40**(2), 312–329.

Seuranen, T., Hurme, M. and Pajula, E. (2005): Synthesis of separation processes by case-based reasoning, *Computers & Chemical Engineering* **29**(6), 1473–1482.

Shah, V. H. and Agrawal, R. (2010): A matrix method for multicomponent distillation sequences, *AIChE Journal* **56**(7), 1759–1775.

Siirola, J. J. and Rudd, D. F. (1971): Computer-aided synthesis of chemical process designs. From reaction path data to the process task network, *Industrial & Engineering Chemistry Fundamentals* **10**(3), 353–362.

Skiborowski, M. (2015): *Optimization-Based Methods for the Conceptual Design of Separation Processes for Azeotropic Mixtures*, Fortschritt-Berichte VDI: Reihe 3, Nr. 946, VDI-Verlag, Düsseldorf.

Skiborowski, M., Harwardt, A. and Marquardt, W. (2013): Conceptual design of distillation-based hybrid separation processes, *Annual Review of Chemical and Biomolecular Engineering* **4**(1), 45–68.

Skiborowski, M., Harwardt, A. and Marquardt, W. (2014a): Conceptual Design of Azeotropic Distillation Processes, *in* A. Górak and E. Sorensen (eds), *Distillation: Fundamentals and Principles*, Elsevier, Amsterdam, pp. 305–355.

Skiborowski, M., Harwardt, A. and Marquardt, W. (2014b): Efficient optimization-based design for the separation of heterogeneous azeotropic mixtures, *Computers & Chemical Engineering* **72**, 34–51.

Smith, E. and Pantelides, C. (1995): Design of reaction/separation networks using detailed models, *Computers & Chemical Engineering* **19**, 83–88.

Smith, R. and Linnhoff, B. (1988): The design of separators in the context of overall processes, *Chemical Engineering Research & Design* **66**(3), 195–228.

Steimel, J., Harrmann, M., Schembecker, G. and Engell, S. (2013a): A framework for the modeling and optimization of process superstructures under uncertainty, *Chemical Engineering Science* **115**, 225–237.

Steimel, J., Harrmann, M., Schembecker, G. and Engell, S. (2013b): Model-based conceptual design and optimization tool support for the early stage development of chemical processes under uncertainty, *Computers & Chemical Engineering* **59**, 63–73.

Stein, O., Oldenburg, J. and Marquardt, W. (2004): Continuous reformulations of discrete–continuous optimization problems, *Computers & Chemical Engineering* **28**(10), 1951–1966.

Sundmacher, K. (2015): Multi-level design of process systems for efficient chemical production and energy conversion, *in* K. V. Gernaey, J. H. Huusom and R. Gani (eds), *Proceedings of the 12th International Symposium on Process Systems Engineering and the 25th European Symposium on Computer Aided Process Engineering*, Elsevier, pp. 25–34.

Sundmacher, K., Zhang, R.-S. and Hoffmann, U. (1995): Mass transfer effects on kinetics of nonideal liquid phase ethyl tert-butyl ether formation, *Chemical Engineering & Technology* **18**(4), 269–277.

Thiel, C., Sundmacher, K. and Hoffmann, U. (1997): Synthesis of ETBE: Residue curve maps for the heterogeneously catalysed reactive distillation process, *Chemical Engineering Journal* **66**(3), 181–191.

Tikhonov, A. N. and Arsenin, V. Y. (1977): *Solutions of Ill-posed Problems*, Vol. 330, Vh-Winston.

Till, J., Sand, G., Engell, S., Schembecker, G. and von Trotha, T. (2003): READOPT: Reaktor-Design-Optimierung durch heuristikgestützte MINLP-Methoden, *Chemie Ingenieur Technik* **75**(8), 1025–1026.

Tschan, M. J.-L., Garcia-Suarez, E. J., Freixa, Z., Launay, H., Hagen, H., Benet-Buchholz, J. and van Leeuwen, P. W. (2010): Efficient bulky phosphines for the selective telomerization of 1, 3-butadiene with methanol, *Journal of the American Chemical Society* **132**(18), 6463–6473.

Tschan, M. J.-L., Launay, H., Hagen, H., Benet-Buchholz, J. and van Leeuwen, P. W. (2011): Telomerisation of buta-1,3-diene and methanol: Superiority of chromanyl-type phosphines in the Dow process for the industrial production of 1-MOD, *Chemistry - A European Journal* **17**(32), 8922–8928.

Ullmann, F. (2001): *Ullmann's Encyclopedia of Industrial Chemistry*, Wiley-VCH, Weinheim.

Ulonska, K., Skiborowski, M., Mitsos, A. and Viell, J. (2016): Early-stage evaluation of biorefinery processing pathways using process network flux analysis, *AIChE Journal, in press* .

Upadhye, A., Qi, W. and Huber, G. (2011): Conceptual process design: A systematic method to evaluate and develop renewable energy technologies, *AIChE Journal* **57**(9), 2292–2301.

Urdaneta, R. (2005): *Targeting and Conceptual Design of Heteroazeotropic Distillation Processes*, Fortschritt-Berichte VDI, Nr. 845, VDI-Verlag, Düsseldorf.

Valera, F. E., Quaranta, M., Moran, A., Blacker, J., Armstrong, A., Cabral, J. T. and Blackmond, D. G. (2010): The flow's the thing... or is it? Assessing the merits of homogeneous reactions in flask and flow, *Angewandte Chemie International Edition* **49**(14), 2478–2485.

Vázquez-Ojeda, M., Segovia-Hernández, J. G., Hernández, S., Hernández-Aguirre, A. and Kiss, A. A. (2013): Design and optimization of an ethanol dehydration process using stochastic methods, *Separation and Purification Technology* **105**, 90–97.

Völkl, L., Geburtig, D., Kiermaier, S., Wasserscheid, P. and Haumann, M. (2016): Pd-catalyzed telomerization of butadiene and methanol with direct catalyst recycling using a liquid-ionic liquid biphasic, continuous process, *Chemical Engineering and Processing: Process Intensification* **99**, 107–114.

Völkl, L., Recker, S., Niedermaier, M., Kiermaier, S., Strobel, V., Maschmeyer, D., Cole-Hamilton, D., Marquardt, W., Haumann, M. and Wasserscheid, P. (2015): Comparison between phosphine and NHC-modified Pd catalysts in the telomerization of butadiene with methanol - A kinetic study combined with model-based experimental analysis, *Journal of Catalysis* **329**, 547–559.

Voll, A. and Marquardt, W. (2012): Reaction network flux analysis: Optimization-based evaluation of reaction pathways for biorenewables processing, *AIChE Journal* **58**(6), 1788–1801.

Wallert, C. (2007): *Konzeptioneller Entwurf und wirtschaftliche Bewertung hybrider Trennprozesse mit Näherungsverfahren*, Fortschritt-Berichte VDI, Nr. 889, VDI-Verlag.

Westerberg, A. W. (2004): A retrospective on design and process synthesis, *Computers & Chemical Engineering* **28**(4), 447 – 458.

Yee, K. F., Mohamed, A. R. and Tan, S. H. (2013): A review on the evolution of ethyl tert-butyl ether (ETBE) and its future prospects, *Renewable and Sustainable Energy Reviews* **22**, 604–620.

Online-Buchshop für Ingenieure

VDI nachrichten

BUCHSHOP

Online-Shops

Fachliteratur und mehr - jetzt bequem online recherchieren & bestellen unter: www.vdi-nachrichten.com/Der-Shop-im-Ueberblick

Täglich aktualisiert: Neuerscheinungen VDI-Schriftenreihen

Im Buchshop von vdi-nachrichten.com finden Ingenieure und Techniker ein speziell auf sie zugeschnittenes, umfassendes Literaturangebot.

Mit der komfortablen Schnellsuche werden Sie in den VDI-Schriftenreihen und im Verzeichnis lieferbarer Bücher unter 1.000.000 Titeln garantiert fündig.

Im Buchshop stehen für Sie bereit:

VDI-Berichte und die Reihe **Kunststofftechnik**:

Berichte nationaler und internationaler technischer Fachtagungen der VDI-Fachgliederungen

Fortschritt-Berichte VDI:

Dissertationen, Habilitationen und Forschungsberichte aus sämtlichen ingenieurwissenschaftlichen Fachrichtungen

Newsletter „Neuerscheinungen":

Kostenfreie Infos zu aktuellen Titeln der VDI-Schriftenreihen bequem per E-Mail

Autoren-Service:

Umfassende Betreuung bei der Veröffentlichung Ihrer Arbeit in der Reihe Fortschritt-Berichte VDI

Buch- und Medien-Service:

Beschaffung aller am Markt verfügbaren Zeitschriften, Zeitungen, Fortsetzungsreihen, Handbücher, Technische Regelwerke, elektronische Medien und vieles mehr – einzeln oder im Abo und mit weltweitem Lieferservice

Die Reihen der Fortschritt-Berichte VDI:

1 Konstruktionstechnik/Maschinenelemente
2 Fertigungstechnik
3 Verfahrenstechnik
4 Bauingenieurwesen
5 Grund- und Werkstoffe/Kunststoffe
6 Energietechnik
7 Strömungstechnik
8 Mess-, Steuerungs- und Regelungstechnik
9 Elektronik/Mikro- und Nanotechnik
10 Informatik/Kommunikation
11 Schwingungstechnik
12 Verkehrstechnik/Fahrzeugtechnik
13 Fördertechnik/Logistik
14 Landtechnik/Lebensmitteltechnik
15 Umwelttechnik
16 Technik und Wirtschaft
17 Biotechnik/Medizintechnik
18 Mechanik/Bruchmechanik
19 Wärmetechnik/Kältetechnik
20 Rechnerunterstützte Verfahren (CAD, CAM, CAE CAQ, CIM ...)
21 Elektrotechnik
22 Mensch-Maschine-Systeme
23 Technische Gebäudeausrüstung

ISBN 978-3-18-395103-1